Emulsion Polymerization of Poly-(Methyl Acrylate) for Flocculation and Dewatering of Oil Sands Tailings.

by

Oscar Njiru

A thesis submitted in partial fulfillment of the requirements for the degree of

Master of Science
in
Chemical Engineering

Department of Chemical and Materials Engineering
University of Alberta

© Oscar Njiru, 2020

Abstract

This work adds to the continuing research efforts in Alberta to manage the accumulation of oil sands tailings and reduce the environmental footprint of oil sands' operations. Oil sands tailings are unwanted by-products of surface-mining bitumen extraction processes. They are usually held in engineered artificial basins called tailing ponds. Mature fine tailings (MFT) are formed after a considerable period of gravity consolidation and are constituted of solids (~30-40 wt. %), traces of residual bitumen (~1-3 wt. %), and water (~60-70 wt. %). MFT predominantly contain negatively-charged fine solids (smaller than 44 μm) that form electrostatically stable suspensions. These stable MFT suspensions are the main concern in tailings treatment: if unattended, they can remain stable for decades. Recent estimates show that more than 1.2 trillion litres of tailings cover over 220 km^2 of land in Alberta. To put this into perspective the volume of oil sands tailings would be enough to fill 480,000 Olympic-sized swimming pools or, to use a Canadian perspective, fill 3 million NFL hockey rinks to 1-inch thickness. Also, remember that a significant portion of these tailings are essentially contaminated water. The main goals in oil sands tailings remediation are to recover and recycle the high amount of water trapped therein and to ultimately reclaim the land they currently occupy.

Industrial dewatering technologies mostly use polyacrylamide (PAM) flocculants. These flocculants hold water in their flocs via hydrogen bonding, making it hard to recover the water. In my thesis, I propose the use of acrylate-based polymers to tackle the aforementioned dewatering challenges posed by PAM flocculants. The main motivation to using these alternative flocculants is their hydrophobic backbones - a property I hope to harness to expel water more effectively from the sediment flocs.

In my thesis, I specifically used poly (methyl acrylate) (PMA). PMA is naturally hydrophobic. Therefore, to achieve the water-solubility required of polymeric flocculants, I hydrolyzed PMA to water-soluble HPMA (hydrolyzed-PMA) and tuned the degree of water solubility of PMA by varying the extent of hydrolysis. Also, being a homopolymer, PMA is comparatively easier and inexpensive to synthesize, especially on an industrial scale. Consequently, it is easy to scale up its production to meet the demands of the oil sands industry.

An integral part of this work was the use of emulsion polymerization to make PMA. This is a technique that is usually preferred for its ability to combine high polymerization rates (short batch cycle time) and high *average molecular weight* (MW). Emulsion polymerization of methyl acrylate allowed me to obtain a stable reaction mixture, high polymer weight fractions per batch, high polymer yields, and polymers with high MW that were comparable to a reference industrial PAM flocculant.

The experimental work was guided by a design of experiment (central composite design) and the responses were modeled using a multiple linear regression model. I used *PMA properties* (degree of hydrolysis (DOH) and MW) as input/predictor variables and key flocculation parameters as output/response variables. The DOH was the sole significant predictor variable for the capillary suction time (CST) model. Supernatant turbidity and the initial settling rate (ISR) models had both the DOH and MW as significant predictor variables, but the DOH still had the dominant effect. This overriding significance of the DOH is, I propose, due to its crucial role in PMA water-solubility, chain extension, and generation of flocculation binding-sites. Generally, supernatant turbidity increased with polymer dosage, which I attributed to the dispersive sodium ions from the caustic solution used for hydrolysis. Flocculation tests on undiluted MFT using a water-soluble high-MW HPMA showed very promising results that exceeded the industrial dewatering requirements for high density tailings flocculation.

In sum, the results presented in this thesis show that the success of HPMA as a tailings flocculant was mainly dictated by its DOH. And higher MW water-soluble HPMA grades were generally better flocculants, especially when used to treat MFT samples with high solids contents.

Dedication

This work is dedicated to my mothers - Wanjiru Wambugu and Njoki Kiai - for supporting my dreams, often at the expense of their own. And in loving memory of my grandparents: Mr. and Mrs. Kiai, and Mr. and Mrs. Njiru, whose memories I deeply cherish.

Acknowledgements

To my thesis advisor, Professor João B. P. Soares, I am deeply indebted. Thank you for creative freedom, for guidance, with patience, and for funding this project. Your forbearances have taught me to be more patient, generous and accommodating with others and even more so with myself. Without your support this work would not have been possible. You have been a full package – an advisor, mentor, role model and friend, all rolled up in one person. It has been an honor and pleasure to work under your supervision.

I would also like to acknowledge the input of the following people who were helpful at various stages of this research. Dr. Linda Botha, a former postdoctoral fellow in our research group, who worked alongside my colleagues Ben and Steph to help initiate this project. Dr. Vahid Vajihinejad, a colleague who helped with the DOE and the CCD. Dr. Marco Antônio Silva, a postdoctoral fellow in our group who helped with MW measurements. The technician Nupur Dabral and fellow colleague Daniel Dixon for their help with NMR analyses. Dr. Xiaoli Tan for his input on topics related to oil sands and for allowing access to research facilities in the Institute for Oil Sands Innovation (IOSI) lab. Technician Lisa Brandt for training on the use of IOSI lab equipment. Mohammed Ghuzi and Shuanglei Peng for their help with some of the flocculation tests.

I am also grateful to my thesis defense committee members: Professor Phillip Choi, Professor Hyun-Joong Chung, Professor João B. P. Soares and the chair, Professor Arvind Rajendran.

Special mention and deep gratitude to Stepan Spitsin, Daniyar Dzhumamukhamedov, Professor Gennady Mikhailovich and Professor Vanchurin Illarionovich for their support during my foundational university years at D. Mendeleev University of Chemical Technology.

To my family, I can never thank you nearly enough for being a constant source of love, even when most of my work takes away from time spent with you. Lastly, I appreciate the friends who have been family over the years I have been away from home.

Table of Contents

1) Introduction

1.1) An Overview of the Alberta Oil Sands 2
1.1.1 Formation 2
1.1.2 Reserves and Their Locations 3
1.1.3. Ore Properties and Extraction Methods 4
1.1.3.1. Properties 4
1.1.3.2. Surface Mining 6
1.1.3.3. In Situ Extraction 7
1.1.4 Economic Significance and Environmental Concerns. 9
1.2) Thesis Outline 12

2) Literature Review

2.1) Oil Sands Tailings and Clay Minerals 14
2.2.1 Hot Water Extraction and Oil Sands Tailings. 14
2.2.2 Properties of Clay Minerals in MFT 20
2.2) Coagulation and Flocculation. 27
2.3) Polymer Flocculants and MFT Dewatering. 30
2.4) Emulsion Polymerization. 35
2.4.1. Introduction - Free Radical Polymerization 35
2.4.1.1. Free Radical Polymerization Techniques 35
2.4.1.2. Free Radical Mechanism and Kinetics 36
2.4.2. Emulsion Polymerization 39
2.4.2.1. Emulsion Polymerization Nucleation and Mechanisms. 40
2.4.2.2. Emulsion Polymerization Intervals 43
2.4.2.3. Emulsion Polymerization Kinetics 45
2.4.2.4. Emulsion Polymerization of Alkyl Acrylates 49

3) Synthesis and Hydrolysis of PMA

3.1) Experimental Design 52
3.2) Polymer Synthesis and Hydrolysis 52
3.2.1. Materials 52
3.2.2. Determination of the Critical Micelle Concentration. 52
3.2.3. Synthesis of PMA 54
3.2.4. Hydrolysis of PMA 56
3.3) Characterization Techniques. 58
3.3.1. DOH: Proton Nuclear Magnetic Resonance (^{1}H-NMR) 58
3.3.2. DOH: Fourier-Transform Infrared Spectroscopy (FTIR) 61
3.3.3. Particle Size Analysis: Dynamic Light Scattering (DLS) 62
3.3.4. Polymer Molecular Weight and Viscosity: FFF and Rheometry 64

4) Flocculation Studies

4.1) MFT Characterization 67
4.2) Statistical Models and Flocculation Tests 69
4.2.1. Capillary Suction Time 69
4.2.2. Supernatant Turbidity 74
4.2.3. Initial Settling Rate (ISR) 80
4.3) High Density MFT Flocculation Tests 84
4.3.1. CST 84
4.3.2. Pressure Filtration 85
4.3.3. Supernatant Clarity: Centrate Solids Content 86
4.3.4 Solids Content 86

5) Conclusions and Future Work

5.1) Main Contributions 88
5.2) Future Work 89

List of Tables

Table 1-1: Comparison of oil recovery yields from various extraction methods [19] 8

Table 1-2: Canada's historical GHG emissions by province and territory 10

Table 2-1: Important properties of typical oil sands' clays. [3] 21

Table 2-2: Water-holding capacity as a function of change in particle size. [41] 23

Table 2-3: A comparison of typical hydraulic conductivities of different saturated soil types.[49], [52] 26

Table 2-4: A table showing T_g values for a range of poly (alkyl acrylates). [124] 50

Table 3-1: Feed composition for PMA synthesis based on the CCD. 55

Table 3-2: A summary of particle size analysis results from DLS. 63

Table 3-3: MW measurements using an FFF. 65

Table 3-4: Viscosity measurements using a Brookfield DV-III rheometer. 65

Table 4-1: MFT properties as characterized by Suncor. 68

Table 4-2: Results from Dean-Stark analysis 68

Table 4-3: Results from atomic adsorption spectroscopy 68

Table 4-4: Key properties that influence clay dispersity. [143], [146] 75

Table 4-3: CST results on undiluted MFT. 84

Table 4-5: Solids content results on undiluted MFT. 86

List of Figures

Figure 1-1:(a) A profile of relevant locations and geological features of the Alberta Oil Sands Deposits.[2] (b) An illustration of oil migration from the original deep source rocks to near-surface locations. [1] Athabasca oil sands deposits have a migration path that is about 360 km long while that for the Peace River Deposits is about 80km.[3] 2

Figure 1-2: Proven oil reserves.[6] 3

Figure 1-3: Oil sands deposits in Alberta.[7] 4

Figure 1-4: Properties of Athabasca bitumen compared to different types of crude oils.[10] 5

Figure 1-5: Summary of the main stages in surface mining. [17] 6

Figure 1-6: A schematic to show water usage and tailings generation for every barrel of bitumen produced in water-based bitumen extraction. [3] 6

Figure 1-7: Main stages in SAGD in-situ bitumen extraction. [17] 7

Figure 1-8: Actual and projected daily bitumen production rates via surface mining and in situ extraction methods. [16] 8

Figure 1-9: Alberta's GHG emissions from different economic sectors. 11

Figure 2-1: Simplified illustration of the key steps in CHWE bitumen recovery. 14

Figure 2-2: Interfacial interactions between bitumen, sand and water during liberation. Equation (**2-2** (Young's equation) offers a mathematical relationship between interfacial tensions from the three phases and their contact angle(Θ). 15

Figure 2-3: Key chemical reactions associated with caustic additives in CHWE: (A) base hydrolysis of naphthenic acid (simplified chemical structure) [30]; and (B) base hydrolysis of (silaceous) sand surfaces. [3] 16

Figure 2-4: Interfacial interactions between air, bitumen and water phases characteristic of the bitumen aeration process. 17

Figure 2-5: Simplified schematic of the main process streams that generate tailings during CHWE.(Adapted from [33]) 18

Figure 2-6: (A) An oil sands ternary diagram showing important boundaries useful for engineering applications.[37] (B) A ternary plot based on Unified Oil Sands Tailings Classification System showing 4 main color partitions based on composition.[39] 19

Figure 2-7: A 1:1 or -TO- structure that is characteristic of kaolinite clays. [42] 21

Figure 2-8: A 2:1 or –TOT- structure found in illite and smectite clays. [43] 21

Figure 2-9: A schematic representation of the electrical double layer on the surface of a dispersed and negatively charged clay particle. Associated electrokinetic potentials are also shown. 23

Figure 2-10: (a) Surface charge of different sodium-treated clay minerals at various pH values. ; (b) A plot showing the degree of dispersion of different clay types as a function of their surface charges. [32], [43] 24

Figure 2-11: An illustration of the interaction forces as described by the DLVO colloidal stability theory. 25

Figure 2-12: The relationship between void ratio and hydraulic conductivity for soils with varying clay content (and plasticity index-PI). [50] 26

Figure 2-13: Colloidal destabilization as a function of (a) pH-control [28], [46] (b) change of electrolyte concentration [54], and (c) variation of ionic strength.[5] 28

Figure 2-14: (A) An illustration of the storage volume reduction that is expected with increase in tailings solids content.[42] (B) An illustration of oil sands tailings' volume % - mass % relationship and atterberg limits. [35] 31

Figure 2-15: (a) PAM. (b) Simplified illustration of proposed intermolecular hydrogen bonding between PAM chains and water molecules. 32

Figure 2-16: Hydrophobic modifications of PAM-based polymers: (a) PNIPAM; (b) PAM-g-PPO copolymer; (c) PAM-g-PEOMA copolymer; and (d) P(NIPAM-AA-NTBA) copolymer. 33

Figure 2-17: HBfPE copolymer showing hydrophilic segments of hydrolyzed methyl acrylate on a hydrophobic polyethylene backbone. 34

Figure 2-18: HPMA homopolymer showing the hydrophilic segments that result from base hydrolysis of the hydrophobic backbone of PMA. 35

Figure 2-19: (A) Autoacceleration as a function of monomer (methyl methacrylate) concentration.[78] (B) Trommsdorff effect and limiting conversion in FRP kinetics. [81] 37

Figure 2-20: The three characteristic steps of free radical polymerization reactions. 38

Figure 2-21: (A) An illustration of a micelle aggregate (50-150 surfactant molecules) in equilibrium with other surfactant molecules in solution. (B) A monomer droplet. (C) Micellar nucleation. (D) Homogenous nucleation. [103] 41

Figure 2-22: Schematic illustration of the conceptual intervals that are characteristic of Harkin's mechanism. [100] 43

Figure 2-23: A A schematic showing a multitude of kinetic events that characterize emulsion polymerization. [104] 48

Figure 3-1: A K-100 tensiometer that was used for surface tension measurements when determining the CMC. 53

Figure 3-2: A plot showing the relationship between surface tension and surfactant concentration. Remnant coagula (coagulums) in the conical flasks served as indicators of colloidal stability at different surfactant concentrations. 54

Figure 3-3: Remnant coagula from: (a) surfactant-free emulsion polymerization with a 10 wt % monomer feed; (b) surfactant-free emulsion polymerization with a 15wt % monomer feed; and (c) conventional emulsion polymerization with a 35wt% monomer feed. 55

Figure 3-4: A proposed PMA base hydrolysis mechanism showing four mechanistic steps: 1 - nucleophilic addition of the hydroxyl ion; 2 - formation of an intermediate species; 3 - Loss of the leaving group; and 4 - deprotonation to form HPMA and gaseous methanol. 56

Figure 3-5: A schematic representation of electrostatic repulsion of the hydroxyl ion by neighboring carboxylate groups, which retards base hydrolysis of ester groups, especially at high degrees of hydrolysis. 57

Figure 3-6: ^{1}H-NMR analysis of HPMA and the corresponding change in water-solubility for relatively low MW samples ($2.14.10^{-2}$ M KPS). 59

Figure 3-7: ^{1}H-NMR analysis of HPMA and the corresponding change in solubility for relatively high MW samples ($1.17.10^{-4}$M KPS). 59

Figure 3-8: ^{1}H-NMR of unhydrolyzed PMA (0 % HPMA). 60

Figure 3-9: ^{1}H-NMR of highly hydrolyzed PMA (~90 % HPMA). 60

Figure 3-10: Tracking the extent of hydrolysis by following the change in the FTIR spectrums corresponding to ester and carboxylate functional groups: (A) unhydrolyzed PMA (milky latex) (B) lowly hydrolyzed PMA (insoluble milky HPMA) (C) moderately hydrolyzed PMA (partly water-soluble translucent HPMA solution) and (D) highly hydrolyzed PMA (clear water-soluble HPMA solution) 61

Figure 3-11: Comparison between the FTIR spectrums of 0 % HPMA (Unhydrolyzed PMA) and ~90 % HPMA. 62

Figure 3-12: (A) Zetasizer Nano ZSP. [138] (B) An intensity distribution of PMA particles at 1.17 $x10^{-4}$ M KPS. 63

Figure 4-1: A Dean-Stark apparatus. [33] 67

Figure 4-2: (A) A schematic of a side view profile, (B) an actual single cell fitted with a filter paper, (C) top view profile and (D) and a complete view of a Type 319 Multi-CST apparatus. [33] 70

Figure 4-3: CST values from: diluted MFT (control); reference commercial PAM; 50% HPMA (1.58x10-3M, KPS) and 70% HPMA (1.58x10-3M, KPS). 70

Figure 4-4: Modelled CST surface response as a function of DOH and initiator concentration. 71

Figure 4-5: A contour plot of the CST surface response as a function of DOH and initiator concentration. 72

Figure 4-6: Observed versus predicted values for the CST model. 73

Figure 4-7: Normal plot of the CST model 73

Figure 4-8: An illustration of the typical increase in supernatant turbidity that was observed with increase in HPMA dosage. ... 74

Figure 4-9: Clay colloidal dispersion (turbidity) due to increase in exchangeable sodium content.[5] 75

Figure 4-10: Illustration of the dual effect that pH and sodium content have on clay colloidal dispersion. (Adopted from [42]and originated from [145]) 76

Figure 4-11: (A) An illustration of the diametrically opposed effects that calcium and sodium ions have on the surface charge of clay minerals at the typical MFT pH (~8).[44] (B) Clay coagulation and dispersion resulting from an increase in calcium and sodium ions.[5], [145] 76

Figure 4-12: A Pareto chart of standardized significant predictor variables. 77

Figure 4-13: Surface response of supernatant turbidity as a function of DOH and initiator concentration. 77

Figure 4-14: A contour plot of the surface response of supernatant turbidity as a function of DOH and initiator concentration. . 78

Figure 4-15: Observed versus predicted values for the turbidity model. 79

Figure 4-16: Normal plot of the supernatant turbidity model. 79

Figure 4-17: The difference in floc size between two HPMA flocculants of equal dosage and hydrolyzed from the same PMA batch ($1.58x10^{-3}$M, KPS) but to different DOH: (A) ~70% HPMA and (B) ~50% HPMA. 80

Figure 4-18: A Pareto chart of standardized significant predictor variables for ISR. 81

Figure 4-19: Surface response of ISR as a function of DOH and initiator concentration. 82

Figure 4-20: A contour plot of the surface response of ISR as a function of DOH and initiator concentration. 82

Figure 4-21: Observed versus predicted values for the ISR model. 83

Figure 4-22: Normal plot of the ISR model. 83

Figure 4-23: CST values from the treatment of undiluted MFT. 85

Figure 4-24: Centrate clarity at optimal dewaterability of HPMA. 86

Figure 5-1: (a) Hydrolyzed poly (styrene-acrylate) copolymer (high Tg and low hydrogen bonding). (b) Partially hydrolyzed PAA homopolymer (high Tg and high hydrogen bonding). (c) Partially hydrolyzed PEA homopolymer (rubbery with low hydrogen bonding). (d) Partially hydrolyzed P-n-BA homopolymer. (e) Partially hydrolyzed P-t-BA homopolymer. (f) Partially hydrolyzed POA homopolymer. 90

List of Abbreviations

API	American Petroleum Institute
CCC	Critical Coagulation Concentration
CCD	Central Composite Design
CEC	Cation Exchange Capacity
CHWE	Clark Hot Water Extraction
CMC	Critical Micelle Concentration
CST	Capillary Suction Time
CT	Composite Tailings
CWR	Clay to Water Ratio
DLS	Dynamic Light Scattering
ESP	Exchangeable Sodium Percentage
FFF	Fluid Flow Fractionation
FTIR	Fourier-Transform Infrared Spectroscopy
GHG	Greenhouse Gases
HBfPE	Hyperbranched Functionalized Polyethylene
^{1}H-NMR	Proton Nuclear Magnetic Resonance
HPAM	Hydrolyzed Polyacrylamide
HPMA	Hydrolyzed Poly (Methyl Acrylate)
ISR	Initial Settling Rate
KPS	Potassium Persulfate
MEHQ	Monomethyl Ether Hydroquinone
MFT	Mature Fine Tailings
MW	Average Molecular Weight
NIPAM	N-IsoPropyl Acrylamide
NST	Non-Segregating Tailings

NTBA	N-Tert-ButylAcrylamide
PAA	Poly (Acrylic Acid)
PAM	Poly (Acrylamide)
PAM-g-PEOMA	Poly(Acrylamide)-graft-Poly(Ethylene Oxide Methyl Ether Methacrylate)
PAM-g-PPO	Poly(Acrylamide)-graft-Polypropylene Oxide
PDI	Polydispersity Index
P-n-BA	Poly (n-Butyl Acrylate)
P-t-BA	Poly (tert-Butyl Acrylate)
PMA	Poly (Methyl Acrylate)
P(NIPAM)	Poly(N-IsoPropyl Acrylamide)
P(NIPAM-AA-NTBA)	Poly(N-IsoPropyl Acrylamide/Acrylic Acid/N-Tert-ButylAcrylamide)
POA	Poly(Octadecyl Acrylate)
SAGD	Steam Assisted Gravity Drainage
SDS	Sodium Dodecyl Sulfate
SFR	Sands to Fines Ratio
SSA	Specific Surface Area
TFT	Thin Fluid Tailings
THF	Tetrahydrofuran
TT	Thickened Tailings
WT	Whole Tailings

List of Symbols

a_s	Interfacial Surface Area Occupied by a Surfactant Molecule
b_i	Coefficient for Linear Terms of the Predictor Variables
b_{ii}	Coefficient for Quadratic Terms of the Predictor Variables
b_{ij}	Coefficient for Interactive Terms of the Predictor Variables
b_o	Constant Coefficient
C_i	Molar Concentration (mol/L) of the Ion of Type i
F_g	Gravitational Force
g	Gravitational Acceleration
I	Initiator
I	Ionic Strength
$[I]$	Initiator Concentration
I^*	Primary Initiator Radical
k_d	Rate Constant for Initiator Dissociation
k_i	Rate Constant for Initiation
k_p	Rate Constant for Propagation
k_{tc}	Rate Constant for Termination by Combination/Coupling
k_{td}	Rate Constant for Termination by Disproportionation
M	Monomer
$[M]$	Monomer Concentration
$[M]_p$	Monomer Concentration in a Polymer Particle
N	Total Number of Latex Particles per Unit Volume
N_A	Avogadro's Number
P_n^*	Polymer Radical with n Monomer Units (Where n is a positive integer)
R	Radius of Solid Particle
R^*	Radical Species
R_i	Rate of Initiation

$[S]$	Surfactant Concentration
T_g	Glass Transition Temperature
X_i & X_j	Coded Values of Predictor Variables.
$\overline{X_n}$	Number-Average Degree of Polymerization
Y_i	i^{th} Predicted Response/Output/Dependent Variable
Z_i	Valence of the Ion of Type i
η	Viscosity of the Dispersing Fluid
μ	The Rate of Volume Increase of Polymer Particle
v	Kinetic Chain Length
v	Terminal Settling Velocity
ρ_f	Density of Fluid Medium
ρ_s	Density of Solid Particle

1) Introduction

1.1) An Overview of the Alberta Oil Sands

1.1.1 Formation

Several theories attempt to explain the formation of Alberta's oil sands. According to the generally accepted biogenic theory, oil sands are a product of ancient marine life subjected to extremely high pressures and temperatures over millions of years. The original product formed was conventional light oil that was located in deep petroleum source rocks hundreds of kilometers to the west. Millions of years ago, as the Rocky Mountains formed, the oil migrated through the permeable sands towards Alberta and upwards closer to the surface (**Figure 1-1**). Later, the light oil underwent biodegradation depleting lighter hydrocarbons and leaving behind the unconventionally heavy oil that is today commonly known as *Alberta oil sands bitumen*. [1]–[5]

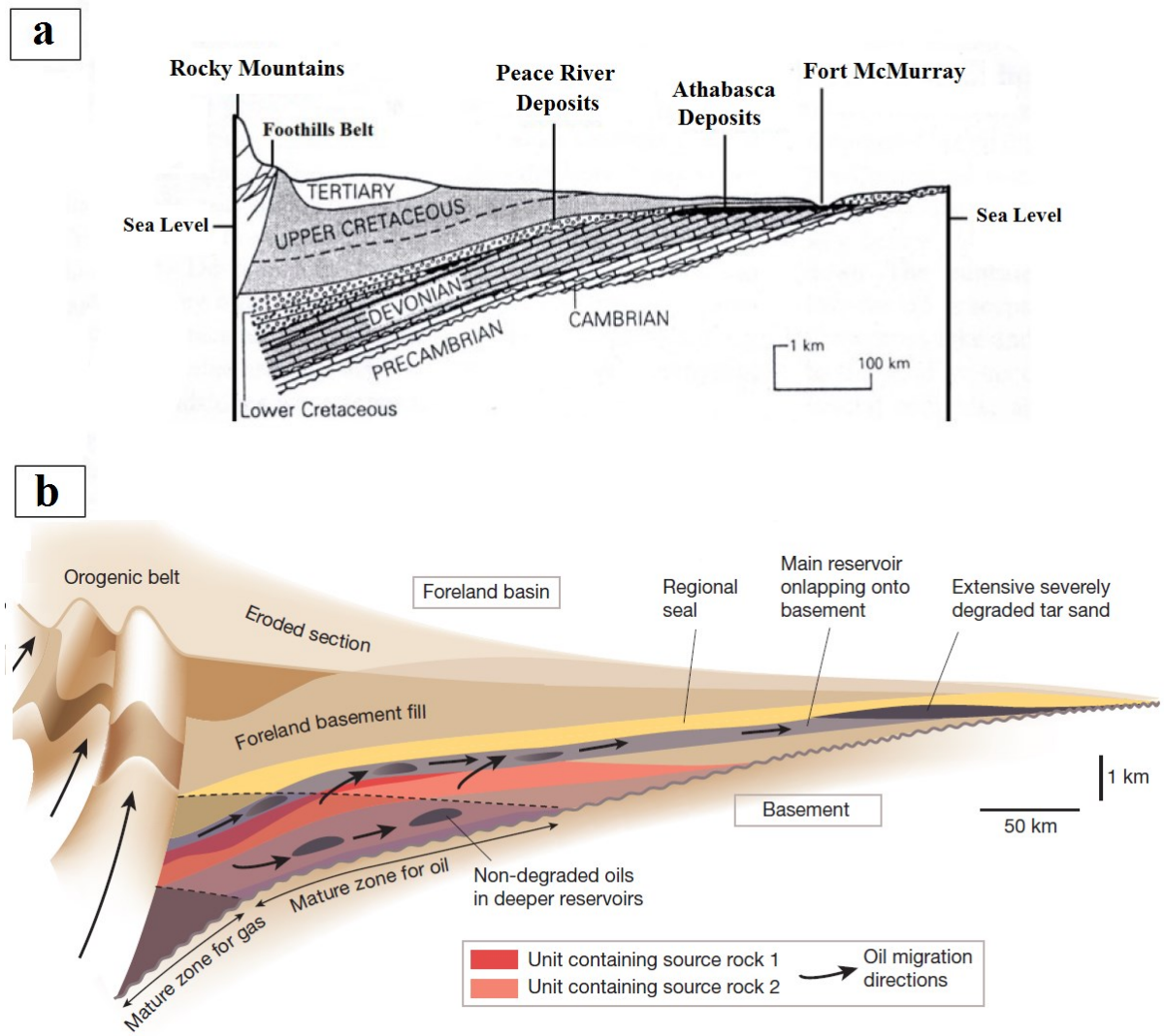

***Figure 1-1**:(a) A profile of relevant locations and geological features of the Alberta Oil Sands Deposits.[2] (b) An illustration of oil migration from the original deep source rocks to near-surface locations. [1] Athabasca oil sands deposits have a migration path that is about 360 km long while that for the Peace River Deposits is about 80 km.[3]*

1.1.2 Reserves and Their Locations

Canada's proven oil reserves, which are almost entirely located in the oil sands in Alberta, are the third largest in the world (**Figure 1-2**).[6] Alberta oil sands are spread out in three different locations: Athabasca, Cold Lake, and Peace River (**Figure 1-3).**[7] To give an appreciation of the size of these reserves, Masliyah et al. suggested that in 2011 the rate of daily oil production could be doubled and the proven reserves would still meet Canada's crude oil demand for over 200 years. Surprisingly, these proven reserves are only a small fraction of the total oil in place: they are a mere 9 % to 10 % of about 1.7 trillion barrels of oil existing in Alberta. To put this in perspective, if the total oil in place could be economically recovered, like the current proven reserves, then the total oil output would be equivalent to the combined output of the entire Middle East. [3]

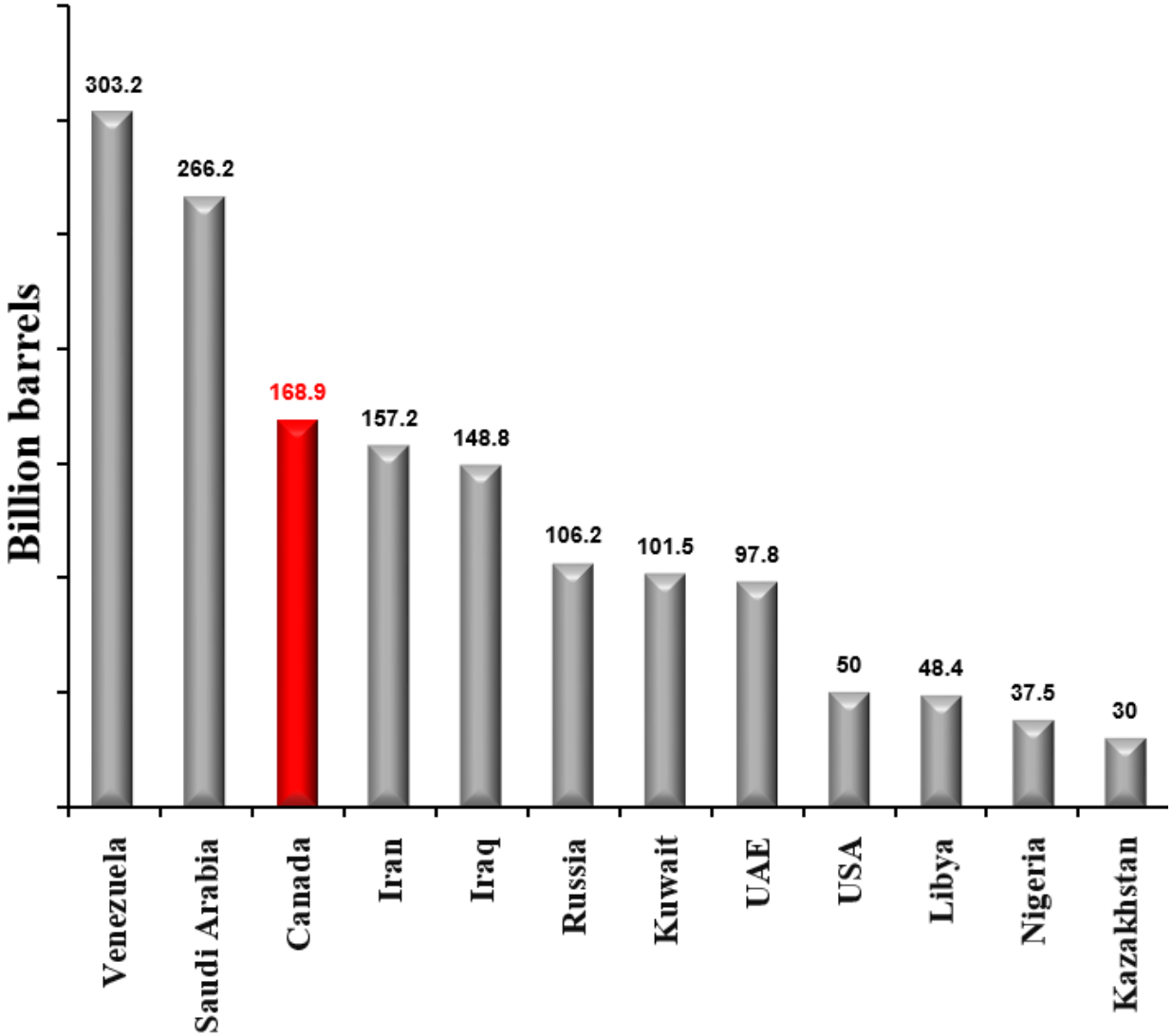

Figure 1-2: *Proven oil reserves.[6]*

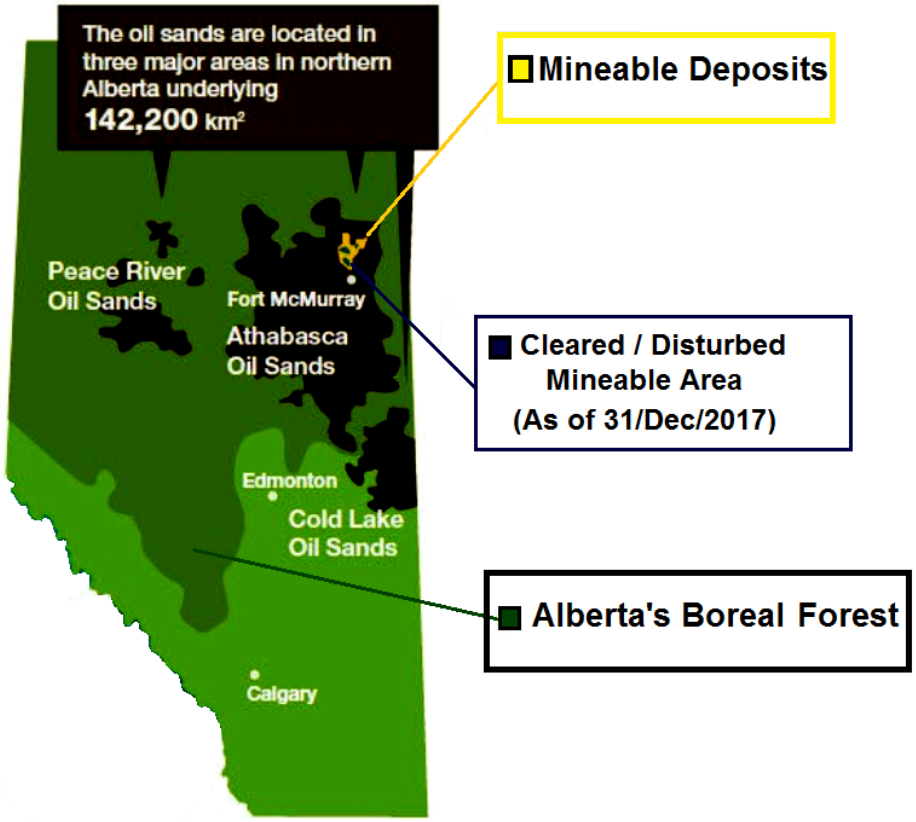

***Figure 1-3**: Oil sands deposits in Alberta.[7]*

1.1.3. Ore Properties and Extraction Methods

1.1.3.1. Properties

Alberta's oil sands are a mixture of solids, water, and bitumen. The solid part forms the bulk of the ore and it is mostly composed of silica sand. The sand is hydrophilic, a unique property of the Alberta's oil sands that is of the utmost importance in water-based bitumen extraction. [3], [8]

The composition of bitumen in Alberta's oil sands varies greatly, even within the same deposit, but the average bitumen content in Athabasca deposits is about 12 wt. %.[9] This composition usually determines the quality of oil sands ore and points to the ores that are more economic to process. The cutoff bitumen content in an oil sands ore that qualifies for economic processability is 7 wt. %.[3] Bitumen is a form of dense petroleum with exceptionally high viscosity (**Figure 1-4**). Athabasca bitumen is estimated to have a viscosity of 300,000 cP, an API gravity of 7.9º and a density of 1015 kg/m^3 at 25 ºC. This viscosity is over 3 orders of magnitude higher than that of light crude oil.[10], [11] Masliyah et al. compared bitumen to cold molasses at room temperature.[8] Unlike conventional oils, bitumen is immobile under reservoir conditions and this

explains why existing extraction methods usually involve heating or diluting bitumen with solvents to lower its viscosity and enhance its recovery.

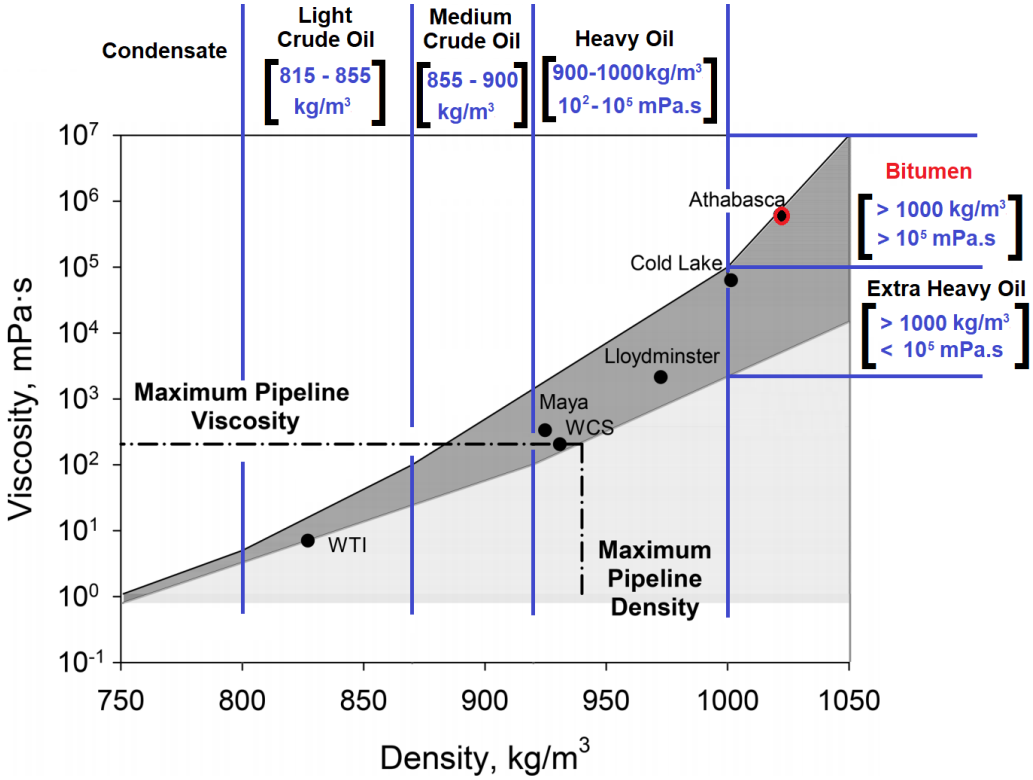

Figure 1-4: *Properties of Athabasca bitumen compared to different types of crude oil.[10]*

The balance of the oil sands ore is water, which can be as low as 0 wt. % in weathered ores and as high as 7 wt. %. The form in which water exists in the ore is a subject of research interest. Previous studies have postulated the existence of a thin water film encapsulating the sand grains.[12]–[14] However, more recent work has shown that this water film hypothesis, although reasonable, lacks empirical basis and is highly unlikely in acidic oil sands ores.[8], [15] The rift notwithstanding, all these studies seem to converge on the hydrophilic nature of mineral solids (sand grains) in the oil sands ore and its utility in bitumen recovery.[3], [8], [15]

1.1.3.2. Surface Mining

Surface mining is a bitumen extraction method that is used for deposits that are near the surface– less than 75 m deep. Currently, the Athabasca deposits are the only ones with deposits shallow enough to allow for surface mining (**Figure 1-3**).[7] These deposits comprise about 20 % of Alberta's oil sands' bitumen reserves. They are estimated to account for almost half of the daily bitumen produced in 2019 (**Figure 1-8**).[16]

The first step in surface mining is to remove the overlaying *muskeg* (water-soaked vegetation or wetlands) and *overburden* (a mixture of clay, silt and sand) to expose the ore for mining. The exposed ore then undergoes a series of stages, as summarized in **Figure 1-5**. This extraction method, which is also known as the Clark hot-water extraction (CHWE) process, uses a significant amount of hot alkaline water to enhance bitumen liberation.[8], [13] Every barrel (~159 litres) of bitumen produced uses about 2.5 m^3 of water and generates about 3.3 m^3 of tailings (**Figure 1-6**).[3] In other words, for every unit volume of bitumen produced, almost 16 times more water is used and over 20 times the unit volume in tailings is generated.

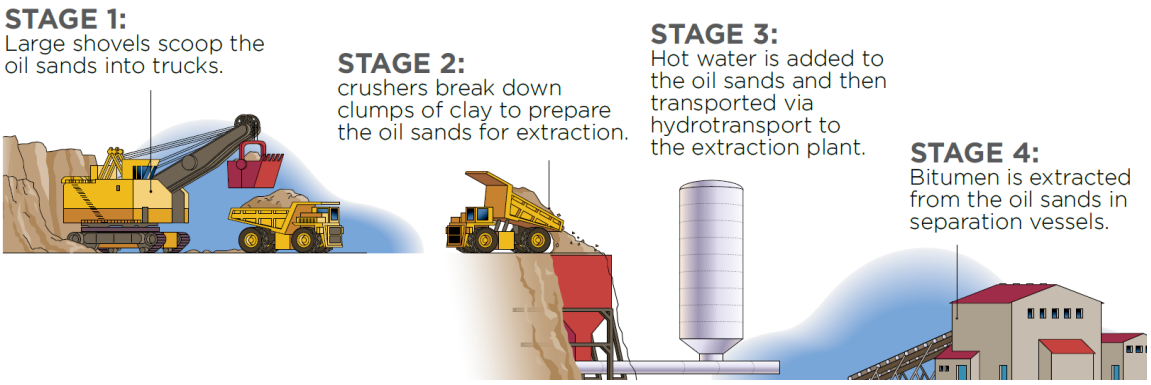

Figure 1-5: *Summary of the main stages in surface mining. [17]*

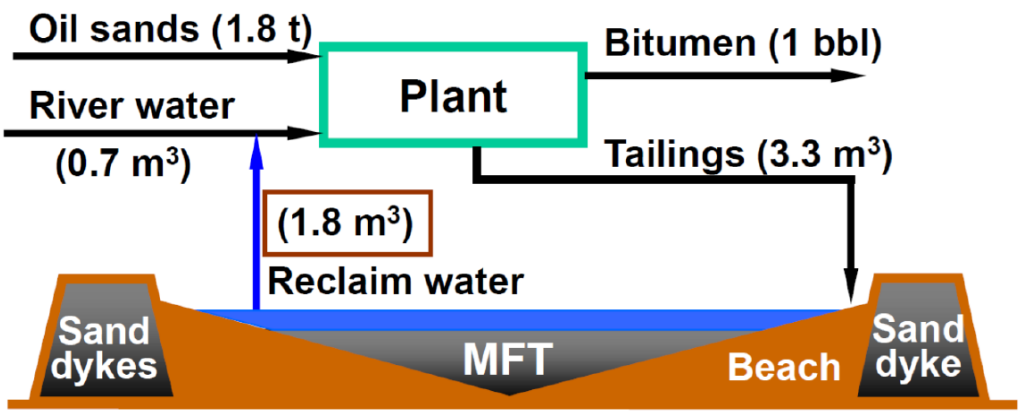

Figure 1-6: *A schematic to show water usage and tailings generation for every barrel of bitumen produced in water-based bitumen extraction. [3]*

1.1.3.3. In Situ Extraction

In situ extraction is a collective term used to describe technologies that are used to extract bitumen *in situ* ("in the original place"), from oil sands deposits that are too deep for surface mining–depths below 200 m. Examples of in situ mining technologies are steam assisted gravity drainage (SAGD), cyclic steam simulation (CSS), toe to heel air injection (THAI) and vapor extraction (VAPEX). These technologies use different approaches to lower the viscosity of bitumen for ease of flow into production wells: SAGD and CSS use steam; THAI uses air for combustion of bitumen in the formation; and VAPEX uses solvents such as vaporized propane.[11] SAGD is the most common among these technologies and its main stages are summarized in **Figure 1-7**.[17] In-situ mining can be used for extraction of about 80% of Alberta's oil sands bitumen reserves. Unlike surface mining, this extraction method does not generate tailings, has minimal land disturbance, and uses significantly less water. However, the use of steam in SAGD makes it an energy intensive technology. This steam generation process usually burns natural gas which in turn leads to higher greenhouse gas (GHG) emissions. It also recovers a comparatively lower amount of bitumen compared to surface mining (**Table 1-1**).

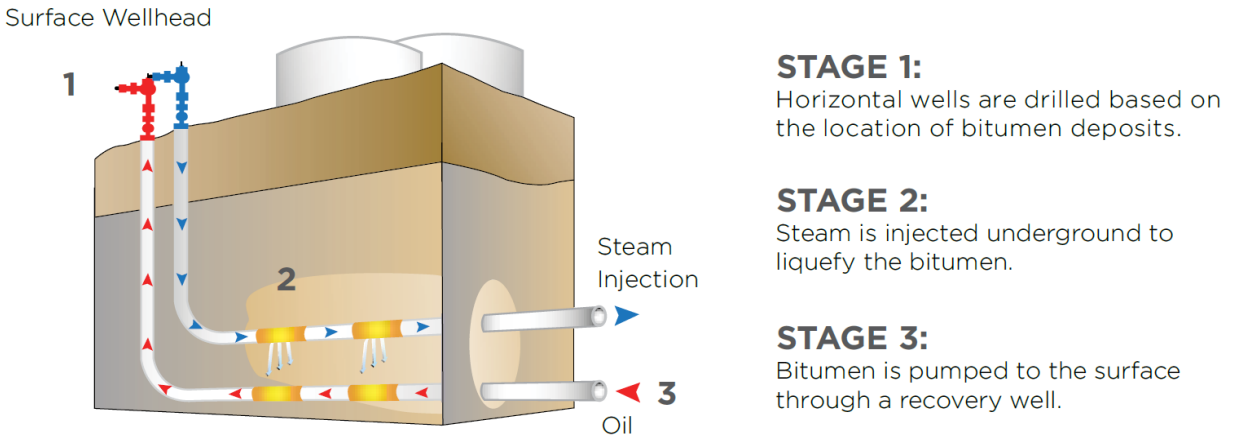

Figure 1-7: *Main stages in SAGD in-situ bitumen extraction. [17]*

The choice of bitumen extraction method is usually determined by the depth of the oil sands ore. If SAGD was used for shallow deposits, for instance, the formation would be too weak and it would most likely result in a steam blow out tragedy. Reversing the roles, if mining was used for deep lying ores, then the cost of removing the muskeg and overburden would be so high that it would offset any economic value from the extracted bitumen. Surface mining, despite being tied to the tailings menace, has several advantages over SAGD. It has a much higher bitumen recovery rate (yield), as shown in **Table 1-1**, lower GHG emissions, higher certainty of bitumen recovery, and it is much easier to stop and start within short notice or in case of an emergency.[18] According

to recent estimates by the Alberta Energy Regulator, surface mining production, though declining, is still projected to produce a significant amount of bitumen: 48.1% of bitumen in 2019 and 43.6% in 2027 (**Figure 1-8**). The Alberta Energy Regulator also expects daily production rates from the oil sands to grow from 2.8 million barrels in 2017 to 3.9 million barrels in 2027.[16] These estimates further underscore the need for research into more efficient and effective ways of treating tailings, especially considering the approximate amount of tailings generated per barrel of bitumen produced (**Figure 1-6**).

Table 1-1: *Comparison of oil recovery yields from various extraction methods [19]*
(Originated from Canadian Centre for Energy).

EXTRACTION METHOD	OIL RECOVERY YIELD
Surface mining	Over 90%
In situ Mining	25-60%
Conventional Heavy Oil	Up to 20%
Conventional Light Oil	Average of 30%

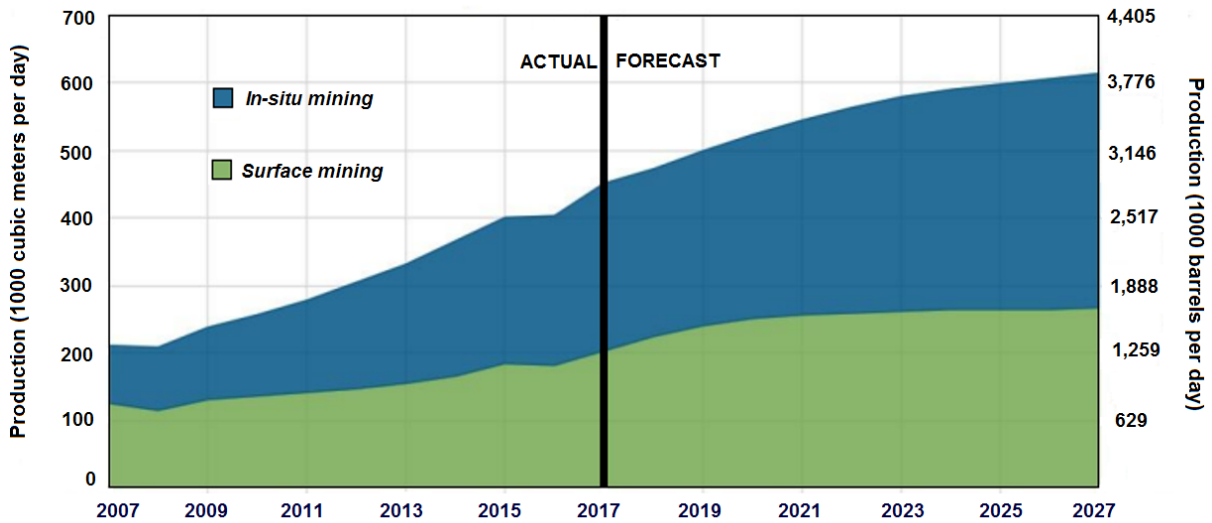

Figure 1-8: *Actual and projected daily bitumen production rates via surface mining and in situ extraction methods. [16]*

1.1.4 Economic Significance and Environmental Concerns.

Alberta is Canada's energy province. According to *Alberta Energy Regulator*, in 2017, about 81 % of Canada's oil and 68 % of Canada's natural gas was from Alberta.[20] The oil sands industry has significant economic impact on both Alberta's and Canada's economies. Based on projections by *Canadian Energy Research Institute* (CERI), provincial and federal government taxes on the oil sands industry for the 2017 to 2027 period will amount to a sum of CAD$256.3 billion. CERI also estimates that oil sands' development between 2017 and 2027 will inject about CAD$1.7 trillion into the Canadian economy and 88 % of the resulting impacts will be felt in Alberta.[21] It is also worth noting that Alberta's oil sands uniquely account for over half of all world oil reserves that are open to the private sector (not state-controlled) and are, therefore, mainly developed by local and international private investors.[22]

The oil sands industry, however, has a significant downside: the environmental pollution resulting from its operations. Top on this list of environmental concerns are tailings generated from water-based extraction of mineable oil sands. Mature tailings or MFT, as mentioned earlier, occupy vast areas of land that needs to be reclaimed. According to *Alberta Environment and Parks Oil Sands Information Portal*, only about 11 % of the total disturbed land has been fully reclaimed since mining began in the 1960s. If untreated, MFT can remain stable for up to 150 years.[23], [24] MFT also contain traces of residual bitumen and toxic organics that are harmful to humans, water birds and aquatic life. Lastly, MFT are predominantly water (up to 70 wt. %), which if effectively recovered, would accelerate the land reclamation process and provide recycled water to help reduce the amount of fresh river water used in water-based bitumen extraction. This research work is focused on tailoring an efficient polymeric flocculant for effective water recovery in tailings remediation.

The other pressing environmental concern is GHG emissions. The *World Resources Institute* places Canada's emissions at almost 2 % of global emissions despite hosting less than 0.5 % of global population. *Environment and Climate Change Canada* estimates that about 10 % of Canada's emissions come from the oil sands.[13] An analysis among provinces and territories shows that Alberta's GHG emissions are the highest in Canada (**Table 1-2**) and as of 2015 almost half of those emissions were from the oil and gas sector (**Figure 1-9**). Technological advancement and process improvements have considerably reduced the amount of emissions per barrel of bitumen produced over the years. However, due to increased production rates in the oil and gas industry, overall emissions from this sector keep rising. Alberta has recorded the highest increase

in the amount of GHG emissions among Canadian provinces for the 2005 to 2017 period. (**Table 1-2**)

A comparison of Alberta's emissions based on extraction methods shows that in situ mining operations emit almost twice as much as surface mining (**Figure 1-9**). As pertains to surface mining, it is worth noting that a fraction of the emissions from this extraction method come from methanogenic oil sands tailings ponds. Methane, the GHG generated from microbial activity (methanogenesis) in these ponds, is multiple times more potent at trapping heat than CO_2, thus, more harmful. [25]–[27] Therefore, this is yet another reason to consider tailings treatment as an exigency.

Table 1-2: *Canada's historical GHG emissions by province and territory*

(Source: Environment and Climate Change Canada, National Inventory Report 1990–2017: Greenhouse Gas Sources and Sinks in Canada, Part 1)

GHG Emissions by Province/Territory, Selected Years

	GHG Emissions (Mt CO_2 eq)[1]								Change (%)
Year	1990	2005	2012	2013	2014	2015	2016	2017	2005–2017
GHG Total (Canada)	602	730	711	722	723	722	708	716	-2.0%
Newfoundland	9.4	9.9	9.4	9.4	10	11	11	11	6.9%
Prince Edward	1.9	2.0	2.1	1.7	1.7	1.7	1.8	1.8	-10%
Nova Scotia	20	23	19	18	16	17	16	16	-33%
New Brunswick	16	20	17	15	14	14	15	14	-28%
Quebec	86	86	80	80	78	78	78	78	-9.8%
Ontario	180	204	169	168	166	165	162	159	-22%
Manitoba	18	20	20	21	21	21	21	22	7.7%
Saskatchewan	44	68	71	73	76	79	76	78	14%
Alberta	173	231	261	271	276	275	264	273	18%
British Columbia	52	63	60	61	60	59	61	62	-1.5%
Yukon	0.5	0.5	0.6	0.6	0.5	0.5	0.5	0.5	-1.3%
NW Territories	NA	1.6	1.5	1.3	1.5	1.7	1.6	1.3	-19%
Nunavut	NA	0.4	0.5	0.7	0.7	0.6	0.6	0.6	33%

NOTES:
1. Totals may not add up due to rounding.
NA = not applicable

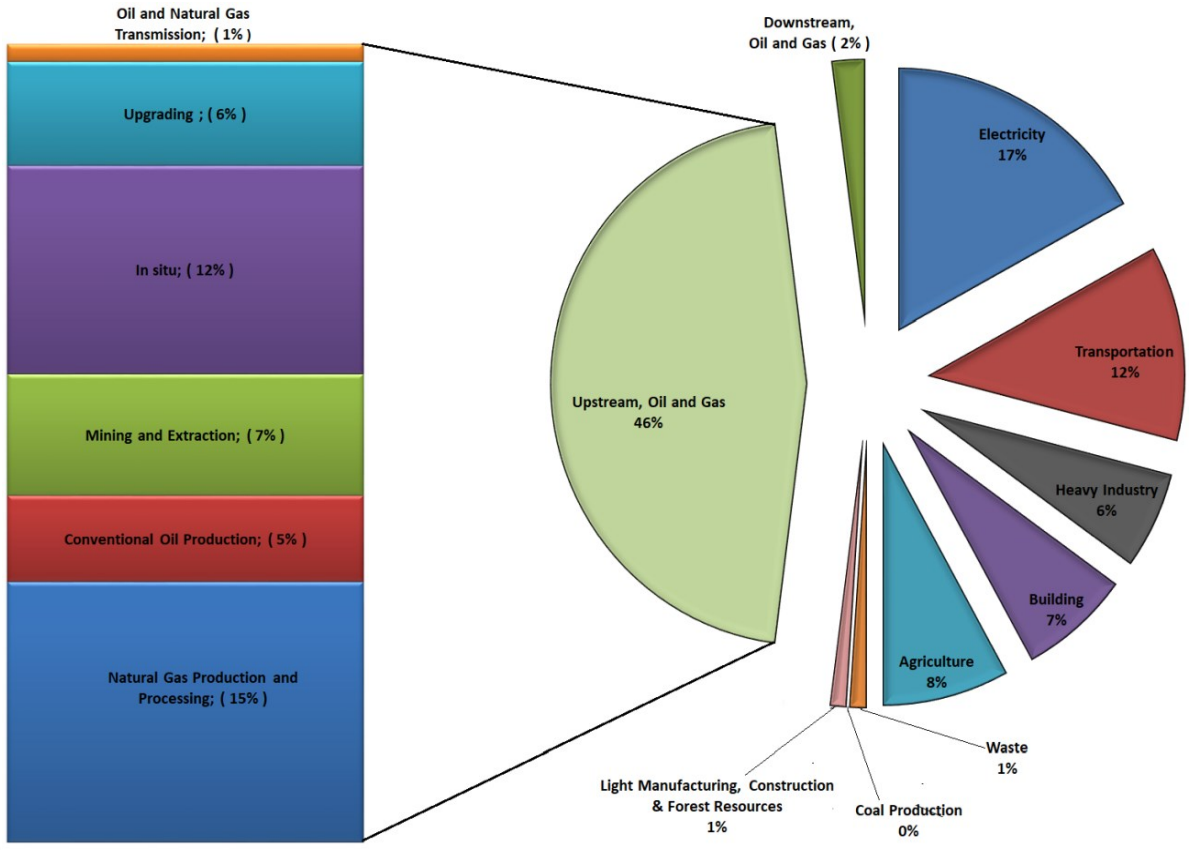

Figure 1-9: *Alberta's GHG emissions from different economic sectors.*

*(**Adapted from** "Investment of Carbon Proceeds into Oil and Gas Production Operations", Canadian Association of Petroleum Producers (CAPP), May 2018. **Originated from** Environment and Climate Change Canada, National Inventory Report 1990–2015: Greenhouse Gas Sources and Sinks in Canada, Part 3, April 13, 2017).*

1.2) Thesis Outline

Chapter 1 is a brief overview of Alberta's oil sands industry, its significance and associated challenges. In particular, it looks at the tailings problem as it relates to bitumen extraction and within the context of Alberta's oil sands industry. The outline of this research work is also highlighted.

Chapter 2 reviews the pertinent technical literature. It revisits surface mining in more detail with particular attention to the science behind relevant conditions used in water-based bitumen extraction. This chapter discusses how efforts to enhance optimal extraction conditions negatively affect tailings treatment. A comprehensive overview looks at common oil sands clay minerals and their relevant properties in relation to tailings treatment. A section of chapter 2 is dedicated to the concepts of coagulation and flocculation as used in tailings treatment, and their practical significance. The role of polymer flocculants, particularly hydrophobically modified flocculants, in tailings dewatering is discussed. At the same time, a case is made for the proposed hydrophobic modification, HPMA. Lastly, emulsion polymerization is reviewed in detail and a justification is given for the use of this technique to synthesize PMA.

Chapter 3 discusses laboratory synthesis of PMA using emulsion polymerization and subsequent base hydrolysis to HPMA. Characterization techniques used are also discussed in this chapter.

Chapter 4 discusses the statistical models and flocculation tests performed using different grades of our proposed novel polymer flocculant on both diluted and undiluted MFT.

Chapter 5 summarizes and discusses the main results of this thesis and makes recommendations for future work.

2) Literature Review

2.1) Oil Sands Tailings and Clay Minerals

2.2.1 Hot Water Extraction and Oil Sands Tailings.

Tailings are not unique to oil sands bitumen extraction. They are common in mineral processing and generally described as the unwanted by-product at the tail-end of most mineral recovery processes. In the global mining industry, millions of tonnes of tailings are annually added to the billions of tonnes already existing. The conventional approach to store these tailings involves impoundment in large artificially engineered structures called tailing dams or ponds. This approach is not only able to contain the high capacity of tailings generated but it also offers comparatively low maintenance and operating costs.[28] In the year 2000, based on consultations with regulatory officials and a detailed literature review, the number of tailing dams from different mineral extraction processes worldwide was estimated to be slightly over 3500.[29] Alberta's oil sands tailings ponds have features that have much in common with those from the mineral processing tailings.

Oil sands tailings are the undesired waste residue at the tail-end of Clark hot water extraction (CHWE) of mineable oil sands. CHWE is a water-based bitumen extraction method developed by Karl Clark in the 1920s, commercialized in the 1960s and modified over time. It uses hot/warm water, a caustic additive and air bubbles to optimize bitumen recovery in mineable deposits. Bitumen recovery in CHWE can be dived into two main steps, bitumen liberation and bitumen aeration (**Figure 2-1**). [3], [8], [12], [13]

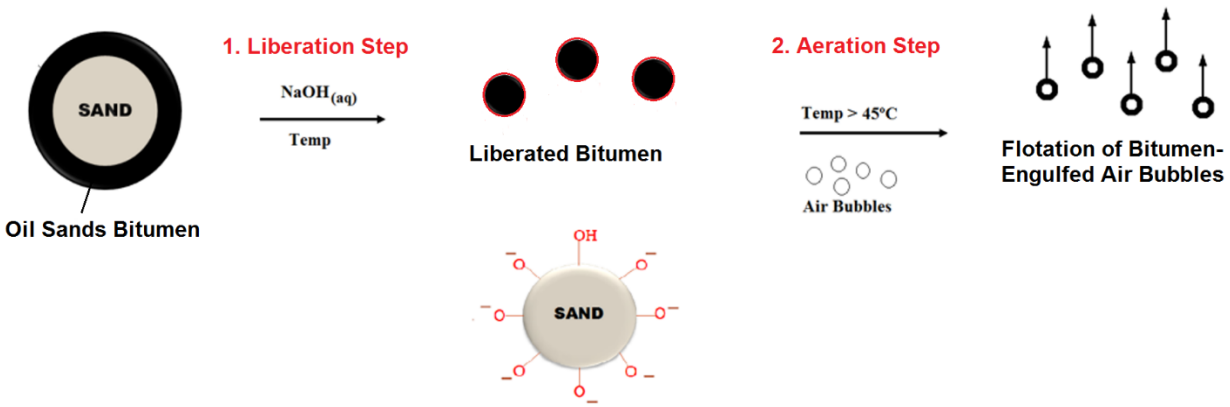

***Figure 2-1**: Simplified illustration of the key steps in CHWE bitumen recovery.*

In CHWE, bitumen liberation is the separation of bitumen from mineral sand grains during bitumen recovery. This water-based detachment of bitumen droplets from the sand grains can be viewed as the replacement of the initial bitumen-sand interface with two new interfaces: the sand-

water and bitumen-water interfaces. This interfacial change can be expressed using an equation that describes the free energy density (J/m^2) associated with the process,[3]

$$\Delta G_{Liberation} = \gamma_{S/W} + \gamma_{B/W} - \gamma_{B/S} \qquad \textbf{(2-1)}$$

Equation **(2-1)**, however, is not practical since the bitumen-sand ($\gamma_{B/S}$) and sand-water ($\gamma_{S/W}$) interfacial tensions are hard to quantify. A simplified and more useful equation that uses the directly measurable bitumen-water interfacial tension ($\gamma_{B/W}$), is obtained by substituting into it the *Young's equation* (Equation **(2-2)**). Equation **(2-3)** is not only easier to quantify experimentally, but it also gives useful thermodynamics information. Based on this equation, the interfacial free energy of bitumen liberation is inherently positive, since $\gamma_{B/W}$ is always positive and sand is not completely wettable (Θ>0). Thus, under normal conditions, bitumen liberation is thermodynamically unfavorable and requires external influence to drive the process.[3]

$$Cos\ \theta = \frac{\gamma_{B/S} - \gamma_{S/W}}{\gamma_{B/W}} \qquad \textbf{(2-2)}$$

*(Where Θ is the contact angle shown on **Figure 2-2**)*

$$\Delta G_{Liberation} = \gamma_{B/W}(1 - Cos\ \theta) \geq 0 \qquad \textbf{(2-3)}$$

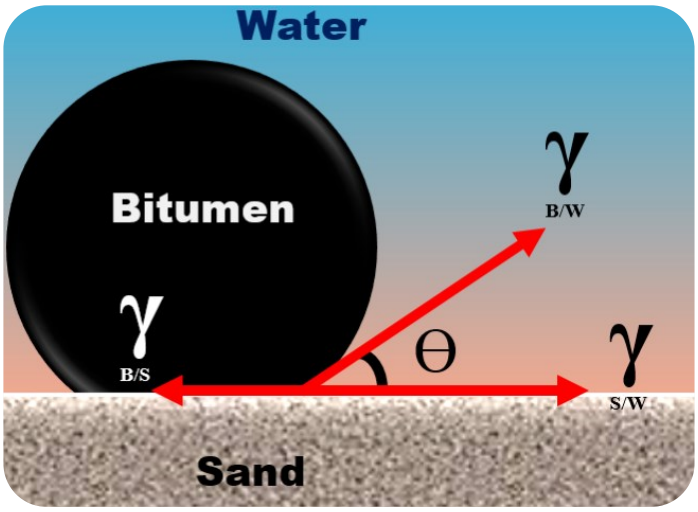

Figure 2-2: *Interfacial interactions between bitumen, sand and water during liberation. Equation 2-2 (Young's equation) offers a mathematical relationship between interfacial tensions from the three phases and their contact angle(Θ).*

One of the innovative approaches used to enable bitumen liberation involves using caustic additives to modify interfacial properties of the system via the hydrolysis of surface active functional groups found in bitumen.[3] For instance, base hydrolysis of naphthenic acids in

bitumen (**Figure 2-3.A**).[30] A fraction (about 2%) of the hydrolyzed naphthenic acids with shorter chains (13-18 carbon atoms) become soluble in water and are released as natural surfactants.[8] These natural surfactants accumulate at the bitumen-water interface and lower the interfacial tension ($\gamma_{B/W}$). According to Equation **(2-2)** and **(2-3)**, lowering $\gamma_{B/W}$ increases cosΘ and decreases the positive free energy associated with bitumen liberation, thus increasing the likelihood of bitumen detachment from the sand grains. The alkaline slurry also hydrolyzes and charges the sand surface (**Figure 2-3.B**) increasing its wettability and decreasing the contact angle (Θ)(increasing cosΘ, see Equation **(2-2)**). And, in this way, it also contributes to lowering the bitumen-liberation free energy (Equation **(2-3)**). A study by Ren et al. on hydrophobic mineral solids that are found in weathered (dehydrated) ores further emphasized the critical role of hydrophilic sand surfaces in bitumen liberation.[31] In addition to engineering interfacial properties, mechanical agitation and high slurry temperature are among other external influences that create conducive hydrodynamic conditions to enable the thermodynamically unfavourable bitumen liberation process. [3], [8]

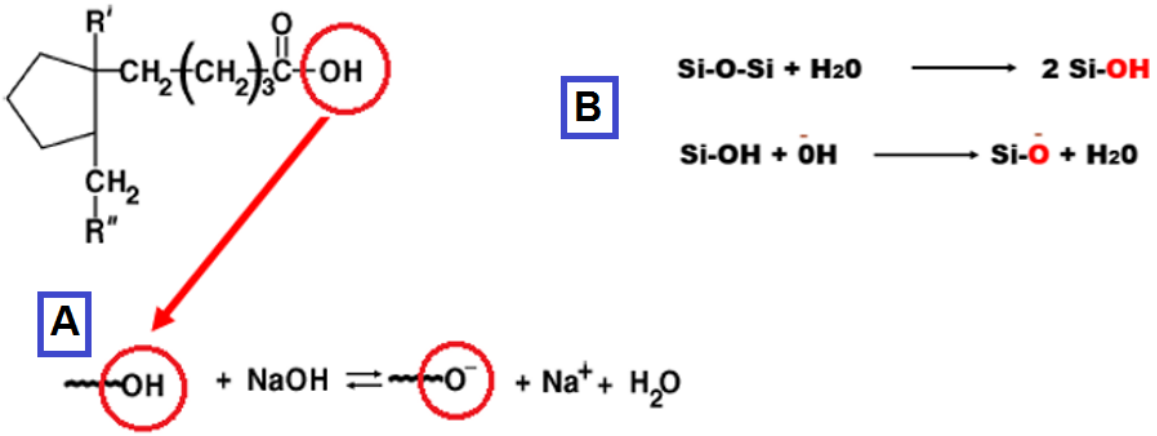

Figure 2-3: *Key chemical reactions associated with caustic additives in CHWE: (A) base hydrolysis of naphthenic acid (simplified chemical structure) [30]; and (B) base hydrolysis of (silaceous) sand surfaces.[3]*

Bitumen aeration, the second step in bitumen recovery, involves attachment (or engulfment) of the liberated bitumen droplets to (or onto) air bubbles. This lowers the bitumen density, increases its buoyancy and allows the resulting bitumen froth to float to the top of the separation vessel for recovery. In absence of aeration, separation would be difficult since liberated bitumen droplets would remain suspended in the slurry due to their high density, which is almost similar to water density, thus, resulting in a poor bitumen yield. The aeration process may also be described as the formation of new bitumen-air interfaces at the expense of the existing bitumen-water and air-water interfaces. The free energy density associated with creation of this new interface is expressed as

follows, [3], [32]

$$\Delta G_{Aeration} = \gamma_{B/A} - \gamma_{B/W} - \gamma_{A/W} \quad \textbf{(2-4)}$$

$$Cos\ \theta = \frac{\gamma_{B/A} - \gamma_{B/W}}{\gamma_{A/W}} \quad \textbf{(2-5)}$$

*(Where Θ is the contact angle shown on **Figure 2-4**)*

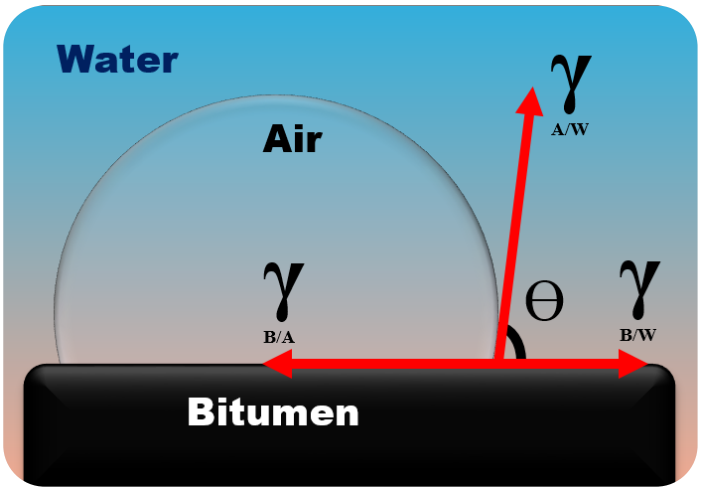

Figure 2-4: *Interfacial interactions between air, bitumen and water phases characteristic of the bitumen aeration process.*

Equation **(2-4)** can be simplified further by inserting the Young's equation (Equation **(2-5)**) to obtain,

$$\Delta G_{Aeration} = \gamma_{A/W}(Cos\ \theta - 1) \quad \textbf{(2-6)}$$

This simplified equation shows that for any contact angle greater than zero, the free energy of aeration is negative. Thus, aeration, unlike bitumen liberation, is a spontaneous process that is thermodynamically stable. This is no surprise since air and bitumen are hydrophobic and their affinity to each other is spontaneous. However, under the alkaline conditions in CHWE, both air and bitumen obtain negative surface charges, which compromises their natural affinity. High slurry pH, although useful for bitumen liberation, tends to be detrimental to bitumen aeration. Under high alkaline conditions, natural surfactants are released onto the bitumen-water interface and further

into the bulk slurry. This lowers bitumen-water and air-water interfacial tensions which results in a smaller contact angle and a lower negative Gibbs free energy of aeration which, in turn, lowers the degree of spontaneity or the ease of bitumen aeration. The optimum pH that favors both liberation and aeration depends on the type of oil sands ore and is within the range of 8.0 to 9.0. In addition, sodium ions present in the caustic additive help to disperse fine solids in order to avert slime coating, optimize flotation and consequently improve bitumen recovery.

In mining, bitumen recovery and tailings management are inextricably linked, and, unfortunately, the optimum conditions for extraction have deleterious effects on tailings treatment. The alkaline slurry pH and high dispersion of sodium treated fine solids (mostly clays) are desired for bitumen recovery but unwanted in tailings treatment, as we shall discuss in the next section. [3], [8]

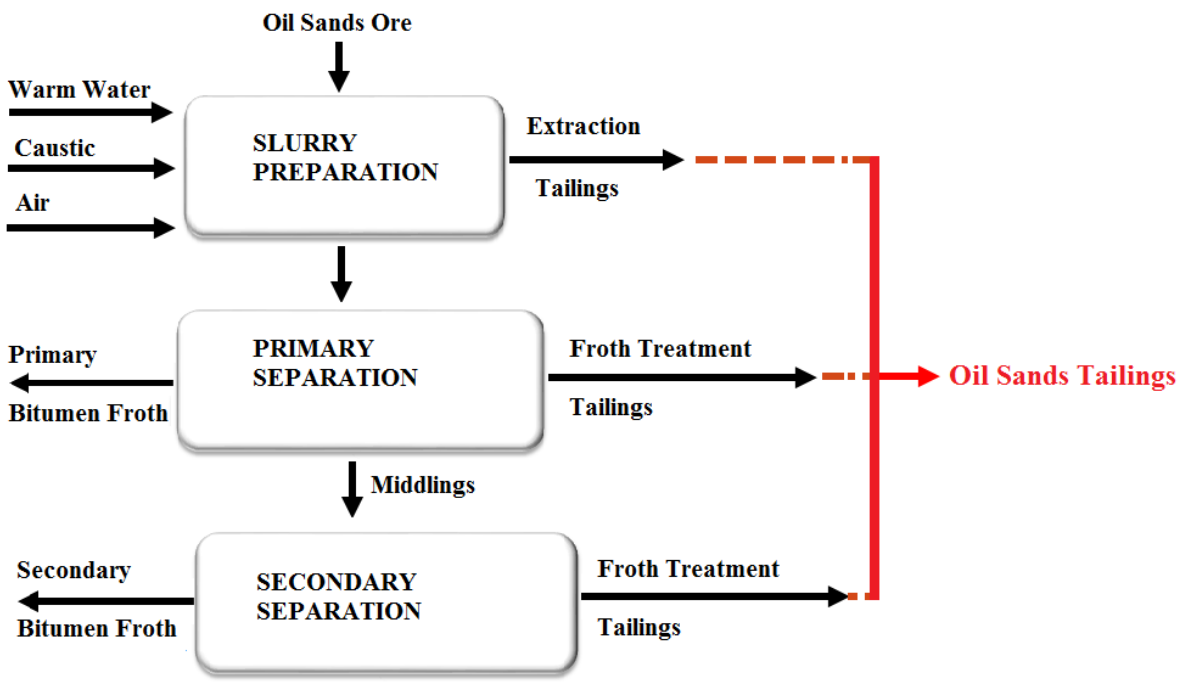

Figure 2-5: *Simplified schematic of the main process streams that generate tailings during CHWE.(Adapted from [33])*

In the course of the CHWE, oil sands tailings are generated from various process streams, as shown in (**Figure 2-5**). These tailings are then impounded in tailing ponds that are surrounded by dykes (sand embankments with high shear strength) for structural integrity. Oil sands tailing ponds occupy massive land areas. Estimates done by the end of 2016 show that these ponds, including associated structures (such as dykes), covered about 257 km^2.[34] The fresh tailings released in these ponds/dams are usually laden with coarse solids that settle fast and often form beaches. The smaller fines remain suspended, with extremely slow settling rates, making it difficult to recover

water and reclaim the pond land.

Over the years, several terms have been used to differentiate oil sands tailings. Thin fine tailings (TFT) refer to oil sand tailings with a nominal solids content that is above 15 % but below 30 %. Mature fine tailings (MFT) is used to refer to oil sands tailings that have been unattended in a pond for several years and have attained a steady nominal solids content that is usually above 30 % and a sands to fines ratio (SFR) that is less than 0.3. Fluid fine tailings (FFT) has a more inclusive definition and it refers to oil sands tailings with nominal solids content greater than 2 wt. % but whose solids content is still less than the required content to reach the *liquid limit* or the *liquid-solid* transition boundary shown on **Figure 2-6A**.[33], [35] The *unified tailings classification chart* (**Figure 2-6B**) represents a more recent (2013) and comprehensive approach of oil sands tailings classification that is based on detailed tailings composition. As shown on **Figure 2-6B**, FFT (highlighted in red) encompasses among others MFT (indicated in blue). Ideally, tailings treatment and initial dewatering should produce a product that is within the non-segregating and pumpable boundaries shown on the ternary plots below (**Figure 2-6A and B**). [33], [35]–[38]

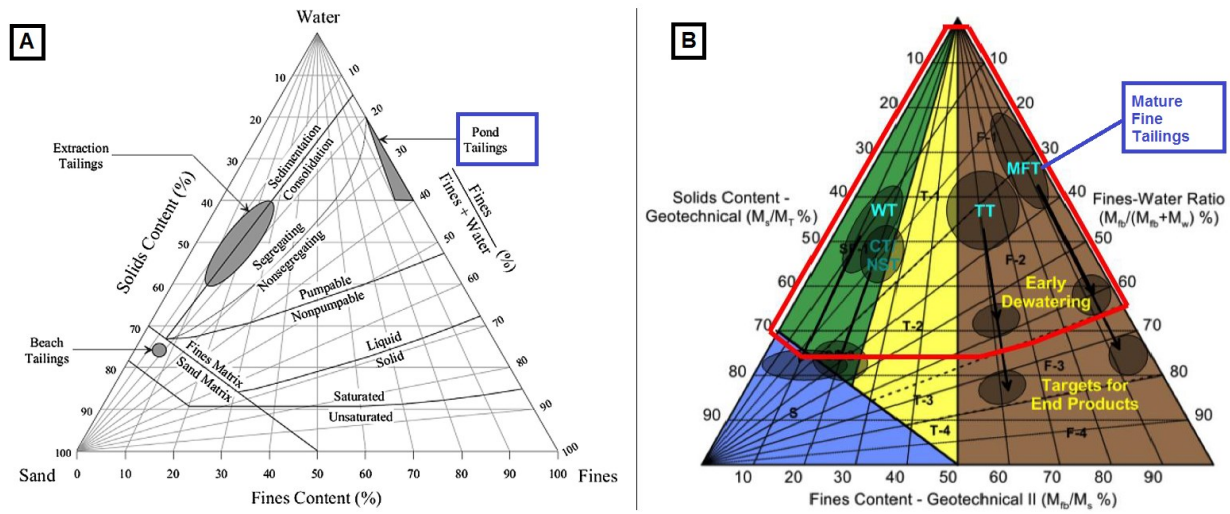

Figure 2-6: *(A) An oil sands ternary diagram showing important boundaries useful for engineering applications.[37] (B) A ternary plot based on Unified Oil Sands Tailings Classification System showing 4 main color partitions based on composition.[39]*

2.2.2 Properties of Clay Minerals in MFT

In MFT, fine solids (particle size<44µm) typically constitute more than 95 wt. % of the solids content and majority of these mineral solids are clays. Clays profoundly affect MFT properties that have important implications in tailings treatment. These minerals are associated with the slow consolidation and high water retention that is characteristic of MFT..[40]–[42] Studying clays in MFT is difficult, but necessary since they comprise a heterogeneous mixture with complex chemistry possessing anisotropic charge distribution, often containing organic materials. This section is not intended to be an exhaustive treatise on clay minerals, but rather a concise overview of key relevant properties of oil sands' clay minerals. Understanding these properties is important for effective MFT treatment.

Kaolinite, illite, chlorite, smectite (montmorillonite), and mixed-layer clays, like illite-smectite and kaolinite-smectite, are the common types of clays in Alberta's oil sands deposits. Their building blocks are siliceous tetrahedral sheets (symbolized as T) and aluminous octahedral sheets (symbolized as O). These structural units are layered differently within the structure of different types of clays. Kaolinites are two-layered with the tetrahedral sheet covalently bonded to the octahedral sheet. These two sheets form a unit layer (a 1:1 layer) which is strongly bound to other unit layers by a series of hydrogen bonds, making kaolinites difficult to delaminate. The compact nature of kaolinite clays explains why they do not swell in water. Kaolinite's structural arrangement as described above can be symbolized as -TO- and is represented on **Figure 2-7**. Illite, chlorite and smectite are three-layered clays, with their unit layers composed of an octahedral sheet sandwiched between two tetrahedral sheets - a 2:1 layer represented as–TOT- (**Figure 2-8**). In Athabasca deposits (McMurray formation), the clay composition of the ore consists of 40-70 wt. % kaolinite, 28-45 wt. % Illite and 1-15 wt. % montmorillonite. MFT suspensions contain the same clay types as the ores, albeit in varying compositions. It is also worth noting that the clay composition in MFT tend to be depth-dependent and can change over time, as different clays settle at different rates.[3], [9], [41], [43]

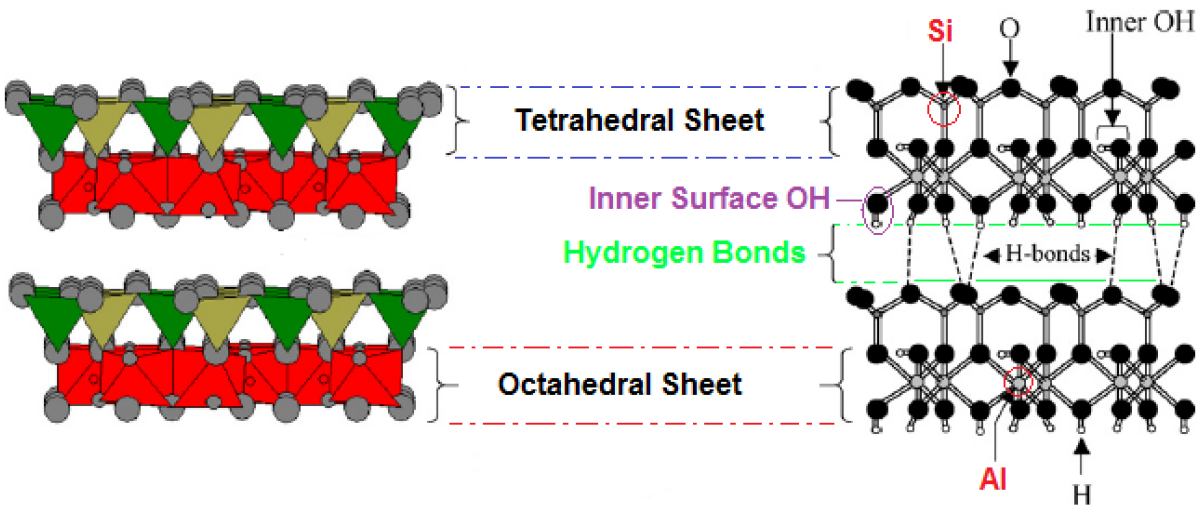

Figure 2-7: *A 1:1 or -TO- structure that is characteristic of kaolinite clays. [44]*

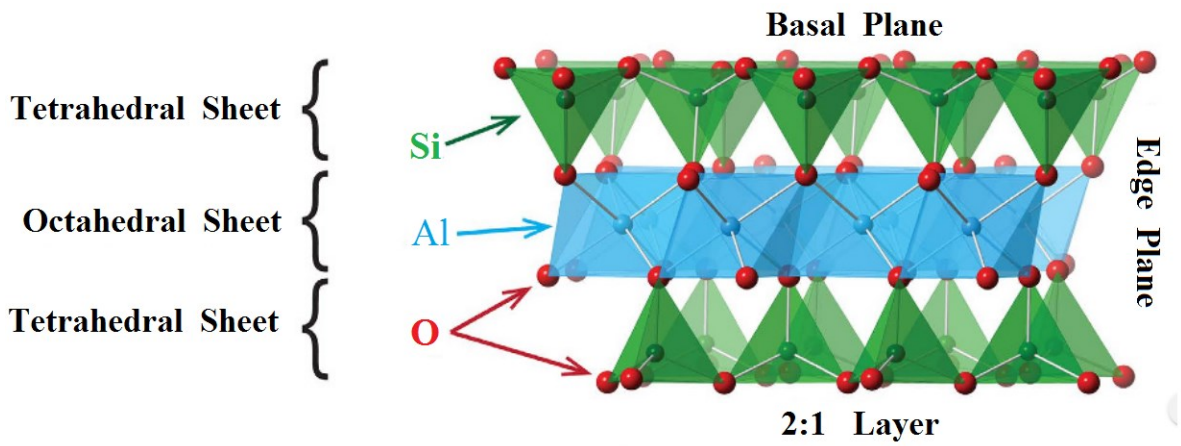

Figure 2-8: *A 2:1 or –TOT- structure found in illite and smectite clays. [45]*

Table 2-1: *Important properties of typical oil sands' clays. [3]*

Clay Type:	Kaolinite	Illite	Chlorite	Montmorillonite
Isomorphic Substitution:	Low in T-Sheet	High in T-Sheet	High in both T- and O-Sheets	
SSA, m^2/g :	10 - 20	65 - 100	42	700 - 840 (Total)
CEC, meq/100g :	3 - 5	10 - 40	10 - 40	80 - 150

Surface charge is responsible for the electrostatic stability of clays, high water retention, and ultimately poor dewatering and consolidation of MFT. One common source of clay surface charge (especially on the basal planes) is isomorphic substitution, or the replacement of higher valence cations by similar-sized low valence cations within imperfect clay crystal lattices. This substitution leads to a net charge deficiency and permanent negative charges. Cations attracted to balance these

permanent charges are referred to as interstitial compensating ions. Cation exchange capacity (CEC) quantifies clay permanent charge by measuring the amount of compensating cations that are available for exchange when the clay is in an aqueous media. The degree to which isomorphic substitution contributes to the overall surface charge varies significantly in different clay types. In smectite clays, for instance, this substitution occurs in both the octahedral and tetrahedral sheets (**Table 2-1**). In smectite clays, particularly, substitution in the O-sheet results in delocalized permanent charges since the compensating cations are unable to access the shielded (sandwiched) O-sheet. As a result, delocalized permanent charges sit on the T-sheets. A phenomenon that weakens the interlayer binding, leading to easy delamination and exposure of the interlayer cations to hydration when the clay is an aqueous medium. This explains the characteristic swelling that is observed in smectite clays, such as montmorillonite, when placed in water. This delamination is also responsible for the exceptionally high specific surface area (SSA) of smectite clays which in total can be as high as 840 m^2/g (**Table 2-1**). High SSA correlates with high water holding capacity and subsequent difficulty in water removal. **Table 2-2** shows the significance of total surface area in relation to the water holding capacity. Generally, clay minerals account for up to 96 % of the water holding capacity in fluid fine tailings (FFT). Due to its high SSA, less than 4 wt. % of montmorillonite can hold up to 19 wt. % water, which is a disproportionately high water-holding capacity compared to other mineral solids. In comparison, kaolinite clays, which are more compact, usually have a much lower SSA and a comparatively low water holding capacity. So, though often present in trace amounts in MFT, smectite and mixed-layer smectite clays possess unique properties that have a predominantly negative effect on tailings treatment. Illite clays have a comparatively low isomorphic substitution which is confined to the T-sheets. Chlorites, despite sharing the same isomorphic substitution with smectites, do not swelling in aqueous solutions due to the presence of a structurally strong octahedral brucite layer that helps counterbalance the permanent charges. As a result, chlorites' delamination and specific surface area are all comparatively low (**Table 2-1**). [3], [5], [42] Clay charges on the edges of clay minerals are usually not derived from isomorphic substitution. They are pH-dependent and change with slurry pH. The surface groups responsible for these charges are protonated to a positive charge at low pH, transition to neutral at a pH corresponding to PZC (point of zero charge) and are negative due to deprotonation in alkaline pH. Kaolinite clays, for instance, have relatively low isomorphic substitution and the overall surface charge is predominantly pH –dependent.[3]

Table 2-2: Water-holding capacity as a function of change in particle size. [42]

Diameter of Sphere, (μm)	Total Surface Area in $1m^3$ of Particles	Volume of Surface Bound Water at 1 μm water layer thickness (m^3)	Wt. % of Bound Water (Solids density $=2650kg/m^3$)
44	$1x10^5$	0.133	5
20	$3x10^5$	0.300	10
10	$6x10^5$	0.600	18
5	$1x10^6$	1.200	31
2	$3x10^6$	3.000	53

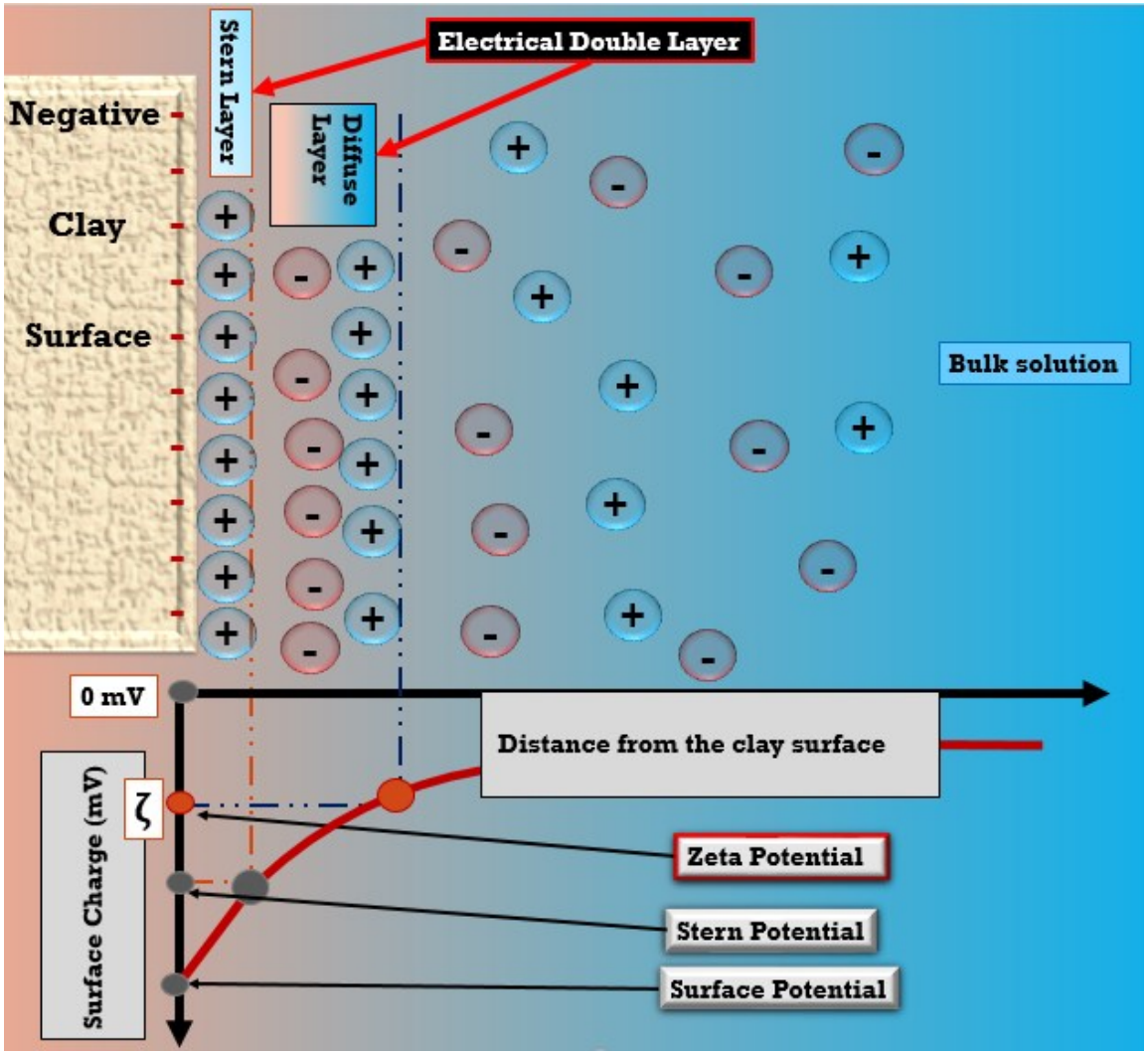

Figure 2-9: *A schematic representation of the electrical double layer on the surface of a dispersed and negatively charged clay particle. Associated electrokinetic potentials are also shown.*

Zeta potential measurements are the most reliable way to empirically quantify the magnitude of surface charge on charged colloidal particles. When a charged particle is dispersed in a fluid medium, two layers of counter ions are formed at the interface. The first layer is firmly adsorbed on the particle surface and it is called the Stern layer. The second layer of ions, which is less loosely anchored, is called the diffuse layer. The Stern layer and the diffuse layer, travel along with the particle in the dispersing fluid/medium and they are referred to as the electrical double layer (EDL). Zeta potential is the electric potential at the boundary of this double layer (at the slipping plane) relative to a point in the continuous phase (in the bulk fluid) (**Figure 2-9**). Zeta potential values range from -100mV to +100mV and particles that are less than -30mV in charge or greater than +30mV tend to form stable colloidal systems. For instance, at a pH range of 8-9 (typical range in oil sands tailings) pure kaolinite, illite and smectite clays treated with sodium possess surface charges that are about -40mv (less than -30mV) (**Figure 2-10a**). And as expected the resulting colloidal dispersion of these highly charged clays was quite high (~ 90% dispersion) (**Figure 2-10b**). These sodium treated pure clays offer useful insight on the interplay between pH, clay surface charges and electrostatic stability, a phenomenon that we would also expect in MFT clays that are obtained from sodium hydroxide treated oil sands ores. [33], [46], [47]

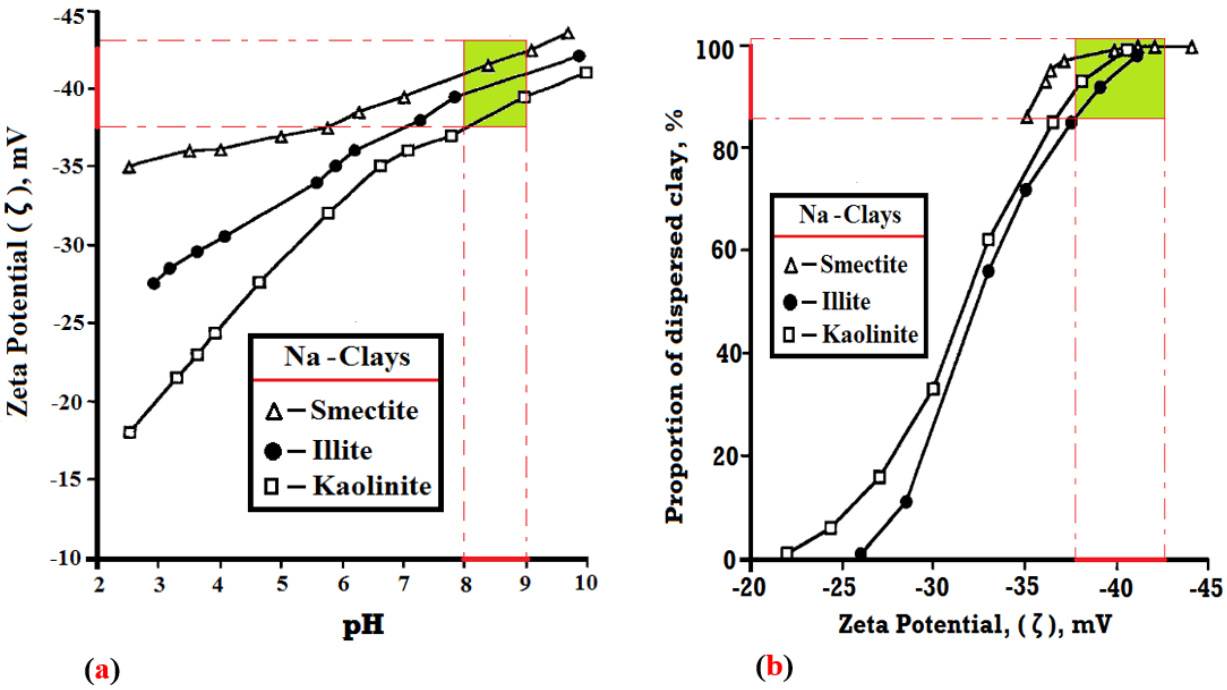

Figure 2-10: *(a) Surface charge of different sodium-treated clay minerals at various pH values. ; (b) A plot showing the degree of dispersion of different clay types as a function of their surface charges. [33], [47]*

Derjaguin-Landau-Verwey-Overbeek (DLVO) theory is a classical theory that considers the effect of repulsive coulombic (electrostatic) forces and attractive van der Waals forces at each

interacting distance to determine colloidal stability (**Figure 2-11**). This theory tends to be reliably accurate in predicting the stability of simple colloidal systems with relatively uniform charge properties and is widely used in nanoscience. MFT suspensions, however, form a complex colloidal system with an array of interaction forces; thus, the DLVO theory in its original form cannot predict MFT colloidal stability. Nonetheless, an understanding of the DLVO theory can further underscore the significance of particle surface charges on colloidal stability. According to the DLVO theory, when the repulsive forces are the dominant contributor to the net interaction energy, then the colloidal system remains stable. In tailings, as charged fine particles (mostly clays) approach each other their double layers overlap, resulting in a repulsive barrier that prevents aggregation and ultimately manifests as strong electrostatic stability of these solids in MFT. [3], [48], [49]

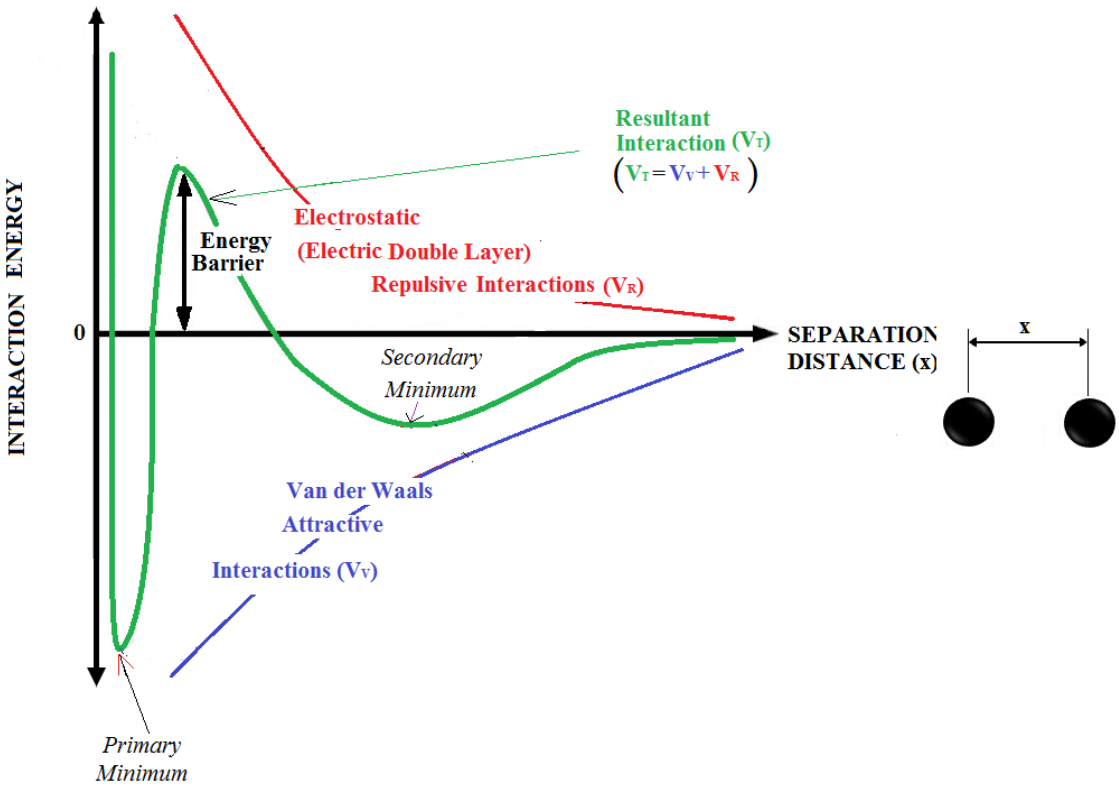

Figure 2-11: *An illustration of the interaction forces as described by the DLVO colloidal stability theory.*

Hydraulic conductivity, K, is another clay property that is often studied in geotechnical engineering, but it also has important implications in tailings management. The hydraulic conductivity of a material is a measure of how fast a fluid can flow through its pores (voids) in relation to the fluid's pressure. A low hydraulic conductivity, therefore, reflects poor water/fluid release. Clays, unlike other soil-types, possess this fluid sealing property which is of practical use in various fields like in the lining of hazardous waste landfills. However, in tailings treatment, low

hydraulic conductivities impede water recovery and subsequent consolidation and are therefore highly undesired. The inverse correlation between clay content and hydraulic conductivity is already well established (**Table 2-3**). In oil sands tailings, clays contribute to the poor water-release of MFT that is characterized by low hydraulic conductivities in the range of 1×10^{-4} to 1×10^{-7} cm/s. [5], [42], [50]–[52] Tavenas et al. showed that soils with a high clay content possess a much lower hydraulic conductivity regardless of their void ratio (**Figure 2-12B**).[5], [53]

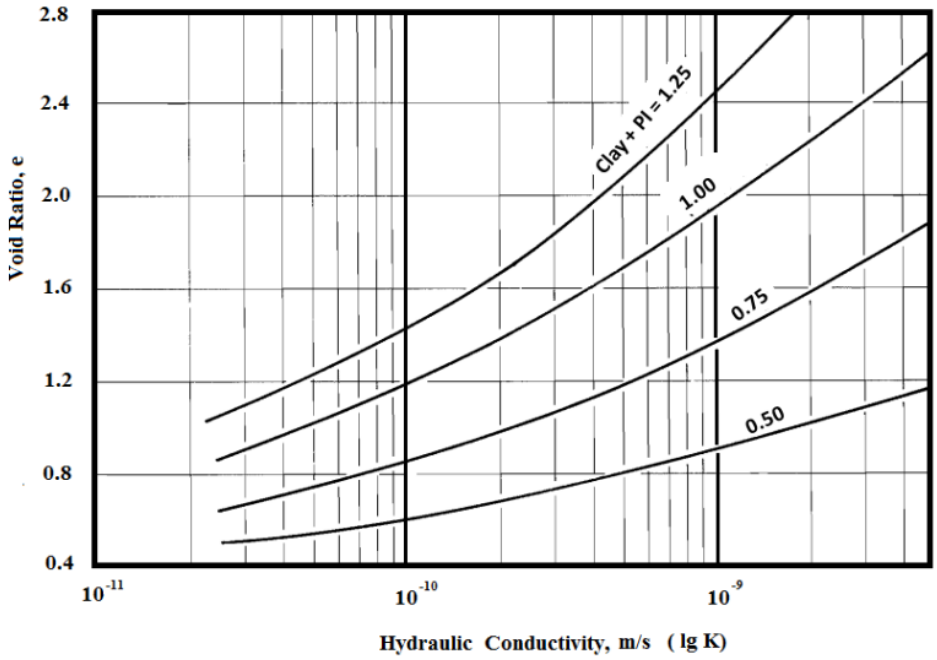

Figure 2-12: *The relationship between void ratio and hydraulic conductivity for soils with varying clay content (and plasticity index-PI). [5], [53]*

Table 2-3: *A comparison of typical hydraulic conductivities of different saturated soil types.*[51], [55]

SOIL TYPE	HYDRAULIC CONDUCTIVITY, *K* (cm/sec)
Clean Gravel	100 – 1.0
Coarse Sand	1.0 - 0.01
Fine Sand	0.01 - 0.001
Silty Sand	0.001 - 0.00001
Clay	< 0.000001

2.2) Coagulation and Flocculation.

Coagulation and flocculation are common terms in tailings, water and wastewater treatment. They are at times used interchangeably. At other times, often in colloid science where the electrical double layer and the DLVO theory are used as the points of reference, coagulation is defined as the irreversible aggregation of colloidal particles in the primary minimum, while flocculation as the reversible aggregation of particles that interact at a range that is no closer than the secondary minimum (**Figure 2-11**). We will briefly explain the use of these two terms as used in the context of this work and as commonly used in water-treatment and mineral processing.[3], [5], [56]

Coagulation will be used to refer to the aggregation of particles into small flocs when repulsive forces between them are neutralized or destabilized. This electrostatic colloidal destabilization weakens the repulsive electrostatic forces or shrinks the electrical double layer, thus, enabling the colloidal particles to approach each other at closer range where attractive van der Waal forces are dominant enough to allow for aggregation. Neutralization of particle surface charges can be achieved by pH-control or addition of a coagulant (electrolyte) solution. In this work, we have used a calcium salt solution as a coagulant. The threshold concentration of inorganic salt coagulants that is needed to initiate aggregation of colloidal particles is known as the critical coagulation concentration (CCC). At the CCC, the energy barrier caused by electric repulsion is eliminated, resulting in spontaneous particle aggregation in the primary minimum. Ionic strength has a linear dependence on both the electrolyte concentration and valence of the ions (Equation **(2-7)**). Consequently, the higher the electrolyte concentration and valence of constituent ions in a coagulant, the higher the ionic strength of the solution and the more effective it is at charge neutralization (shrinkage of the electrical double layer). **Figure 2-13** illustrates the role(s) of pH-control, electrolyte concentration, and ionic strength play in neutralizing surface charge (destabilizing a colloidal dispersion).[3], [57], [58]

$$\boldsymbol{I = \frac{1}{2}\sum_{i=1}^{n} C_i Z_i^2} \qquad \textbf{(2-7)}$$

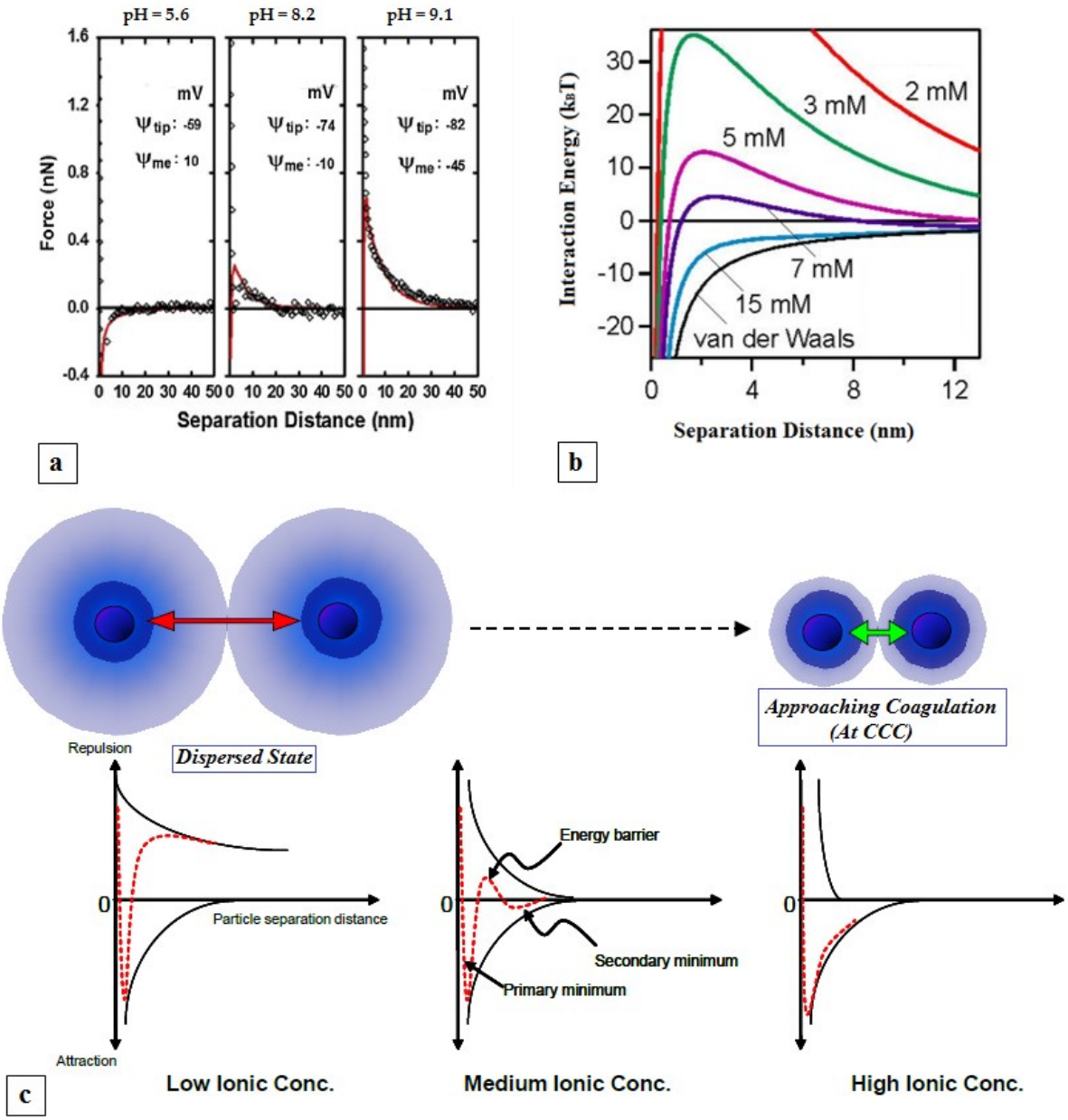

Figure 2-13: *Colloidal destabilization as a function of (a) pH-control [28], [48] (b) change of electrolyte concentration [57], and (c) variation of ionic strength.[5]*

Flocculation, on the other hand, will be used to refer to aggregation and subsequent sedimentation of the destabilized particles by polymer bridging. Polymer bridging is the formation of flocs by the simultaneous attachment of a water-soluble polymer to several particles. Desirable polymer flocculants usually possess high molecular weights and can attach at multiple points and on several particles' surfaces making the adsorption on particles practically irreversible. Coagulation usually precedes flocculation so as to aggregate fine solids and reduce the linkage points during polymer bridging (flocculation). Consequently, flocs from polymer bridging are larger, denser, and settle visibly faster by gravitational sedimentation. This relationship between the floc size and rate of sedimentation is usually approximated using Stokes' Law. According to

Stokes' Law, the settling velocity is proportional to the density of the solid and a square of the particle's size (Equation **(2-8)**).

$$\upsilon = \frac{2gR^2(\rho_s - \rho_f)}{9\eta} \qquad \textbf{(2-8)}$$

The gravitational force acting on the particle is proportional to a cube of the particle's size (Equation **(2-9)**).

$$F_g = \frac{4\eta g R^3(\rho_s - \rho_f)}{3} \qquad \textbf{(2-9)}$$

Working with a dilute laminar suspension, assuming that the viscosity and density of the dispersing fluid remain constant, and that the suspended solids have roughly the same density, we can use a Stokes' Law approximation to gain a useful perspective of the sedimentation process. A 200 µm particle (a size typical of a visible floc) will settle 100 times faster than a 20 µm particle (~size of a fine mineral solid, < 44 µm), 10,000 times faster than a 2 µm particle and 1000,000 times faster than a 0.2 µm particle (size of an ultra-fine clay mineral). Despite the simplistic assumptions made when using Stokes' Law, this analogy makes a case for polymer induced flocculation. It is hard to overestimate the importance of flocculation in accelerating the initial sedimentation rate of fine solids in tailings treatment. [3], [42], [51], [58]–[61]

2.3) Polymer Flocculants and MFT Dewatering.

Polymers have a vast array of applications: as carriers in drug delivery applications, as scaffolds in tissue engineering, as viscosity improvers in enhanced oil recovery and lubricants in hydraulic fracturing, as retention aids in paper fabrication, as synthetic soil conditioners in agriculture, and as flocculants in water, wastewater and sludge treatment.[59], [62]–[69]

In oil sands tailings, polymer flocculants accelerate the sedimentation of fines and increase the hydraulic conductivity of the sediments, thus enhancing initial tailings dewatering and rapid densification which, consequently, helps hasten the drying and reclamation process. In the grand scheme of things, polymeric flocculants contribute to both water recovery and subsequent land reclamation – the two main challenges associated with tailings treatment. Currently, polymer flocculants are used in thickeners and are incorporated in most commercial dewatering technologies. For example, in thin lift dewatering, an industrial dewatering technology, oil sands tailings are intercepted and treated with polymer flocculants to accelerate flocculation and initial dewatering. The resulting compaction of the polymer-treated tailings significantly reduces their volume and forms a high-density trafficable paste. This paste is then placed in thin layers on inclined ground to allow for further dewatering and natural desiccation. Mechanical dewatering technologies such as centrifugation and filtration also use polymer flocculants to enhance flocculation, dewatering and densification. Storage volume reduction and water recovery are two features associated with polymer-treated tailings which are extremely important, especially considering the current inventory of tailings. Generally, in high-density thickeners, in-line flocculation and centrifugation technologies, all of which use polymer flocculants, the solids content of MFT increases from ~ 30 wt. % to ~ 50 wt. %, a densification that corresponds to a ~ 50 % saving in storage volume. Additional processes like filtration, consolidation and drying help further densify the treated tailings from ~ 50 wt. % to ~ 80 wt. %, which offers an extra reduction in storage volume of about ~ 45 %. Treated MFT at 60 wt. % solids requires less than a third of the total storage volume that would be required for the same amount of fines from composite tailings (CT) at 80 wt. % solids consolidation. Based on Kaminsky's estimation, increasing tailings solids content from about 10 wt. % to 60 wt. % saves almost 90 % in storage volume (**Figure 2-14A**). In tailings treatment, this initial densification happens along with initial dewatering and the retrieved water is recycled. Dried tailings with a solids content of 75 wt. % to 80 wt. % (47 vol. % to 40 vol. %), within the plastic limit range, are considered to have the desired long-term stiffness and strength (50 kPa to 100 kPa) required for reclamation. **Figure 2-14B** offers yet

another perspective on oil sands tailings' volume reduction; to move from 50 wt. % solids to the desired 75 wt. % to 80 wt. % you end up losing 67 % to 75 % of the water in the tailings. [5], [35], [42], [59]

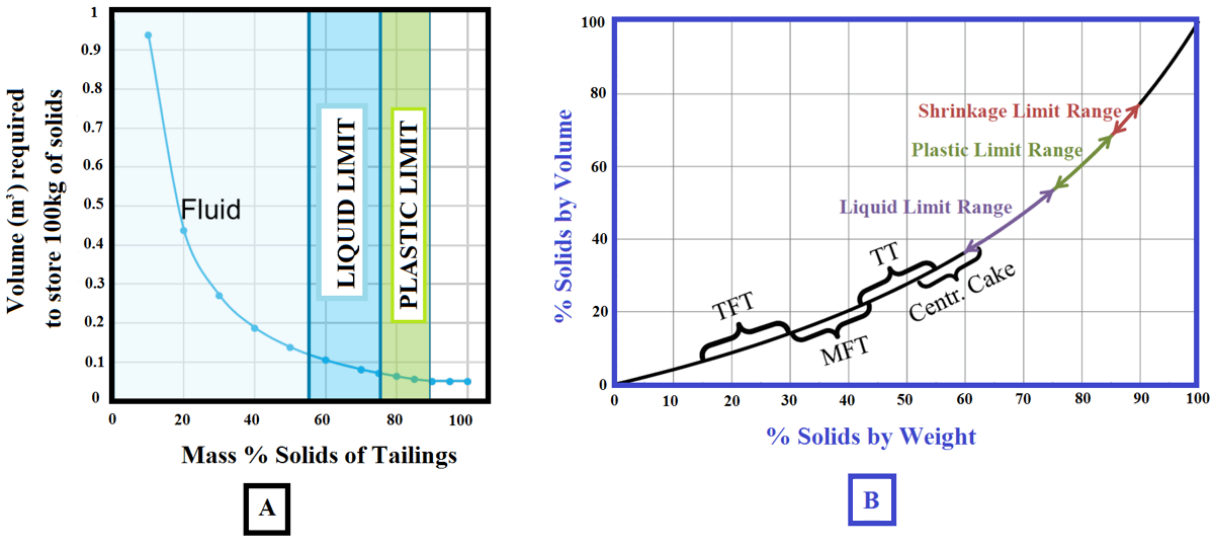

Figure 2-14: *(A) An illustration of the storage volume reduction that is expected with increase in tailings' solids content.*[42] *(B) Another illustration of oil sands tailings' volume % - mass % relationship and atterberg limits.* [35]

The main polymer flocculants used in industrial oil sands tailings treatment are PAM-based flocculants. These flocculants have had a proven record of success in other industrial applications and it is, therefore, no surprise that they were the first polymer flocculants considered for industrial oil sands tailings treatment. Solubility in water (hydrophilicity) and high molecular weight are key desirable properties in PAM flocculants. These properties avail numerous active sites of the flocculant for interaction with the dispersed particles leading to effective adsorption of the flocculant on multiple particle surfaces. Thus, PAM flocculated tailings form relatively large flocs with high initial settling rates and rapid initial dewatering. These polymers, however, tend to hold water in their flocculated sediments, where the polymer concentration is much higher, which could ultimately lead to poor long term pore water recovery and by extension poor consolidation. This water release problem is most likely due to hydrogen bonding of water molecules with PAM chains as shown in **Figure 2-15b**. Hydrogen bonds are weak dipole-dipole bonds that are formed between hydrogen and highly electronegative atoms like oxygen and nitrogen. PAM flocculants replicate their structural units (monomers) up to millions of times within their high MW chains, which would in turn significantly amplify the strength of the hydrogen bonds due to their amide groups and the associated water retention capacity. [35], [42], [59], [70]–[74]

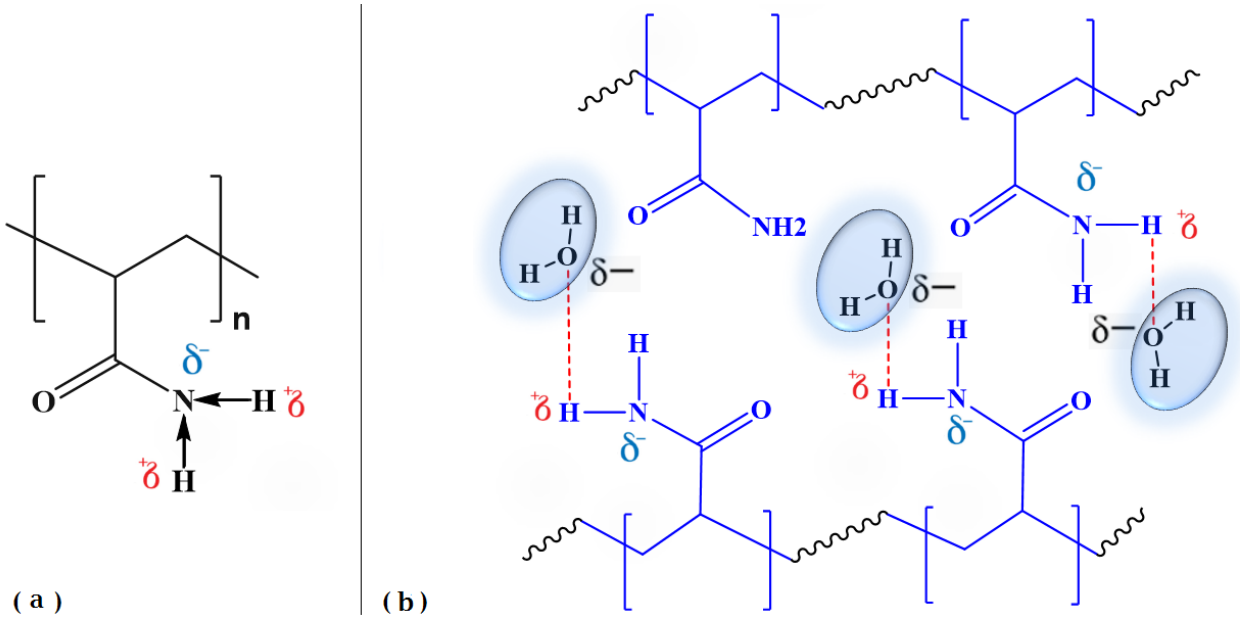

Figure 2-15: *(a) PAM. (b) Simplified illustration of proposed intermolecular hydrogen bonding between PAM chains and water molecules.*

Several studies have looked at the effect of hydrophobic groups in water-soluble polymer flocculants used in tailings treatment. [70]–[73], [75] Li et al. investigated the use of poly(n-isopropyl acrylamide) (PNIPAM) (**Figure 2-16a**) as an oil sands tailings flocculant. The hydrophobic properties of non-ionic PNIPAM are thermal responsive and the transition from hydrophilic to hydrophobic state only happens at temperatures above PNIPAM's lower critical solution temperature (LCST) – in this case above 32º C . This LCST value was dependent on the molecular structure and it increased notably when ionic PNIPAM was used instead. Therefore, despite its promising performance, this hydrophobic modification could only be used at elevated temperatures and heating the current tailings inventory to temperatures above PNIPAM's LCST is not an economically viable option. [75] Reis et al., motivated by previous PNIPAM studies, decided to use poly(acrylamide)-graft-polypropylene oxide (PAM-g-PPO) hydrophobic modification (**Figure 2-16b**) as an alternative flocculant. PAM-g-PPO showed promising results on dewaterability that were also attributed to the hydrophobic segments.[72] Hripko et al. worked on yet another hydrophobic PAM modification, poly(acrylamide)-graft-poly(ethylene oxide methyl ether methacrylate) (PAM-g-PEOMA) (**Figure 2-16c**), drawing from the success of PAM-g-PPO. PAM-g-PEOMA also showed remarkably good dewaterability compared to the industrial PAM-based reference flocculant when more than 30 % of hydrophobic grafts were added to the PAM backbone. [71] Gumfekar et al. used poly(n-isopropyl acrylamide/acrylic acid/n-tert-butylacrylamide) copolymer (P(NIPAM-AA-NTBA)) (**Figure 2-16d**) which possessed two types of hydrophobic comonomer segments, NIPAM and NTBA, that were credited with the improved

water release of this flocculant. Flocculation tests on P(NIPAM-AA-NTBA) were run at 50ºC to initiate the transition of PNIPAM's structural conformation from hydrophilic to hydrophobic state. Again, based on the foregoing argument, using PNIPAM modifications is not practical for industrial-based tailings treatment.[73]

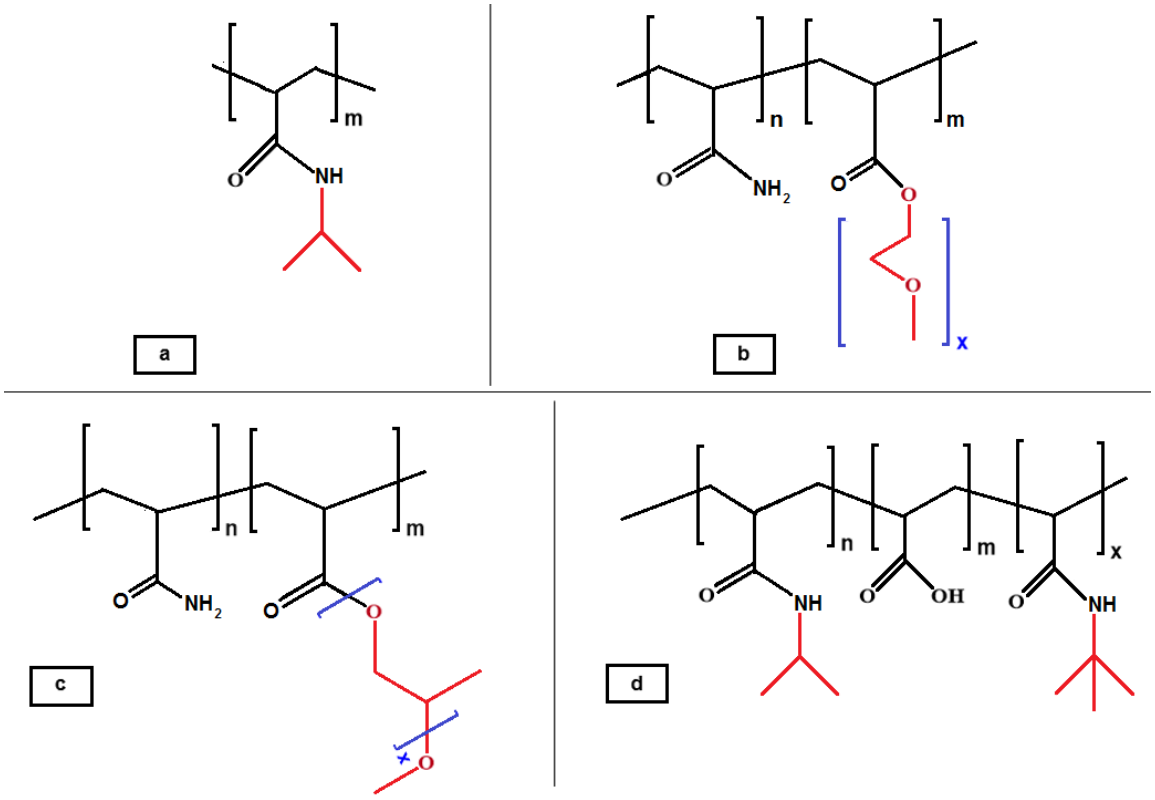

Figure 2-16: *Hydrophobic modifications of PAM-based polymers: (a) PNIPAM; (b) PAM-g-PPO copolymer; (c) PAM-g-PEOMA copolymer; and (d) P(NIPAM-AA-NTBA) copolymer.*

In summary, almost all the current hydrophobic modifications of PAM flocculants are copolymers that are comparatively more expensive and difficult to synthesize, especially on an industrial scale. Moreover, the techniques used to synthesize these copolymers make it difficult to attain molecular weights that compare to those of current industrial flocculants without significantly lowering polymerization rates. In polymer flocculants, high molecular weight chains result in increased binding sites, which increases the flocculation and adsorption capacity. However, at very high molecular weights of about $18x10^6$ Da, chain entanglement becomes a limiting factor and ultimately results in poor interaction with small particles.[76] Thus, it is advisable to have a polymerization technique that allows you to obtain a range of MWs including the very high limits so as to test the optimum flocculation capacity of your flocculant.

Studies on hydrophobically modified flocculants that are not based on PAM also show promising dewatering ability that is attributed to their hydrophobic functional groups.[70], [77],

[78] Botha et al. synthesized hyperbranched functionalized polyethylene (HBfPE) (**Figure 2-17**) by functionalizing a purely hydrophobic polyethylene backbone with methyl acrylate and then hydrolyzing the methyl acrylate segments. The hydrolyzed methyl acrylate segments acted as active binding sites allowing for both water-solubility and interaction with dispersed particles in tailings whereas the hydrophobic backbone helped repel water. Hydrophobic segments seem to not only repel water but they also promote interaction with fugitive bitumen and other organic compounds that coat clay particles, thus, adding extra polymer adsorption sites. HBfPE is, however, a copolymer that uses palladium catalysts under thorough conditions in the course of its synthesis, making it expensive and difficult to scale up. Also, high MW HBfPE polymers that compare to industrial PAM could not be obtained. [70], [74], [79], [80]

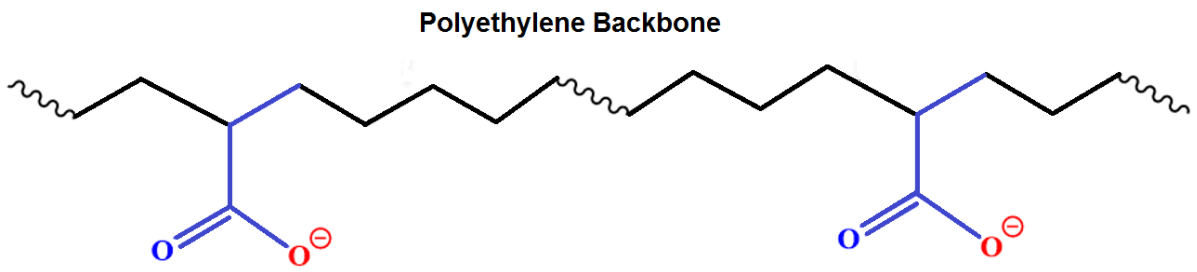

Figure 2-17: *HBfPE copolymer showing hydrophilic segments of hydrolyzed methyl acrylate on a hydrophobic polyethylene backbone.*

Inspired by the success of prior studies on hydrophobically modified flocculants and particularly HBfPE, we decided to try out a novel approach to synthesizing these types of polymers. In our research, we proposed the use of a homopolymer that is comparatively easier and cheaper to synthesize and hence economical to scale up. Our proposed flocculant, also possessed a hydrophobic backbone for water repulsion and could be hydrolyzed to attain the desired water-solubility and anionic charge for interaction and flocculation of fine solids. Moreover, the polymerization technique used was such that very high molecular weights could be obtained at high rates of reaction while maintaining surprisingly low viscosities of the reaction mixture. This technique is also water-based, therefore, a more environmentally friendly approach compared to solvent-based alternatives. MW could also be varied significantly and high MW that compared to industrial flocculants could also be attained. PMA, our proposed flocculant, was synthesized via emulsion polymerization to form a hydrophobic PMA latex solution which was then hydrolyzed to water-soluble HPMA (**Figure 2-18**). Thus, just like in HBfPE, we ended up with a hydrophobic backbone and ionic active sites for clay and water interactions.

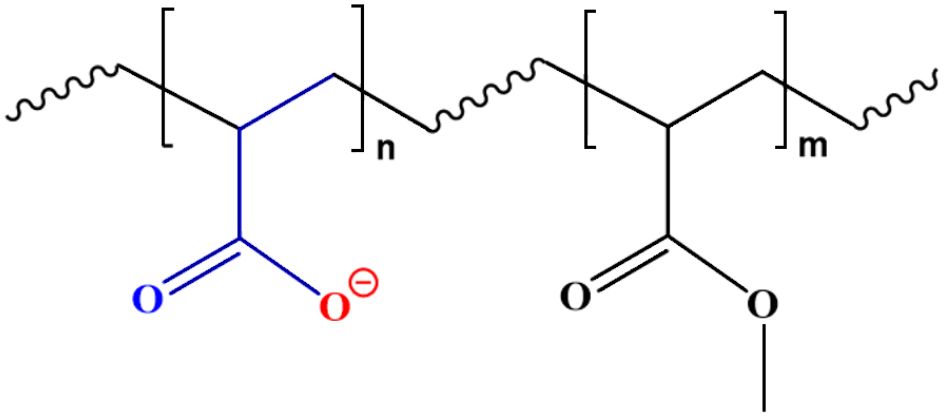

Figure 2-18: *HPMA homopolymer showing the hydrophilic segments that result from base hydrolysis of the hydrophobic backbone of PMA.*

2.4) Emulsion Polymerization.

2.4.1. Introduction - Free Radical Polymerization

Free radical polymerization is used to make a wide range of polymers. In 2001, it was estimated that free radical polymerization accounted for almost 40 billion pounds of polymers produced in the United States alone. [81] In more recent estimates, free radical polymerizations processes account for about 45 % and 40 % of the global plastic and synthetic rubber production, respectively. [82] In essence, free radical polymerization is initiated by the generation of a primary free radical that serves as an active center for the successive addition of monomer molecules. The monomers usually contain a vinyl group. A common characteristic of chain addition polymerizations such as free radical polymerization is reaching high degrees of polymerization at very early stages of the reaction (very low conversions). Lovell et al. puts this in perspective using an example whereby 1 mole of a monomer with a conversion of approximately 10^{-17} % is considered enough to yield a polymer molecule with 60,000 monomer-unit segments. [83]

2.4.1.1. Free Radical Polymerization Techniques

Free radical polymerizations are usually carried out using four main techniques: bulk, solution, suspension, and emulsion polymerization. Bulk polymerization is the simplest to set up and has minimal polymer contamination as it involves just the monomer and a monomer-soluble initiator. However, as conversion increases, the reaction mixture quickly becomes viscous and mixing and heat removal becomes quite difficult leading to a *gel effect* (**Figure 2-19**). The only way to effectively run bulk polymerization is to operate at low monomer conversions, which is not an economically viable option on an industrial scale.

Solution polymerization uses solvents that act as diluents and help to lower the viscosity and assist in heat transfer/removal. This technique makes mixing and thermal control easier, therefore solving the main problems associated with bulk polymerization. Solvents, however, may be expensive and require separation steps (evaporation or precipitation) to recover them and purify the polymer product, further raising production cost.

Based on the kinetics of bulk and solution polymerization, diluting the monomer in solution polymerization lowers both the polymerization rate and the average polymer molecular weight. Organic solvents are also a source of toxic volatile organic compounds (VOCs) which may pollute the environment if poorly disposed.

Suspension polymerization is a better alternative to overcome the challenges posed by bulk polymerization. It involves the use of a monomer that is insoluble in water and can be suspended in the form of droplets in an aqueous phase by strong agitation and use of stabilizers (dispersants). Since a monomer-soluble initiator is used, each droplet is analogous to a bulk polymerization microreactor. Therefore, droplet kinetics are also similar to those of bulk polymerization. Constant strong agitation is required to maintain the stability of the polymer beads in suspension and it may be difficult to control properties of the polymer beads. This technique is also comparatively unreliable when used to synthesize polymers that possess a low *glass transition temperature* (T_g) such as methyl acrylate because the polymer beads coagulate easily if the temperature of the reaction mixture is above the polymer T_g. [81], [83]

Emulsion polymerization, the method of choice to synthesize the polymer flocculants in this thesis, solves most of the problems associated with the methods described above. It will be discussed later in this chapter.

2.4.1.2. Free Radical Mechanism and Kinetics

The mechanism of free radical polymerization can be divided into three main steps: initiation, propagation and termination (**Figure 2-20**) The Initiation step generates primary free radicals via initiator decomposition. Propagation involves the addition of monomers to the primary radicals resulting in a growing polymer chain with an active end group (polymer radical). Termination is the final step in which polymer radicals stop growing either by combination or disproportionation. For simplicity, we will ignore the effect of chain transfer reactions.

The polymerization kinetics for bulk and solution processes are such that, at low conversions, the *rate of polymerization* (R_p) and the *kinetic chain length* (v) can be predicted with Equation **(2-10)** and **(2-11)**, respectively.

$$R_p = -\frac{d[M]}{dt} = k_p[M]\left(\frac{fk_d[I]}{k_t}\right)^{0.5} \propto [M][I]^{0.5} \qquad \textbf{(2-10)}$$

$$v = \frac{k_p[M]}{2(fk_tk_d[I])^{0.5}} = \left(\frac{k_p^2}{k_t}\right)\frac{[M]}{2R_p} \propto [M][I]^{-0.5} \qquad \textbf{(2-11)}$$

At higher conversions, however, especially when the initial monomer concentration is high, the viscosity of the reaction mixture increases as the concentration of polymer chains increases, reducing the mobility of the polymer radicals. Thus, it becomes harder for active end groups to get close enough to undergo termination reactions, causing the rate of termination (proportional to k_t) to drop. Since R_p and v are inversely proportional to the square root of k_t – see Equations **(2-10)** and **(2-11)** – the rapid drop in k_t, typical at higher conversions, translates as an auto-acceleration of the rate of polymerization and an increase in polymer molecular weight, a phenomenon known as gel effect or *Trommsdorff effect* (**Figure 2-19**). [81], [83], [84]

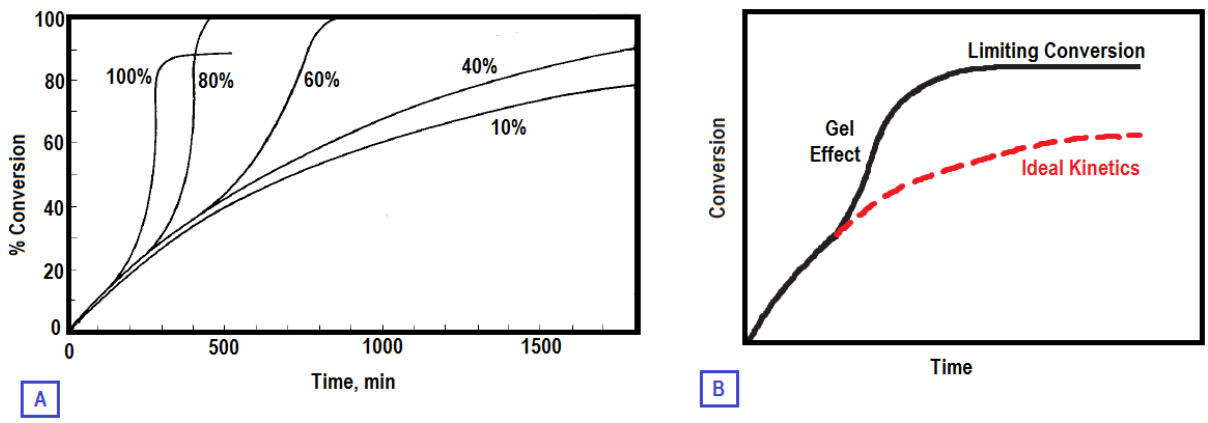

Figure 2-19: *(A) Autoacceleration as a function of monomer (methyl methacrylate) concentration.*[81] *(B) Trommsdorff effect and limiting conversion in FRP kinetics.* [84]

In the industry, Trommsdorff effect usually results in extremely viscous reaction mediums with very poor heat dissipation which can easily lead to runaway reactions that ruin equipment, at best, or cause fatal explosions, at worst. Moreover, for batch and solution polymerization, the only way

to increase both R_p (shorten batch cycle times) and increase polymer molecular weight, is to increase the monomer concentration, as shown in Equation ((**2-12**) and ((**2-13**).

COUPLING: $$\overline{X_n} = 2\upsilon \propto [M][I]^{-0.5} \quad \textbf{(2-12)}$$

DISPROPORTIONATION: $$\overline{X_n} = \upsilon \propto [M][I]^{-0.5} \quad \textbf{(2-13)}$$

This variable, however, can only be adjusted within a narrow range, considering the high possibility of gel effect at higher conversions (**Figure 2-19A**). Raising the initiator concentration, on the other hand, will increase R_p but at the expense of dropping the polymer molecular weight. The reverse is also true: an increase in the polymer molecular weight can only be achieved at the expense of a reduction in R_p (Equation **(2-10)** and **(2-11)**). Moreover, the homogeneous polymerization (solution or bulk) of monomers with an inherently low $\frac{k_p^2}{k_t}$, such as isoprene or methacrylonitrile, result in very low polymerization rates (R_p) to obtain kinetic chain lengths that are as low as ~ 10^4. In addition, incomplete monomer conversion may result if the propagation rate is also influenced by poor mobility of the polymer radicals (**Figure 2-19B**). [81], [83]–[87]

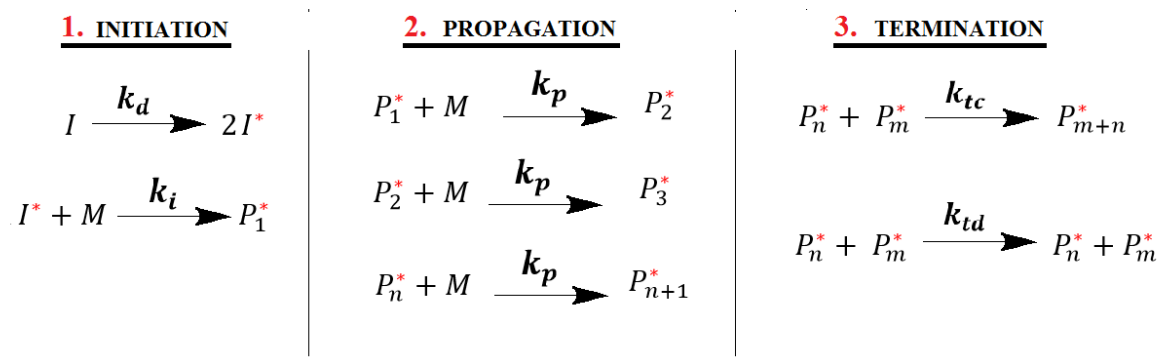

Figure 2-20: *The three characteristic steps of free radical polymerization reactions.*

2.4.2. Emulsion Polymerization

Emulsion polymerization is another alternative way to conduct free radical polymerization. It was first reported in the industry in 1927 and patented and commercialized in the 1930s.[88] However, its first major industrial application did not happen until the Second World War, when it was harnessed to produce synthetic rubber (copolymer of 1,3-butadiene and styrene) following Japan's strategic cut-off of natural rubber sources in southeast Asia. This technique has since found a broad array of applications, such as: water-based paints and coatings, paper coatings, sealants and adhesives, binders for non-woven fabric, plastic pigments, additives for construction materials such as Portland cement, mortar and concrete, a variety of core-shell products (some used for high-impact materials), drug delivery systems and other specialty polymers. [81], [84], [88]–[94]

Emulsion polymerization, as a general term, encompasses many variations like conventional emulsion polymerization, inverse emulsion polymerization, mini-emulsion polymerization, and micro-emulsion polymerization. [81], [95]–[103] Conventional emulsion polymerization, also referred to as macro-emulsion polymerization, is the technique used in this thesis and will be the sole subject of this review section.

Conventional emulsion polymerization is an oil-in-water (o/w) method with four key components: monomer, water, surfactant and initiator. The monomers that can be polymerized with this technique have reduced water solubility, ranging from very low (~ 0.03 wt. % for styrene at 20 ºC) to relatively high (~ 7 wt. % for acrylonitrile at 20 ºC). Water is the continuous phase in which the organic phase is dispersed. The use of water as a dispersing medium makes this a cheaper and greener technique vis-à-vis solvent-based technologies. Water is also ideal for heat dissipation purposes because of its high specific heat capacity and high enthalpy of vaporization, both properties deriving from its dense intermolecular hydrogen bonds network. These properties enable water to absorb high heats of polymerization without drastically changing temperature and with minimal risk of fire hazards.

Surfactants are also an important component in emulsion polymerization. They are amphiphilic – possessing a polar head and a hydrophobic tail – and readily absorb on interfaces where they lower the surface tension and stabilize colloidal dispersions. Surfactant molecules easily dissolve in the aqueous phase at low concentrations, but beyond a certain critical concentration (CMC-*critical micelle concentration*) they aggregate and form *micelles* (aggregates with hydrophobic inner cores and polar exteriors) (**Figure 2-21A**). In an emulsion system, the monomer ("oil phase") is partitioned such that some of it is dissolved in the micelles' hydrophobic pockets while most of

the remaining monomer (as high as over 95 %) is dispersed as droplets that are stabilized by surfactant molecules. In summary, surfactants help to generate micelles and to stabilize both the monomer droplets and the synthesized polymer particles. [84], [104]–[107]

2.4.2.1. Emulsion Polymerization Nucleation and Mechanisms.

Emulsion polymerization shares the same three-step (initiation, propagation and termination) mechanism that is typical of homogenous free radical polymerization, but they happen in a more complex system. In emulsion polymerization, all the mechanistic steps happen in a heterogeneous colloidal system, where the reagents are partitioned among the water, the micelles, the polymer particles, and the monomer droplets (**Figure 2-21A** and **B**).

Polymer particles are central to any discussion on emulsion polymerization mechanisms and their formation is commonly referred to as *nucleation*. Nucleation studies are essential since polymer particles are the principal locus of emulsion polymerization and these particles influence subsequent polymer properties and the reaction kinetics. The type of nucleation in an emulsion polymerization system is mainly dictated by surfactant concentration and partly by the water-solubility of the monomer.

At high surfactant concentration (above the CMC) there are numerous micelles in solution and monomers with low water-solubility, such as styrene, mainly undergo micellar (or heterogeneous) nucleation, whereas hydrophilic monomers, such as acrylonitrile, undergo both micellar and homogenous nucleation simultaneously. *Micellar nucleation*, as the name suggests, occurs in the monomer swollen micelles. In conventional emulsion polymerization, primary free radicals are generated in water because the initiators used are water-soluble. Surface-active polymer radical species, generated in the aqueous phase, penetrate the micelles where the monomer concentration is much higher than in solution (40 fold higher for styrene) and a rapid propagation of the polymer chain ensues forming a polymer particle (**Figure 2-21C**). Growth of the polymer chain continues until another polymer radical species enters the surfactant-stabilized particle and terminates the chain. The first qualitative emulsion polymerization mechanism was proposed by Harkins and was solely centered on micellar nucleation. Harkins had reviewed most of the wartime research on production of synthetic rubber in the United States. So, his inclination towards micellar nucleation was influenced by the hydrophobic monomers used during his time like styrene and butadiene (constituents of synthetic rubber).

On the other hand, at low surfactant concentrations (below the CMC), micelles are absent and all emulsion polymerization monomers undergo homogeneous nucleation. Surfactant-free emulsion polymerization of water-insoluble monomers, such as styrene, is also characterized by homogeneous nucleation. *Homogeneous nucleation*, unlike micellar nucleation, happens in the aqueous phase where the polymer chain propagates until it becomes insoluble, collapses onto itself and precipitates out of the water phase. A collapsed chain (or a series of collapsed chains) forms a latex particle analogous to a micellar particle that is stabilized by surfactant molecules and in which propagation of polymer continues (**Figure 2-21D**).

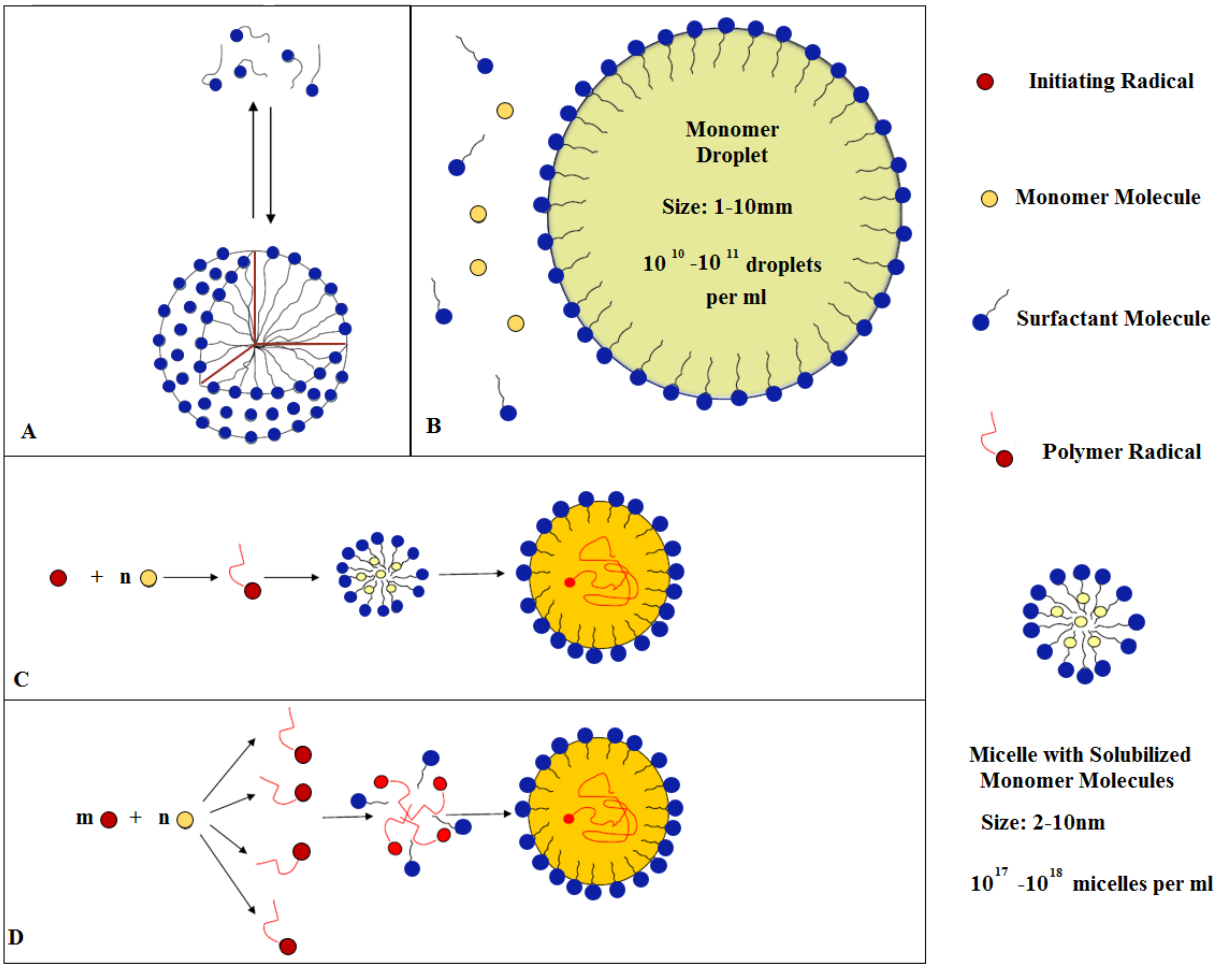

Figure 2-21: *(A) An illustration of a micelle aggregate (50-150 surfactant molecules) in equilibrium with other surfactant molecules in solution. (B) A monomer droplet. (C) Micellar nucleation. (D) Homogenous nucleation. [106]*

Nucleation inside monomer droplets (droplet nucleation) is infinitesimally small (< 0.1%). Micelles, though smaller in size, by far outnumber droplets and so their cumulative surface area is more than two orders of magnitude higher; thus, they have a much higher probability of capturing polymer radicals. Droplet nucleation is only prominent in mini- and micro-emulsion polymerization where monomer droplets are comparatively small and numerous enough to avail an effective surface area for polymer radical capture.

Coagulative nucleation is yet another nucleation mechanism: it occurs when small unstable latex particles (precursor particles) from any of the above mechanisms grow via coagulation as opposed to polymerization. Above the CMC, however, when the surfactant concentration is enough to stabilize even the precursor particles, the contribution of this type of nucleation is substantially reduced.

In conclusion, in practice most emulsion polymerization reactions involve a combination of some or all of these nucleation mechanisms occurring simultaneously, albeit in varying degrees. The predominance of one type of nucleation mechanism over the other(s) is determined by the type of monomer, the surfactant concentration, and other polymerization conditions. It is practically impossible to have a blanket mechanism that covers all events for all emulsion systems and equally difficult to incorporate all the relevant mechanistic aspects in a mathematical model. Emulsion nucleation mechanisms remain an active subject of research. [81], [84], [87], [105], [106], [108]–[114]

2.4.2.2. Emulsion Polymerization Intervals

Harkins' postulation of emulsion polymerization mechanism has since been modified to accommodate more systems. It is often conceptually divided into three main stages (or intervals): a particle formation (nucleation) stage and two particle growth stages (**Figure 2-22**).

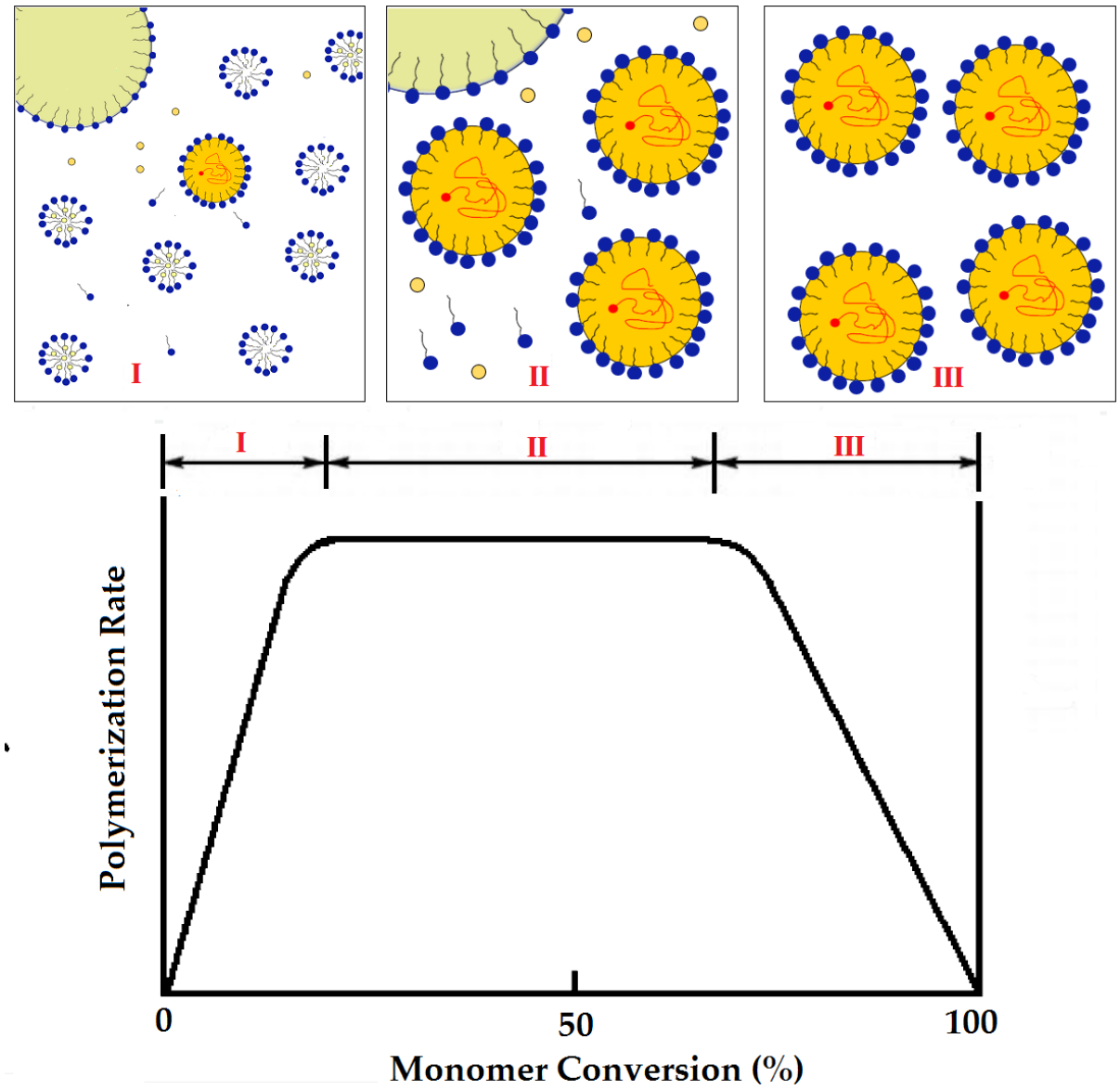

Figure 2-22: *Schematic illustration of the conceptual intervals that are characteristic of Harkin's mechanism. [115]*

The first stage (nucleation stage) is the shortest of the three and it happens at low monomer conversion (**Figure 2-22**). This stage is characterized by generation of polymer particles and a corresponding rise in polymerization rate. At this stage, most of the micelles present in the reaction mixture do not form particles but instead disintegrate to provide surfactant molecules that are needed to stabilize the polymer particles that are being generated. In micellar nucleation, for example, only 1 in about 1000 (0.1 %) of the initial micelles participates in particle formation,

with the rest disintegrating so as to provide colloidal stability. The disappearance of all the micelles marks the transition to the second interval.

In the second interval, the number of polymer particles should ideally remain constant as growth of the already existing particles takes precedence. However, even in the absence of micelles, homogeneous nucleation can still proceed as long as the surfactant concentration is greater than 0.05 mM. Monomer that is consumed by the growing polymer chains, as the particles grow, is rapidly replenished by monomer that diffuses from the aqueous solution which, in turn, is compensated by dissolution of monomer from the droplets. Monomer droplets act as monomer reservoirs that help keep the polymer particles saturated with monomer and, in this way, facilitate the propagation of polymer chains. At this stage, the rate of polymerization is relatively constant since the number of polymer particles and the particle's monomer concentration are both fairly constant.

Consumption of all monomer droplets marks the end of the second stage and the beginning of the third and last stage. In the last interval, in the absence of monomer droplets, both the concentration of monomer in the particles and the reaction rate gradually drop as polymerization proceeds. Usually, 100% monomer conversion is achievable by the end of this stage.[81], [83], [105], [106], [112], [115]

2.4.2.3. Emulsion Polymerization Kinetics

In a typical emulsion polymerization recipe, the initiator can generate 10^{16}-10^{18} radicals per second per unit volume of the aqueous continuous phase. The distinctiveness of emulsion polymerization primarily lies in its ability to compartmentalize this flux of radical species in discrete polymer particles. This segregation of free radicals comes with several advantages. The viscosity of the reaction medium, for instance, no longer depends on polymer molecular weight since almost all polymer chains are encapsulated in the latex particles. A particle can hold as many as 10,000 chains. As a consequence, the viscosity of the reaction mixture is usually close to that of the dispersing medium, water in this case. This low viscosity makes it possible to synthesize latexes with high weight fractions of polymer, lower the mixing energy, and accelerate the rate of heat removal during polymerization. The compartmentalization of free radicals also changes the reaction kinetics significantly, and for the better. The isolation of the loci of polymerization means that radicals within different particles cannot terminate. As a result, the rate of reaction (R_p) is usually higher than that of bulk, solution, or suspension systems operating under the same temperature. This technique is also favorable to scale up since it can generate high-yield batches in shorter times. In addition, the polymers produced via emulsion polymerization usually have higher average molecular weights than those made via other techniques at similar initiator concentrations. More importantly, unlike homogenous polymerizations, both the R_p and the molar masses can be increased simultaneously. [83], [84], [89], [90], [105], [107], [116]

Smith and Ewart were the first to quantitatively describe Harkins' qualitative mechanism. They showed how the kinetics of emulsion polymerization depended on initiator and surfactant concentrations. According to their theory, *the rate of polymerization* (R_p) in an emulsion system depends on the *number density of polymer particles* (N_p) which, in turn, is linearly dependent on the surfactant and initiator concentrations (see Equation **(2-14)** and Equation **(2-15)**).

$$N = k\left(\frac{R_i}{\mu}\right)^{\frac{2}{5}}(a_s[S])^{\frac{3}{5}} \propto [I]^{0.4}[S]^{0.6} \qquad \textbf{(2-14)}$$

$$R_p = \frac{-d[M]}{dt} = k_p[M_p]\bar{n}\frac{N}{N_A} \propto [S]^{0.6}[I]^{0.4} \qquad \textbf{(2-15)}$$

In emulsion polymerization, the number average degree of polymerization and the kinetic chain length are equal and they depend on the number of polymer particles - Equations **(2-16)** and **(2-17)**.

$$\overline{X_n} = \frac{Nk_p[M_p]}{R_i} \propto [S]^{0.6}[I]^{-0.6} \quad \textbf{(2-16)}$$

$$\upsilon = \overline{X_n} \propto [S]^{0.6}[I]^{-0.6} \quad \textbf{(2-17)}$$

As expressed in the equations discussed above, it is possible to simultaneously increase N_p, R_p, and the polymer molecular weight by increasing the surfactant concentration.

The rate of polymerization is also influenced by the average number of radicals per particle ($\bar{n}$). The value of $\bar{n}$ is dictated by the type of monomer used and the reaction conditions. Smith and Ewart, just like Harkins, based their work on a styrene-based system (low water-solubility monomer) which, under a wide range of reaction conditions, usually gives values of $\bar{n}$ that are equal to 0.5. This means that, at any moment, on average, half the number of polymer particles contain a polymer radical. Systems for which $\bar{n}$ = 0.5 are called Case 2 systems. These systems are characterized by monomers with low water-solubility, negligible *radical desorption*, and small-sized particles that can only hold one polymer radical at a time and instantly undergo bimolecular termination when a second radical enters the polymer particle. Case 2 systems are also called *zero-one systems* since at any given moment their particles have either zero or one radical.[81], [90], [117] Smith-Ewart's classical kinetic theory can only reliably predict the rate of polymerization for Case 2 systems and usually works at relatively low monomer conversions (Interval II), nonetheless, this theory is foundational to modern day understanding of emulsion polymerization kinetics.

Systems that deviate from Case 2 kinetics are referred to as Case 1 ($\bar{n}$ < 0.5) or Case 3 ($\bar{n}$ > 0.5) systems. Case 1 systems have, on average, fewer polymer radicals per particle mostly due to a high rate of radical desorption. Typical case 1 monomers include methyl acrylate and vinyl acetate. They are characterized by relatively high water-solubility and also tend to possess a high monomer chain-transfer constant. Radical exit/desorption is one of several kinetic events that characterize emulsion polymerizations (**Figure 2-23**). The mechanism for this interfacial process is chain transfer to monomer forming small monomer radicals which can easily diffuse into the water phase.[107], [109]

Case 3 systems are characterized by large-sized particles and low termination rates, thus, have two or more radicals in some of the particles ultimately averaging to $\bar{n}$>0.5. Butyl acrylate and methyl methacrylate are monomers that exhibit case 3 behavior under certain conditions. It is also not uncommon for Case 2 systems to transition to Case 3 at high monomer conversions (Interval III), when termination becomes diffusion-controlled and the particle size is relatively large. Case 3 systems, particularly, show a significant increase in rate of polymerization (R_p) even when the number of particles (N) is constant.[81], [83], [105], [109], [118]

According to kinetic studies by Banerjee et al., batch emulsion polymerization of methyl acrylate deviated from classical Case 2 kinetics. The steady-state polymerization rate depended less on surfactant concentration, as is reflected by the drop in the value of the exponent from the classical ~0.6 to ~0.3 – See Equations **(2-18)**, **(2-19)** and **(2-20)**. Moreover, based on this study, the monomer-water ratio had a significant influence on methyl acrylate kinetics. At a monomer-water ratio that was above the monomer's solubility (> 0.58 mol/L, at 50 ºC), the polymerization rate was independent of monomer concentration and depended mostly on initiator concentration as described by Equation **(2-18)**.

$$R \; \alpha \; [M]^0 [I]^{0.46 \pm 0.04} [S]^{0.30 \pm 0.03} \qquad \textbf{(2-18)}$$

Conversely, in a highly diluted emulsion system (below the monomer's solubility < 0.58 mol/L, at 50 ºC) (Equation **(2-19)**) and in the absence of surfactants (where particle formation was exclusively via homogeneous nucleation) (Equation **(2-20)**) the steady-rate of polymerization depended mostly on monomer concentration. [119]

$$R' \; \alpha \; [M]^1 [I]^{0.42 \pm 0.04} [S]^{0.25 \pm 0.05} \qquad \textbf{(2-19)}$$

$$R'' \; \alpha \; [M]^1 [I]^{0.40 \pm 0.04} \qquad \textbf{(2-20)}$$

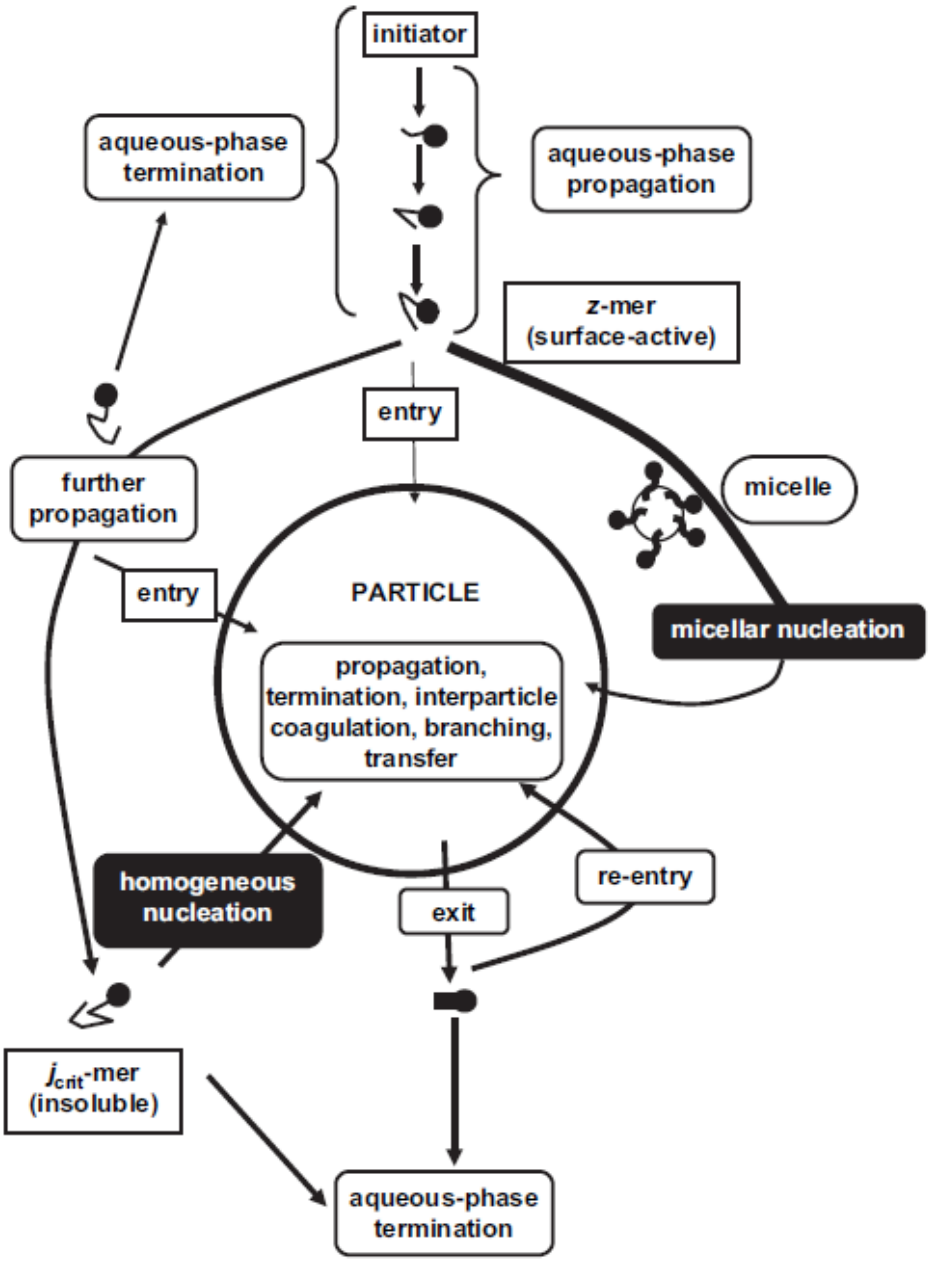

Figure 2-23: *A schematic showing a multitude of kinetic events that characterize emulsion polymerization. [107]*

2.4.2.4. Emulsion Polymerization of Alkyl Acrylates

Alkyl acrylates, also known as acrylate esters, can only be effectively polymerized via emulsion free radical polymerization. These acrylates are characterized by high rates and heats of polymerization. Methyl acrylate (MA) polymerization, for example, is highly exothermic with a heat of polymerization of -77 kJ/mol, which is higher than that of methyl methacrylate (MMA) (-58 kJ/mol). The polymerization rate constants of alkyl acrylates also exceed those of corresponding methacrylates. For instance, the k_p of MA is an order of magnitude higher than that of MMA. These differences can be explained by the lower steric hindrance in alkyl acrylates, as opposed to alkyl methacrylates, which makes it easier for their monomer molecules to quickly add to the polymer radical.

Bulk polymerization of methyl acrylate is impractical – it sets off an autoacceleration almost instantly, forming an immobile crosslinked network at very low conversions.

Solution polymerization, on the other hand, is characterized by high viscosity of the polymerizing medium that is dependent on the MW. High viscosity of the reaction mixture is mostly attributed to branching and crosslinking during polymerization due to abstractions of tertiary hydrogens in favor of more stable tertiary radicals. Thus, solution polymerization presents serious viscosity problems particularly when dealing with high MW polymers, not to mention the additional cost of solvents, their retrieval and the risk of chain transfer among other solvent-related problems that were previously mentioned. The downsides of these *homogenous techniques* (bulk and solution polymerization) far outweigh any potential benefits, making them unsuitable for commercial production of poly (alkyl acrylates).

The next alternative, suspension polymerization, when used on alkyl acrylates, would yield tacky and soft polymer beads that tend to easily agglomerate due to the low T_g values of poly (alkyl acrylates) (**Table 2-4**). Suspension polymerization also avails fewer variables to control relevant polymer properties.

In contrast, emulsion polymerization offers better thermal, viscosity, and latex stability. It also has the added advantages of better property control, use of water as solvent, and possibility of achieving higher polymerization rates and polymer molecular weights simultaneously. Emulsion polymerization overcomes the challenges posed by all other free radical polymerization techniques and is, thus, most apt for synthesis of alkyl acrylates and for commercial scale up. Hence the choice of this technique for the synthesis of PMA in this thesis. [81], [120]–[127]

Table 2-4: *A table showing T_g values for a range of poly (alkyl acrylates).* [128]

Poly-(Alkyl Acrylates)	**T_g (ºC)**
Poly (Methyl Acrylate) – PMA	+10
Poly (Ethyl Acrylate) – PEA	-23
Poly (n - Propyl Acrylate) – P-n-PA	-42
Poly (i - Propyl Acrylate) – P-i-PA	-2
Poly (n - Butyl Acrylate) – P-n-BA	-53
Poly (i - Butyl Acrylate) – P-i-BA	-33
Poly (tert - Butyl Acrylate) – P-t-BA	+38
Poly (Octadecyl Acrylate) – POA	+41

3) Synthesis and Hydrolysis of PMA

3.1) Experimental Design

A central composite design was used to study the effect of varying key properties of PMA on its performance as a flocculant in MFT treatment. This statistical design of experiments helps analyze the effects of chosen predictor variables on particular response variables using fewer experiments, as opposed to a "one variable at a time" approach.[129], [130] The predictor variables used in this investigation were initial initiator concentration and the DOH. These variables are independent of each other, as is required in a central composite design. The initiator concentration was used to regulate the polymer molecular weight based on the inverse relationships shown in Equations **(2-16)** and **(2-17)**. The other predictor, DOH, dictated the charge density (number of negative carboxylate flocculation sites) on the polymer chains, chain conformation and the water-solubility of the chains (their hydrophilicity).

3.2) Polymer Synthesis and Hydrolysis

3.2.1. Materials

Methyl acrylate (MA) (99 %, with ≤ 100 ppm monomethyl ether hydroquinone), potassium persulfate (KPS) (≥ 99.0 %), sodium dodecyl sulfate (SDS) (≥ 98.5 %) and sodium hydroxide (anhydrous ≥ 97 %) were obtained from Sigma Aldrich and used as received. Deionized water was used as the dispersing medium. The quality of water used for polymer synthesis is important since the presence of mineral ions can influence colloidal stability in emulsion latex solutions.[81]

3.2.2. Determination of the Critical Micelle Concentration.

The CMC of SDS is estimated to be within 7-10 mM at 20-25 ºC by Sigma Aldrich. We started our experimental work with an empirical verification of the CMC and a series of preliminary estimations to determine the convenient surfactant concentration for our recipe. As was briefly mentioned in the literature review, the CMC is the surfactant concentration beyond which surplus surfactant molecules will aggregate to form micelles. At concentrations below the CMC, surfactant molecules dissolve in water and accumulate at the water-air interface where they gradually lower the surface tension. At the CMC, however, the surfactant saturates the air-water interface and further increase in their concentration has negligible effect on surface tension. Thus, by tracking how surface tension changes with surfactant concentration, one can determine the CMC.

A K-100 tensiometer (**Figure 3-1**), an equipment that measures the change in surface tension using the Wilhelmy plate method, was used for empirical determination of the CMC at 23 ºC. The SDS concentration beyond which there was no further drop in surface tension (~ 8.2 mM) was used as the CMC estimate (**Figure 3-2**). This value also falls within the range prescribed by Sigma Aldrich. Based on preliminary polymerization tests, we evaluated colloidal stability at varying surfactant concentrations and found out 45 mM SDS (approximately 5.5 times the value estimated for the CMC) was the optimum SDS concentration for our recipe.

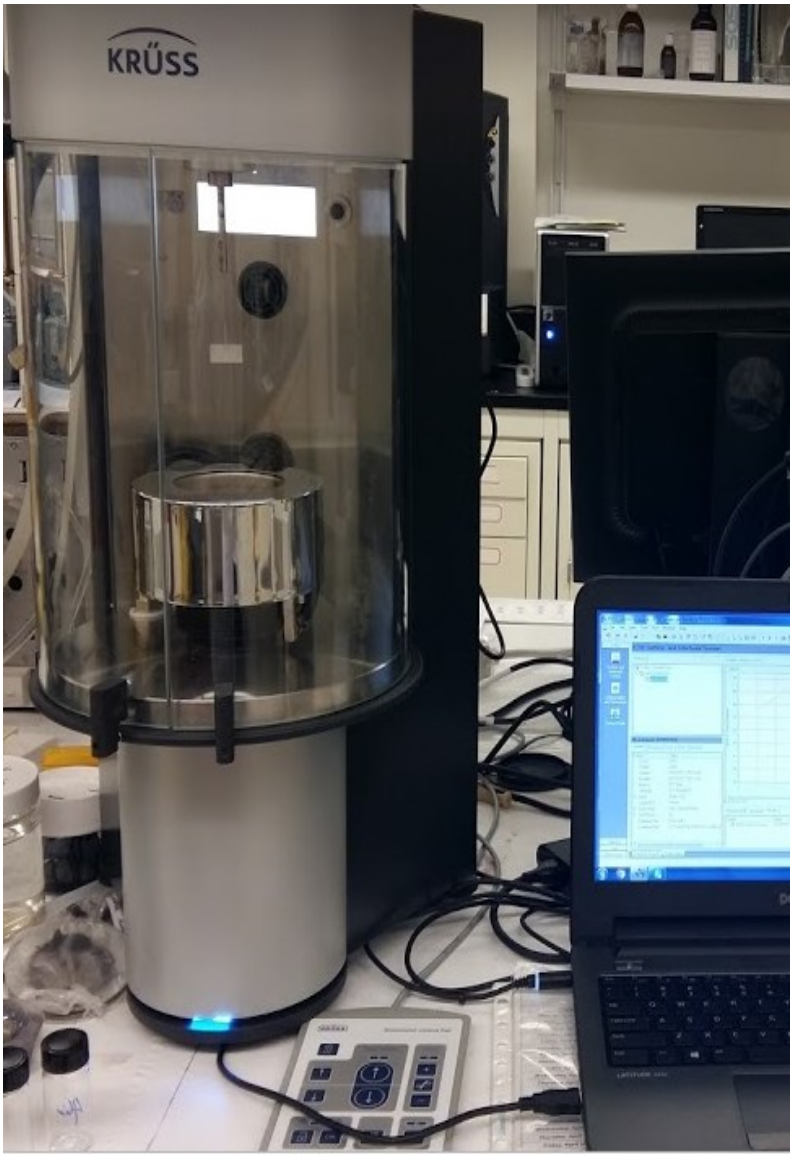

Figure 3-1: *A K-100 tensiometer that was used for surface tension measurements when determining the CMC.*

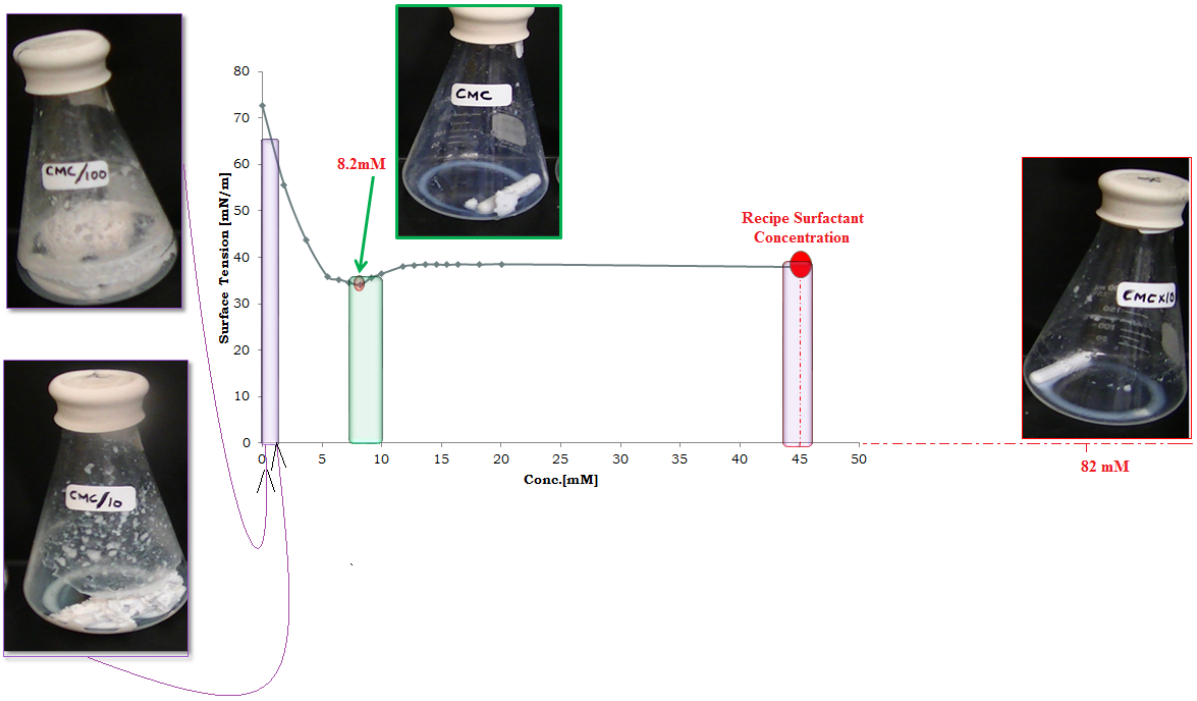

Figure 3-2: *A plot showing the relationship between surface tension and surfactant concentration. Remnant coagula (coagulums) in the conical flasks served as indicators of colloidal stability at different surfactant concentrations.*

3.2.3. Synthesis of PMA

PMA synthesis was run based on the feed composition shown in **Table 3-1**. Deionized water made the balance in all batches and constituted approximately 64 wt. % of the reaction mixture. The monomer-water ratio of these feed compositions was 6.3 mol/L, which is greater than the solubility of methyl acrylate in water (0.58 mol/L). Presumably, this system would follow the kinetics described by Equation **(2-18)**.

Generally, anionic surfactants like SDS are used within a range of 0.2 wt % to 3 wt % of the amount of water.[81] Our recipe, however, maintained a surfactant concentration that translated to about 1.3 wt. % on the amount of water - approximately 5.5 times above *CMC* (See **Figure 3-2**). The decision to keep the surfactant to water ratio relatively low (with regard to the permissible range) was based on preliminary HPMA flocculation tests in which the supernatant became turbid. We hypothesized (then) that surfactant molecules could be dispersing the fine solids in MFT and causing the undesired supernatant turbidity. Thus, we decided to keep the surfactant concentration as low as possible, provided that it was still possible to offer the required colloidal stability during emulsion polymerization.

Polymerizations were run in 250 ml three-necked round-bottomed flasks fitted with a water condenser. The reaction formulation components were purged with nitrogen for 15 minutes to deoxygenate them prior to heating. The reactor was placed in an oil bath and the oil temperature

was set to 65-67 ºC, which is well above the Kraft Point (minimum temperature to form micelles) for SDS. The polymerization time was 4 hours for each batch and the stirring rate was set at 200 rpm (using a magnetic stir bar).

Table 3-1: *Feed composition for PMA synthesis based on the CCD.*

Log [I]	-3.93	-3.60	-2.80	-2.00	-1.67
Initiator Concentration, M	1.17×10^{-4}	2.51×10^{-4}	1.58×10^{-3}	1.00×10^{-2}	2.14×10^{-2}
Surfactant Concentration	2.91×10^{-2} M (0.84 wt. %)				
Monomer Concentration	4 M (35 wt. %)				

Emulsion polymerization, using SDS, played a critical role to the success of our synthesis. Results from surfactant-free polymerization attempts were all poor: in the absence of surfactant, monomer feeds of 10 wt. % and 15 wt. % lost approximately half of the polymer yield to coagulation and the remaining latex had only about 5% solids content (**Figure 3-3a** and **b**). In surfactant-free polymerization, lowering the monomer/water ratio was the main variable that improved colloidal stability, which, I suppose, worked by minimizing the rate of collisions and subsequent coagulation of the latex particles. This monomer-reduction approach, however, resulted in low polymer yield per batch and required multiple batches to attain the same yield as a single conventional emulsion polymerization.

In contrast, polymerization in the presence of 0.84 wt. % SDS allowed us to not only elevate the monomer feed to 35 wt. %, but to also obtain latex solids contents that were as high as 30 wt. % (**APPENDIX C**) with minimal coagulation (**Figure 3-3c**). In other words, using SDS not only significantly improved colloidal stability, but it also allowed access to higher weight fractions of polymer per batch.

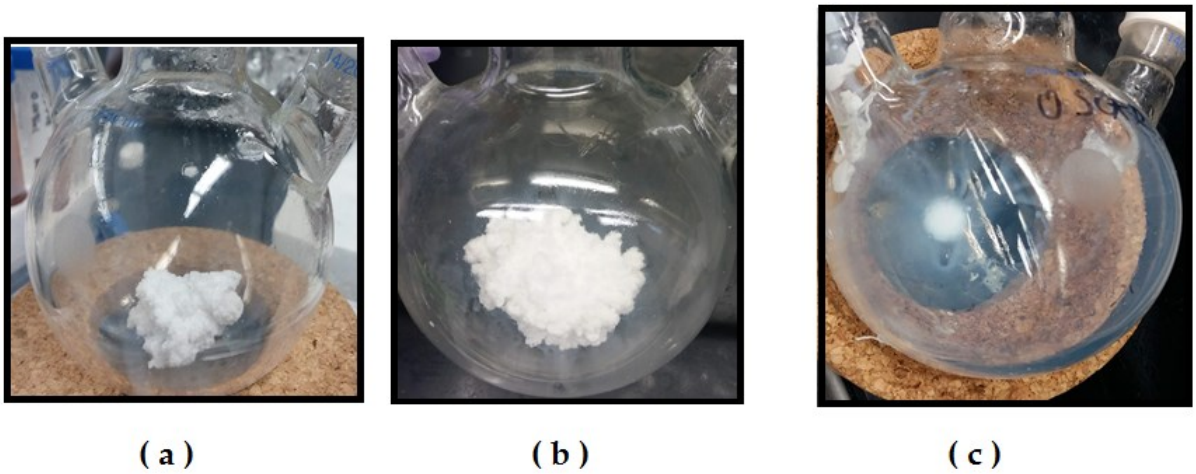

Figure 3-3: *Remnant coagula from: (a) surfactant-free emulsion polymerization with a 10 wt. % monomer feed; (b) surfactant-free emulsion polymerization with a 15 wt. % monomer feed; and (c) conventional emulsion polymerization with a 35 wt. % monomer feed.*

3.2.4. Hydrolysis of PMA

Hydrolysis of PMA to convert it into water-soluble HPMA was carried out using a caustic solution in the presence of heat. **Figure 3-4** shows a proposed reaction mechanism, which borrows from well-studied saponification (base hydrolysis of esters) reactions. Unlike acid hydrolysis, base hydrolysis yields carboxylate ions that make PMA soluble in water and also act as binding sites during flocculation. The proposed mechanism is also uniquely characterized by a rapid deprotonation step that is highly favorable as it helps drive the equilibrium of the preceding steps towards formation of HPMA.[131], [132]

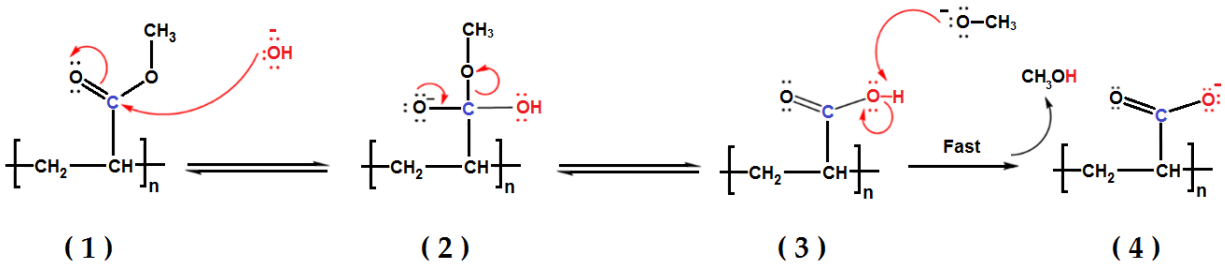

Figure 3-4: *A proposed PMA base hydrolysis mechanism showing four mechanistic steps: 1 - nucleophilic addition of the hydroxyl ion; 2 - formation of an intermediate species; 3 - Loss of the leaving group; and 4 - deprotonation to form HPMA and gaseous methanol.*

PMA was filtered through a Whatman Grade 50 filter paper (capable of retaining particles with diameters higher than 2.7 µm) to remove any traces of coagulum from the latex before proceeding with the hydrolysis. Moreover, to determine the average solids content for each batch, 3 ml triplicate samples of the homogenous filtered PMA were dried using an OHAUS MB27 moisture analyzer until the mass of the dried samples was constant (**Appendix C**). PMA was hydrolyzed in its latex emulsion state so as to maintain its colloidal stability. Hydrolysis was run in a 1 L glass beaker using an oil bath set at 80 ºC for 12 hours. As hydrolysis progressed, there was significant change in solution viscosity which necessitated occasional dilution with DI water and continuous mixing using both a magnetic stirrer and an overhead mixer with an anchor impeller. Caustic solution was added using a syringe pump and the amount added was based on theoretical stoichiometric calculations that factored in the initial monomer feed and the gravimetric polymer yield. Empirical values of degrees of hydrolysis did not exactly match with theoretical calculations. The deviation was especially pronounced at higher degrees of hydrolysis and higher MWs. These deviations may be explained by previous studies on base hydrolysis of PMA that have suggested that electrical effects of neighboring carboxylate groups may retard the reaction of the unhydrolyzed ester groups.[133]–[135] Studies on alkaline hydrolysis of PAM also show a progressive decrease in reaction rates as hydrolysis progresses due to increased electrostatic

repulsion of hydroxyl ions by both the neighboring carboxylate units and other remote carboxylate groups on proximate polymer chains.[136]–[138] From a mechanistic point of view, this progressive electrostatic shielding (**Figure 3-5**) could be preventing the nucleophilic addition of the hydroxyl ion (**Figure 3-4– step 1**) making it practically impossible to reach complete hydrolysis.

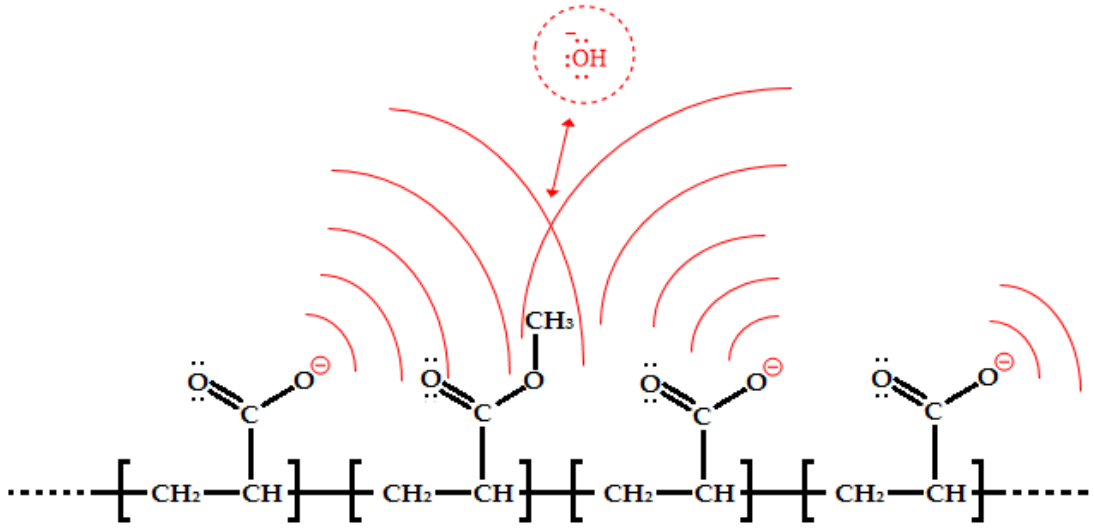

Figure 3-5: *A schematic representation of electrostatic repulsion of the hydroxyl ion by neighboring carboxylate groups, which retards base hydrolysis of ester groups, especially at high degrees of hydrolysis.*

3.3) Characterization Techniques.

3.3.1. DOH: Proton Nuclear Magnetic Resonance (^{1}H-NMR)

We used ^{1}H-NMR to determine the DOH by tracking the loss of hydrogen atoms attached to the methyl ester group due to hydrolysis. i-NMR software was used to overlap and compare ^{1}H-NMR data from different samples (**Figure 3-6** and **Figure 3-7**). DOH was determined based on the integration of the peak areas from processed NMR data. Peak Integration values show the amount of hydrogen atoms within the analyzed sample and the chemical shift of these peaks is dictated by the nature of the particular functional groups, such as –CH, -CH_2 and –OCH_3. NMR data from unhydrolyzed PMA was considered to be 0 % HPMA (or 100 % PMA) and was used as a reference point against which the other calculations were made. For example, the ratio of integration peaks for the unhydrolyzed reference PMA that is shown on **Figure 3-8** was calculated as follows,

$$\frac{Methyl\ group\ Integration\ \ Peaks(OCH_3)}{Backbone\ Integration\ \ Peaks\ (-CH, -CH_2)} = \frac{53.72}{46.29} = \frac{1.16}{1} \qquad \textbf{(3-1)}$$

In comparison, the ratio of integration peaks for its highly hydrolyzed variation that is shown in **Figure 3-9** was calculated as described below,

$$\frac{Methyl\ group\ Integration\ \ Peaks(OCH_3)}{Backbone\ Integration\ \ Peaks\ (-CH, -CH_2)} = \frac{0.11}{1} \qquad \textbf{(3-2)}$$

The remnant methyl groups in the HPMA sample above and the corresponding DOH were calculated as shown in Equation **(3-3)** and Equation **(3-4)**, respectively.

$$\%\ OCH_3 = \frac{0.11}{1.16} X100 = 9.5\ \% \qquad \textbf{(3-3)}$$

$$\%\ COO^- = \frac{1.16 - 0.11}{1.16} X100 = 90.5\ \% \qquad \textbf{(3-4)}$$

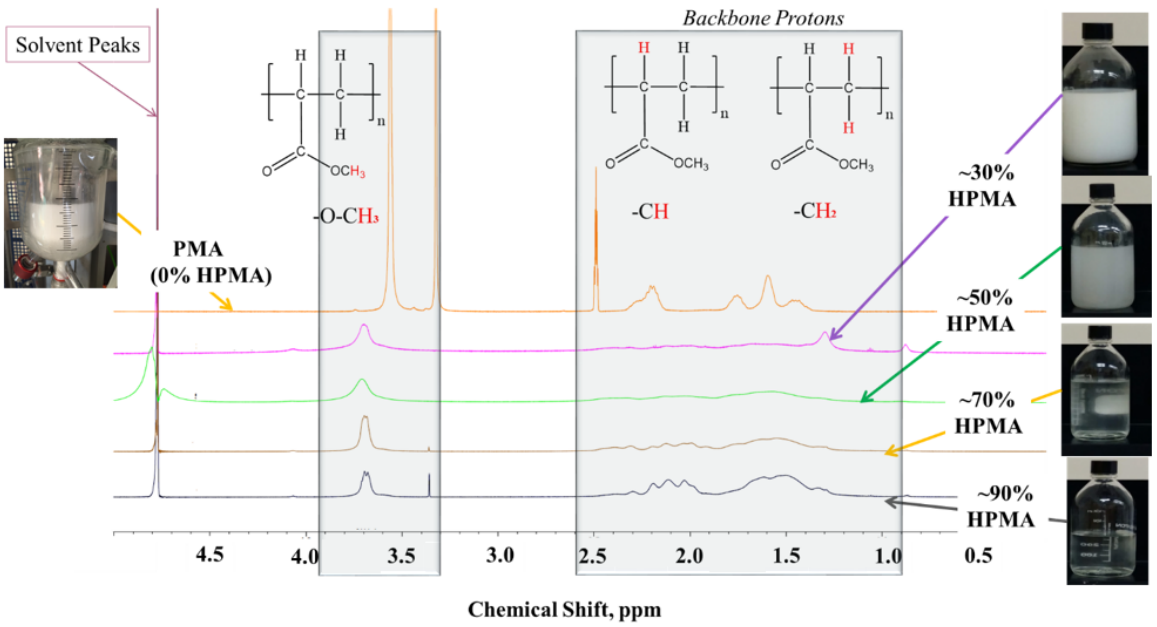

Figure 3-6: *^{1}H-NMR analysis of HPMA and the corresponding change in water-solubility for relatively low MW samples (2.14.10^{-2} M KPS).*

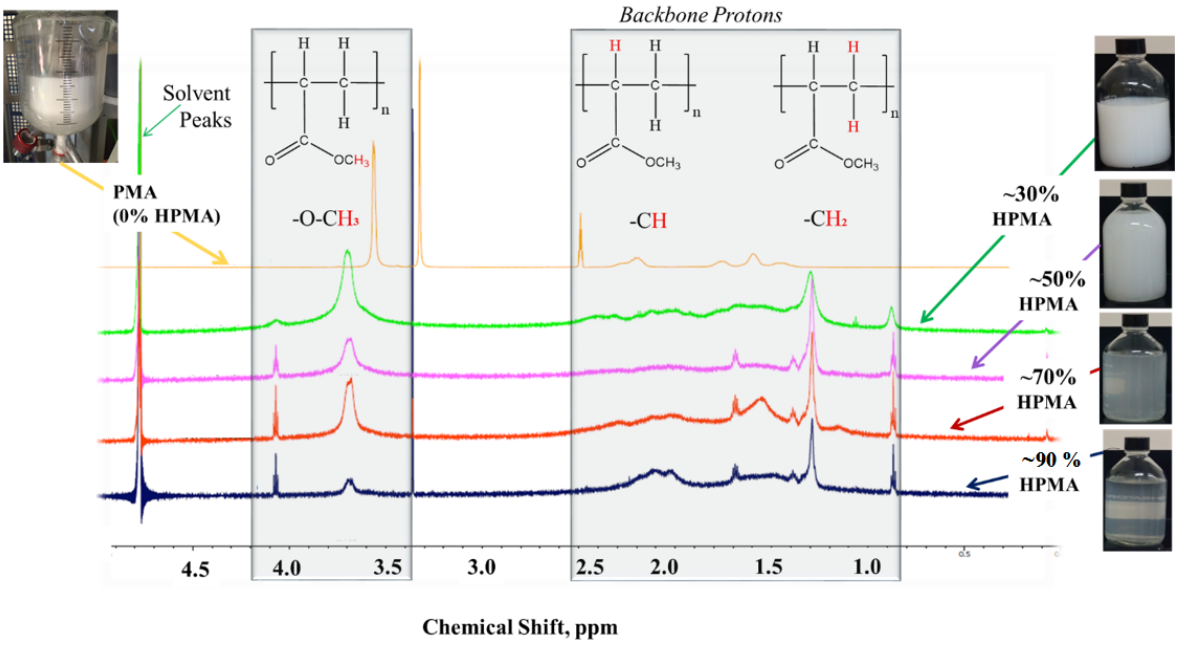

Figure 3-7: *^{1}H-NMR analysis of HPMA and the corresponding change in solubility for relatively high MW samples (1.17.10^{-4} M KPS).*

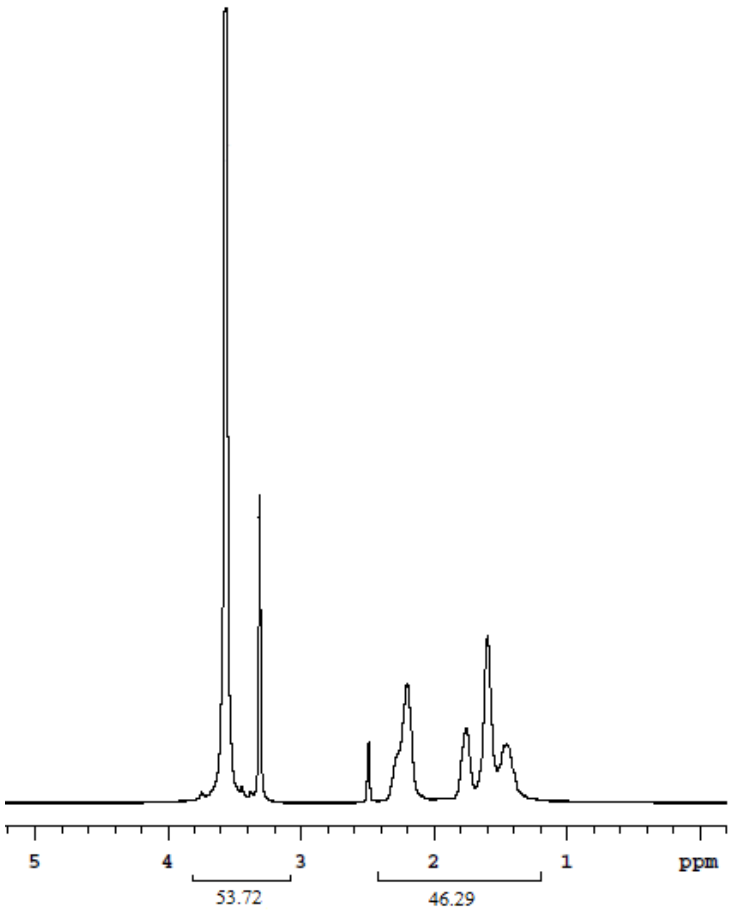

Figure 3-8: *^{1}H-NMR of unhydrolyzed PMA (0 % HPMA).*

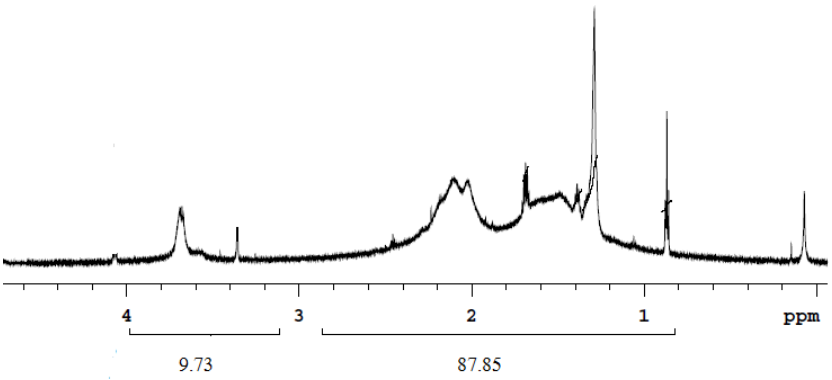

Figure 3-9: *^{1}H-NMR of highly hydrolyzed PMA (~90 % HPMA).*

3.3.2. DOH: Fourier-Transform Infrared Spectroscopy (FTIR)

FTIR is yet another technique that can be used to characterize both PMA and HPMA. This analytical technique works by identifying functional groups on the sample based on their unique infrared spectrum absorption across a wide wavelength range. The equipment used for our characterization was an Agilent Technologies Cary 600 Series FTIR Spectrometer with the scans set at 16 runs and using ATR (attenuated total reflection). All sample solutions were initially completely dried using a freeze dryer before FTIR analysis. Samples at different degrees of hydrolysis showed substantial changes in the FTIR spectrums corresponding to changes in functional groups due to hydrolysis. For instance, there was considerable change in the spectrum corresponding to the stretching vibrations of the carbonyl groups in esters (~1735 cm^{-1}) and carboxylates (~1579 cm^{-1} for asymmetric vibration and ~1406 cm^{-1} for asymmetric vibration).[139], [140] Spectrum signals from ester groups represented the methyl groups in PMA, whereas the carboxylate groups' signals were due to the hydrolyzed segments in HPMA. As can be seen from **Figure 3-10** and **Figure 3-11**, as hydrolysis progressed the signal from methyl group gradually disappeared while the carboxylate signal became stronger.

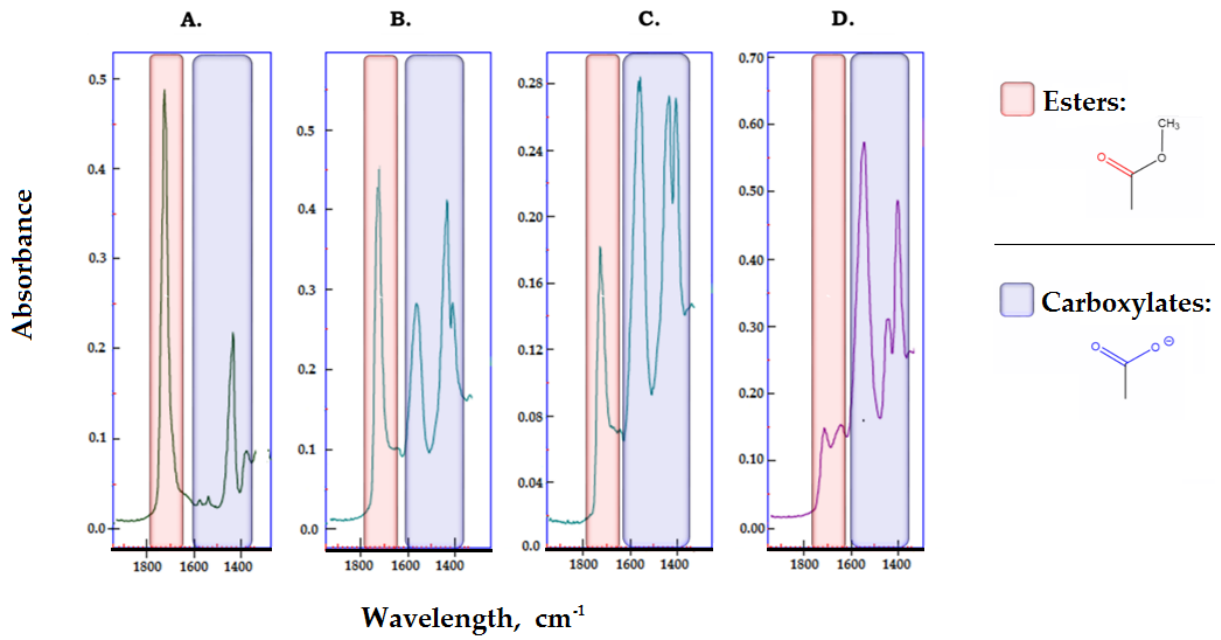

Figure 3-10:*Tracking the extent of hydrolysis by following the change in the FTIR spectrums corresponding to ester and carboxylate functional groups: (A) unhydrolyzed PMA (milky latex) (B) lowly hydrolyzed PMA (insoluble milky HPMA) (C) moderately hydrolyzed PMA (partly water-soluble translucent HPMA solution) and (D) highly hydrolyzed PMA (clear water-soluble HPMA solution)*

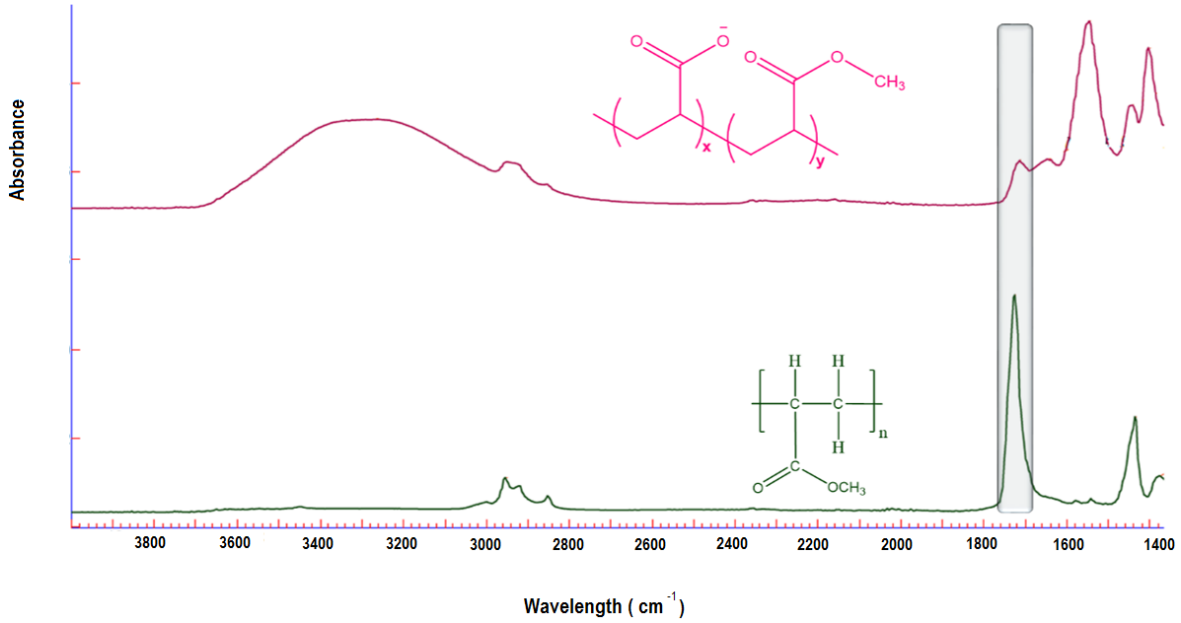

Figure 3-11: *Comparison between the FTIR spectrums of 0 % HPMA (Unhydrolyzed PMA) and ~90 % HPMA.*

3.3.3. Particle Size Analysis: Dynamic Light Scattering (DLS).

DLS, also known as quasi elastic light scattering (QELS) or photon correlation spectroscopy (PCS), was used to characterize the size of PMA latex particles. In emulsion polymerization, particle size analysis is usually used to determine the quality of latex polymer products and to calculate particle concentration (N) in kinetic studies. DLS was used after several failed attempts at using a field emission scanning electron microscope (FE-SEM) and a transmission electron microscope (TEM) for size analysis.

PMA possesses a T_g that is below standard room temperature, which makes it difficult to prepare dry samples for imaging at room temperature. Moreover, PMA samples are easily damaged by the electron beams used in FE-SEM and TEM. Ideally, imaging a PMA sample would require a cryo-SEM. Unlike the aforesaid imaging techniques, DLS, which is non-invasive and generally much easier to run, allowed us to directly characterize polymer particles in their dispersed latex form. This technique works by determining particle diffusion using scattered laser light from the Brownian motion of latex particles and converts this information to size and size distribution using the Stoke-Einstein equation. DLS results are primarily obtained in the form of intensity-weighted distributions and mean particle diameters (Z-average or Z_{ave}). The Z_{ave} values are synonymous with the particles' hydrodynamic diameter. By definition, the hydrodynamic

diameter is the diameter of a hard sphere possessing the same diffusion rate (or possessing an equivalent translational diffusion coefficient) as the particle being measured.[141]

A Zetasizer Nano ZSP equipment was used for DLS particle size analysis (**Figure 3-12A**). All test samples were first filtered through a 0.22 µm syringe filter to remove any traces of coagulum and dust particles. The samples were then diluted to form a near translucent suspension (about 2-3 drops in 20 ml DI water). The unimodal particle size intensity distributions that were obtained were all relatively narrow (**Appendix A** and **Figure 3-12B**) which, I suppose, is an indicator of desirable colloidal stability and, by extension, a confirmation that the surfactant concentration was sufficient. I also observed that low initiator concentrations (~10^{-4} M) yielded comparatively larger particle sizes than higher concentrations (~10^{-2} M) (**Table 3-2**). To better explain the trend in particle size we would need to replace the current *ab-initio* system with a *seeded* system and to also have a deeper understanding of the nucleation mechanism(s) and the reaction kinetics of this system.

Table 3-2: *A summary of particle size analysis results from DLS.**

Initiator Concentration, M	1.17 x10^{-4}	2.51x10^{-4}	1.58 x10^{-3}	1.00 x10^{-2}	2.14 x10^{-2}
Z_{AVE}, nm	121.5	113.8	106.8	101.0	100.3

Values in this table are averages of triplicate results shown in* ***Appendix A*

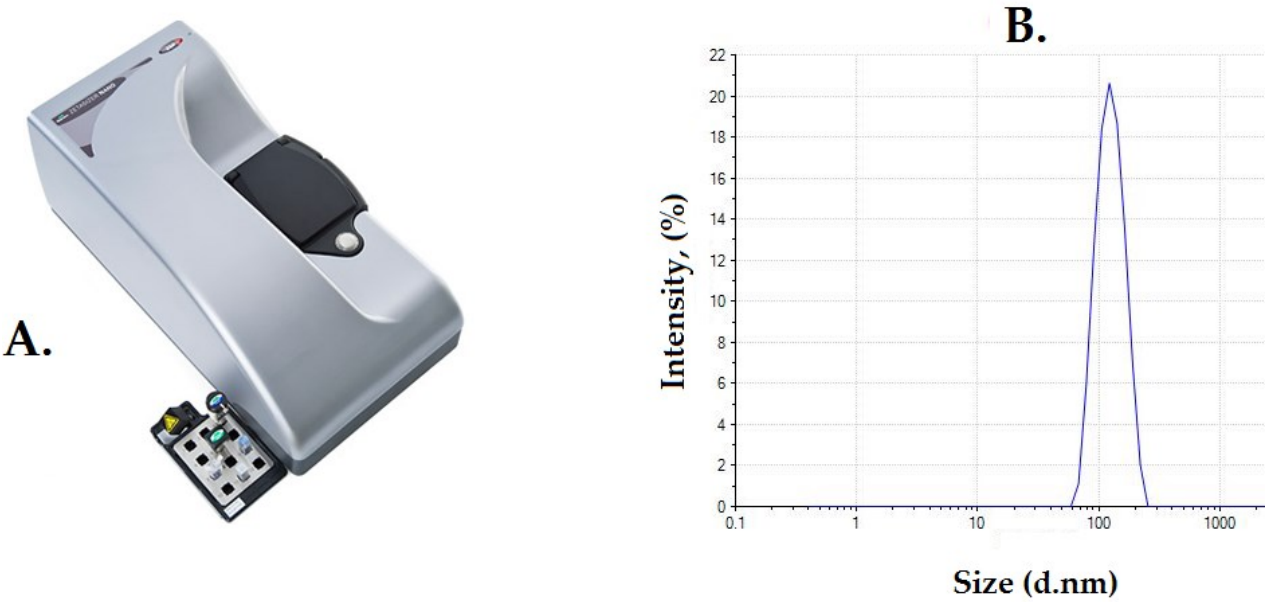

Figure 3-12: *(A) Zetasizer Nano ZSP.* [142] *(B) An intensity distribution of PMA particles at 1.17 x10^{-4} M KPS.*

3.3.4. Polymer Molecular Weight and Viscosity: FFF and Rheometry

High molecular weight polymers usually exceed the upper limit measurements of the commonly used gel permeation chromatography (GPC) columns. Therefore, to overcome this equipment limitation we used a field flow fractionation (FFF) column which is more reliable for high molecular weight measurements. Since PMA is insoluble in water and in common organic solvents such as THF, it was first hydrolyzed to water-soluble HPMAs. Tests were run at the two extremes of initiator concentrations where we expected the highest and lowest molecular weight values based on the inverse relationship discussed in Equations **(2-16)** and **(2-17)**. For comparison, we also measured the molecular weight of our reference industrial PAM. As expected, the lowest initiator concentration yielded polymers with molecular weights higher than those made with the highest initiator concentration.

Hydrolysis of hydrophobic PMA to water-soluble HPMA caused a drastic change in solution viscosity. The transition from a milky low-viscosity latex suspension to a highly viscous and clear HPMA solution corresponded with a massive swelling of the polymer solution. Viscosity of polymer solutions has been, for a long time, a subject of research interest in oil recovery. Therefore, we used literature from this field to explain our observations. Primary oil recovery and conventional waterflooding can leave about 67 % of the original oil in place (OOIP) still trapped in reservoirs. Viscous polymer-water solutions increase the sweeping efficiency, which in turn significantly raises the efficiency of oil recovery. Studies on the most commonly used polymer in enhanced oil recovery, PAM, have shown that water solutions of hydrolyzed PAM (HPAM) tend to have higher viscosities than those of corresponding unhydrolyzed PAM. As a result, very low concentrations of HPAM can still yield high viscosities – an economic and desirable aspect that is harnessed in oil recovery. High viscosity in HPAM solutions is attributed to electrical repulsions of negative carboxylate groups that result in chain extensions and an increase in their hydrodynamic volume.[143]–[146] Viscosity changes in HPMA solutions can similarly be interpreted within this framework. That is, the swelling of highly hydrolyzed PMA solutions is a consequence of inter- and intramolecular electrical repulsions of negative carboxylate groups leading to extension and dispersion of HPMA chains that were initially encapsulated in PMA latex particles.

A programmable Brookfield DV-III Rheometer was used to empirically quantify this change in viscosity. As expected, lowly hydrolyzed HPMA solutions hardly showed any change in viscosity, supposedly due to lack of sufficient negative carboxylate ions to facilitate the extension of the

polymer chains, leaving most of them still 'packed' in latex particles. Conversely, highly hydrolyzed PMA samples (water-soluble HPMAs) had viscosities that were much higher even at extremely low concentrations (0.1 wt. %). Viscosity measurements can also serve as a qualitative way to evaluate the molecular weight of equally hydrolyzed samples. In general, solutions of high molecular weight polymers are highly viscous.

Table 3-3: *MW measurements using an FFF.*

Sample	**Mw (g/mol)**	**PDI**
Reference PAM	17,540,000	3.40
HPMA (1.17 x10^{-4}M KPS); DOH ≅ 70 %	18,110,000	3.67
HPMA (1.17 x10^{-4}M KPS); DOH ≅ 90 %	16,980,000	3.95
HPMA (2.14 x10^{-2}M KPS); DOH ≅ 90 %	3,432,000	4.82
HPMA (2.14 x10^{-2} KPS); DOH ≅ 70 %	3,970,000	4.60

Table 3-4: *Viscosity measurements using a Brookfield DV-III rheometer.*

Temp=24.3ºC ; Mixing Rate =200 rpm ; Shear Rate =186 s^{-1}		
Sample	**Concentration, wt. %**	**Viscosity, cP ≡ mPa.s**
PMA (1.17 x10-4 M KPS); Unhydrolyzed	Undiluted	~2
Reference PAM	0.1	22.3
HPMA (1.17 x10^{-4}M KPS); DOH ≅ 70 %	0.1	22.5
HPMA (1.17 x10^{-4}M KPS); DOH ≅ 90 %	0.1	17.2
HPMA (2.14 x10^{-2}M KPS); DOH ≅ 70 %	0.1	12.6
HPMA (2.14 x10^{-2}M KPS); DOH ≅ 90 %	0.1	10.3

4) Flocculation Studies

4.1) MFT Characterization

MFT was obtained from Suncor and was characterized as summarized in **Table 4-1**. Additional characterization included a dean stark analysis to verify the MFT composition (**Table 4-2** and **Figure 4-1**) and an ions analysis using atomic adsorption spectroscopy (AAS) (**Table 4-3**). The instrument used for AAS was a VARIAN 220 FS atomic absorption spectrophotometer. MFT composition (mineral solids and bitumen content) results obtained from dean stark analysis were congruent with the characterization results from Suncor. As expected, ions analysis results showed predominantly high sodium ions in both the MFT and process water which is mainly due to the use of caustic additives in surface mining. The process water analyzed herein was also successfully used to hydrolyze PMA in a trial test. The use of recycled water in the production of HPMA flocculant is a potential benefit that might be harnessed in the future after resolving problems associated with supernatant turbidity.

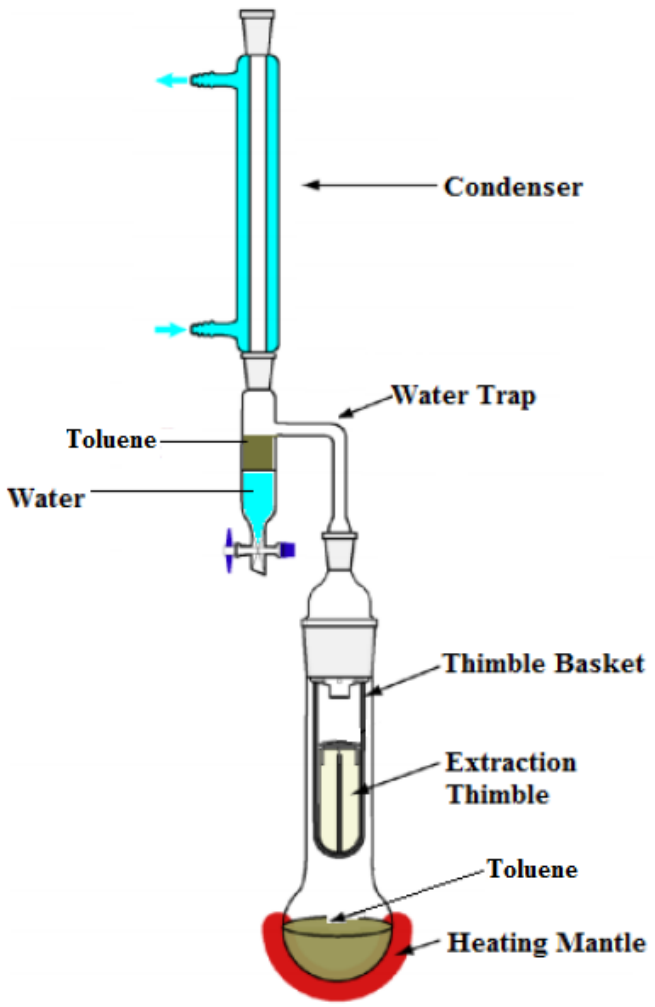

Figure 4-1: *A Dean-Stark apparatus. [33]*

Table 4-1: *MFT properties as characterized by Suncor.*

Label	Mineral Solids (Wt. %)	Bitumen (Wt. %)	Clay Mineral (Wt. %)	CWR	SFR	Bulk Density (kg/m3)	pH	Conductivity (µs/cm)
ES-2575	33.32%	1.2%	82.3%	0.419	0.013	1253	8.0	2667

Table 4-2: *Results from Dean-Stark analysis*

Bitumen (wt. %)	Water (wt. %)	Solids (wt. %)
1.10	65.10	33.80

Table 4-3: *Results from atomic adsorption spectroscopy*

MFT Water Ions Analysis (ppm)			
Na^+	K^+	Ca^{2+}	Mg^{2+}
938.0	16.1	24.4	10.6
Process Water Ions Analysis (ppm)			
Na^+	K^+	Ca^{2+}	Mg^{2+}
905.0	12.0	16.7	10.5

4.2) Statistical Models and Flocculation Tests.

The responses (output variables) in our CCD were typical key flocculation parameters: capillary suction time (CST), supernatant turbidity, and initial settling rate (ISR). A multivariable linear regression analysis was used to model these responses and obtain statistical models showing the effects of the input variables (predictors) on our flocculation parameters (responses variables),

$$Y_i = b_o + \sum_{1}^{n} b_i X_i + \sum_{1}^{n} b_{ii} X_i^2 + \sum_{1}^{n-1} \sum_{i+1}^{n} b_{ij} X_i X_j \qquad \textbf{(4-1)}$$

For flocculation, 100 g MFT (diluted using DI water to 10 wt. % based on solids content) was transferred to 250 ml glass beaker (diameter of 7 cm). The diluted MFT sample was mixed at 400 rpm for 2 minutes using an overhead electric mixer with a three-star axial impeller (diameter of 5 cm) so as to obtain a homogeneous slurry. A coagulant solution of Ca^{2+} from $CaCl_2$ was added (2000 ppm Ca^{2+} based on solids) and the slurry was mixed again for 1 minute at 400 rpm. HPMA flocculant was then added and mixed at 200 rpm until the polymer was evenly dispersed and visible flocs emerged. The mixing rate was lowered to 200 rpm on adding HPMA because the flocs formed were shear sensitive and relatively easy to break at high shear. The shear sensitivity, we suppose, is due to the elastomeric nature of PMA as characterized by its low T_g. The values of the output variables that were used in the CCD were those obtained at approximated optimal polymer dosages (polymer dosages corresponding to the lowest CST value) as shown in **Appendix D**.

4.2.1. Capillary Suction Time

CST is a flocculation parameter that is usually used to quantify the dewatering ability of treated MFT. The equipment used to measure CST was a Type 319 Multi-CST Triton apparatus fitted with Triton filter papers (7 cm × 9 cm) (**Figure 4-2**). This equipment records the time taken for water released from polymer-treated MFT slurries to pass through two electrode sensors, from R_1 to R_2 (**Figure 4-2C**), as it travels radially through an absorbent filter paper. The shorter the CST time recorded, the better the dewaterability. Our initial hypothesis suggested that HPMA would have better dewatering ability than commercial PAM-based flocculants due to its inherently hydrophobic backbone. Therefore, this output variable also offered a quantitative way to empirically verify our hypothesis. The trend in CST results also helped us approximate where the optimal polymer dosage lies. Overdosing of the flocculant results in a gel matrix that blocks water-

release pathways, which, consequently, results in higher CST values. **Figure 4-3** shows the typical rise in CST past the optimal dosage due to 'overdosing. CST values that were used were obtained from an average of three measurements from three separate 5 ml aliquots of the treated MFT.

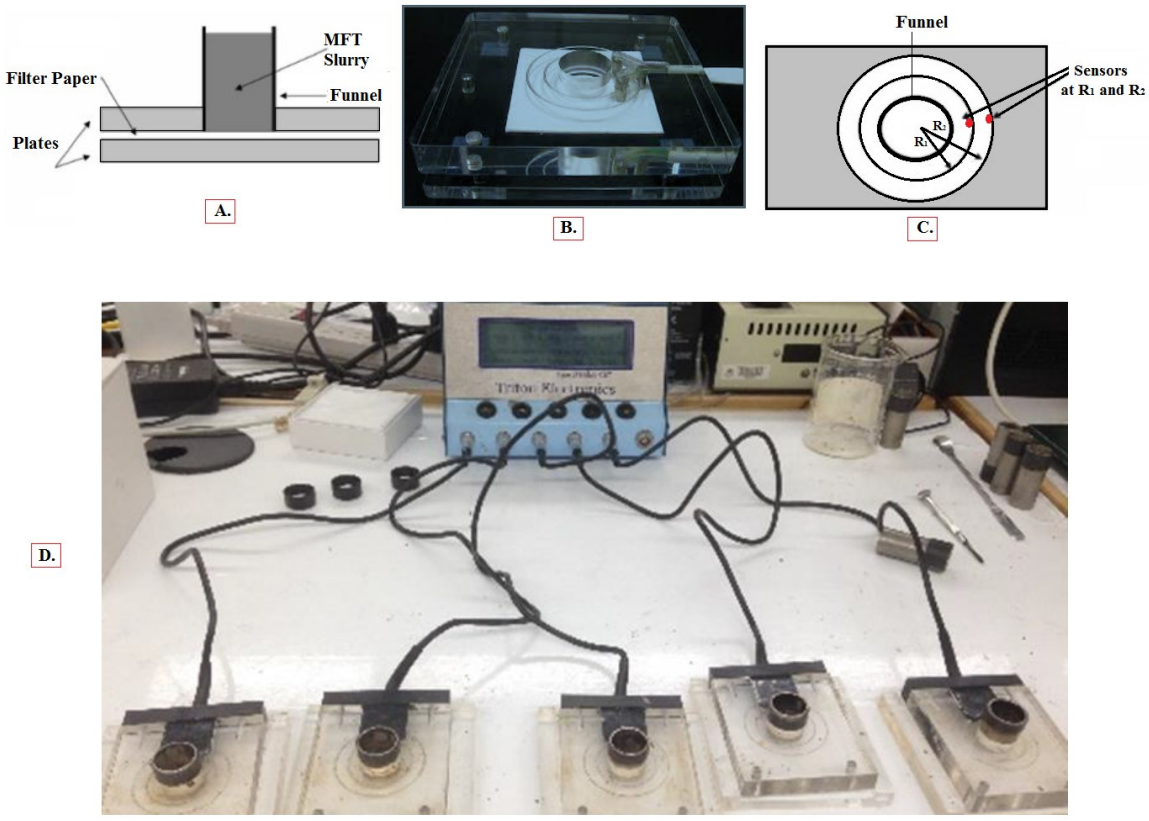

Figure 4-2: *(A) A schematic of a side view profile, (B) an actual single cell fitted with a filter paper, (C) top view profile and (D) and a complete view of a Type 319 Multi-CST apparatus. [33]*

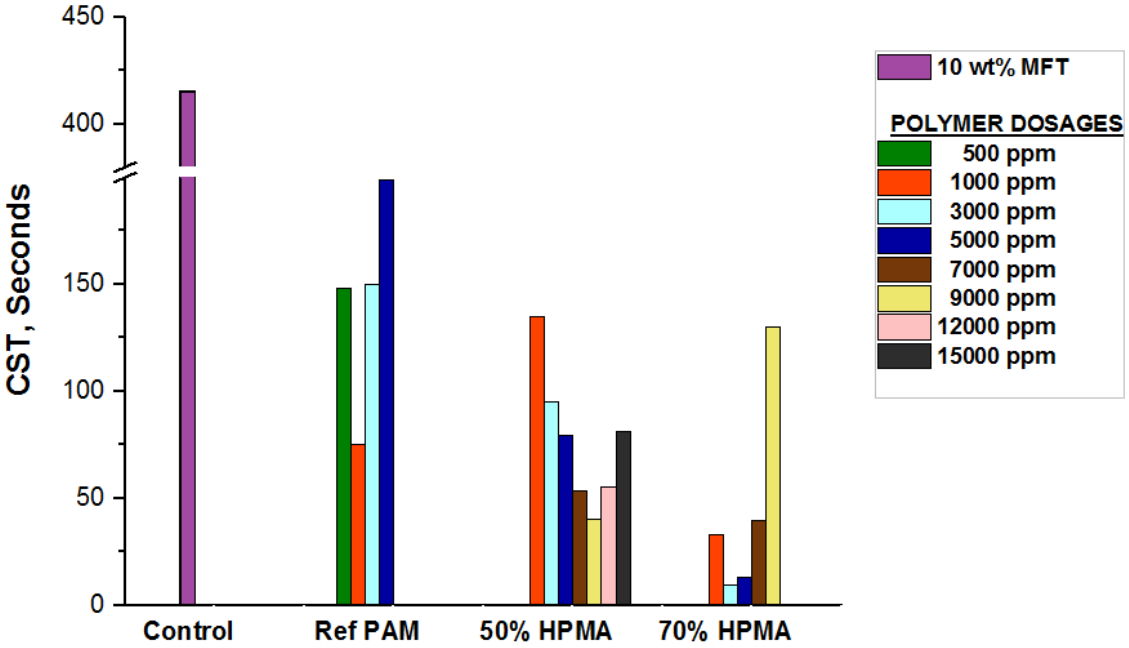

Figure 4-3: *CST values from: diluted MFT (control); reference commercial PAM; 50 % HPMA ($1.58x10^{-3}$M, KPS) and 70 % HPMA ($1.58x10^{-3}$M, KPS).*

Initiator concentration (MW) was statistically insignificant in relation to this response variable and the only significant predictor was the DOH. After dropping the insignificant variable, we obtained the following empirical model that was based on coded factors,

$$\mathbf{CST = 13.83 - 30.30\ DOH - 17.96\ DOH^2} \qquad \textbf{(4-2)}$$

The surface response and the corresponding contour profile of the CST model are shown on **Figure 4-4** and **Figure 4-5**, respectively. According to this model, as the DOH was lowered below water-solubility (~50%) there was a significant increase in both the CST values and the polymer dosage used. These observations, we suppose, can best be understood by referring back to the brief discussion in the previous chapter on the significance of carboxylate groups in HPMA. In summary, we concluded that the lower the DOH, the fewer the anionic active-sites, the poorer the extension of polymer chains and the lower the chains' water-solubility. As a result, in lowly hydrolyzed PMA grades floc formation was poor due to the limited flocculation sites. Also, low water-solubility and poor chain extension avail only a fraction of the polymer for flocculation in aqueous media and this, we suggest, explains the need of higher dosages to make up for the deficiency. In general, CST test results showed that water-soluble HPMA grades outperformed the reference commercial PAM (**Figure 4-3**) as initially predicted in our hypothesis.

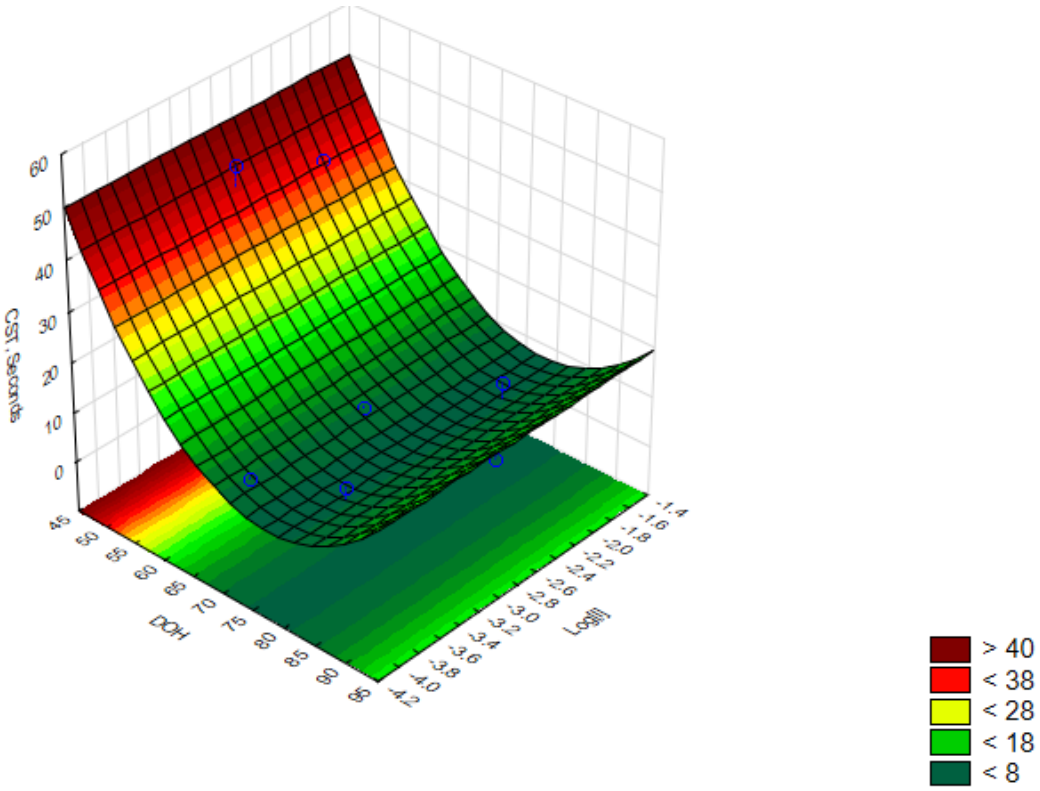

Figure 4-4: *Modeled CST surface response as a function of DOH and initiator concentration.*

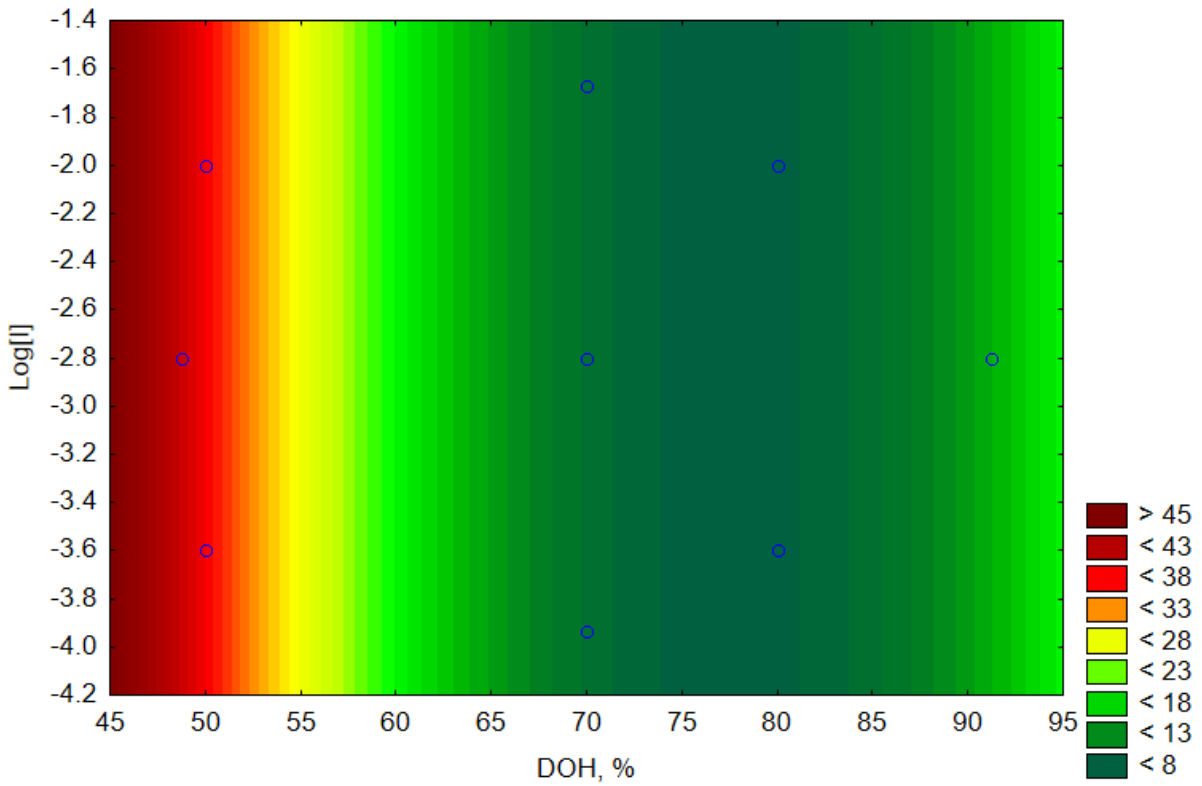

Figure 4-5: *A contour plot of the CST surface response as a function of DOH and initiator concentration.*

Moreover, the values of the coefficients of determination (R^2 and R^2_{adj}) for this model were quite high, which indicates that the model was able to capture most of the variation from this response (**Figure 4-6**). The model also met the basic regression assumptions of normality (See **Figure 4-7**) and unpredictability/non-linearity (See CST residual plot - **APPENDIX E**) in the residuals.

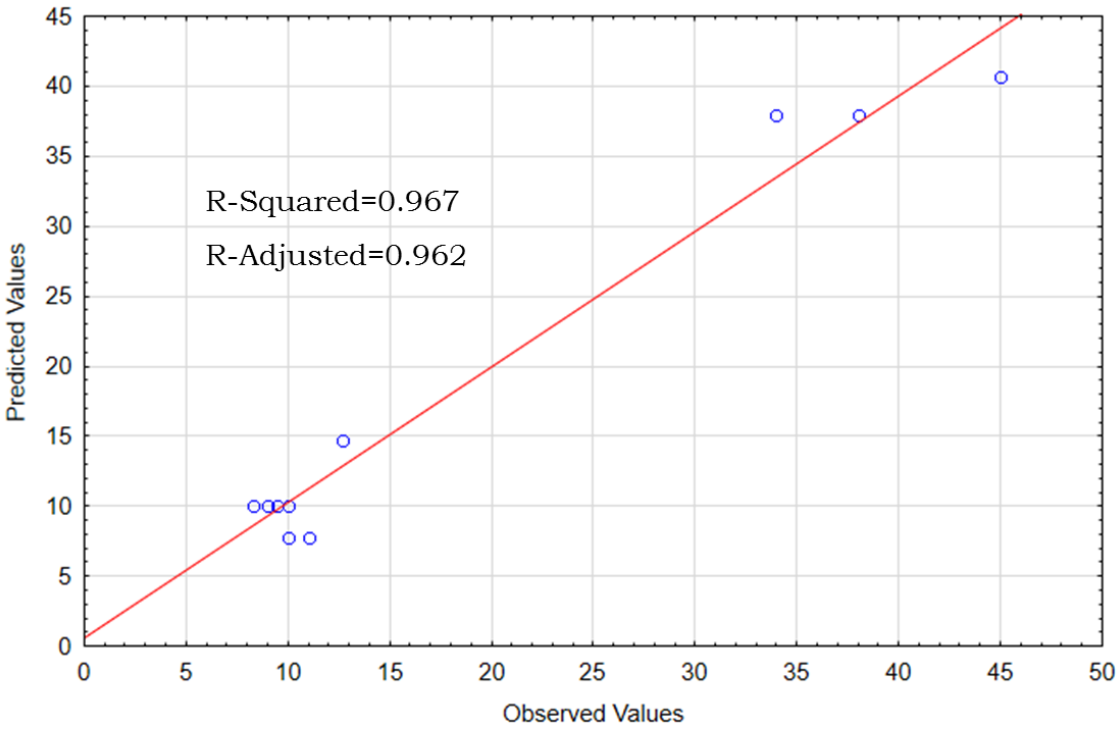

Figure 4-6: *Observed versus predicted values for the CST model.*

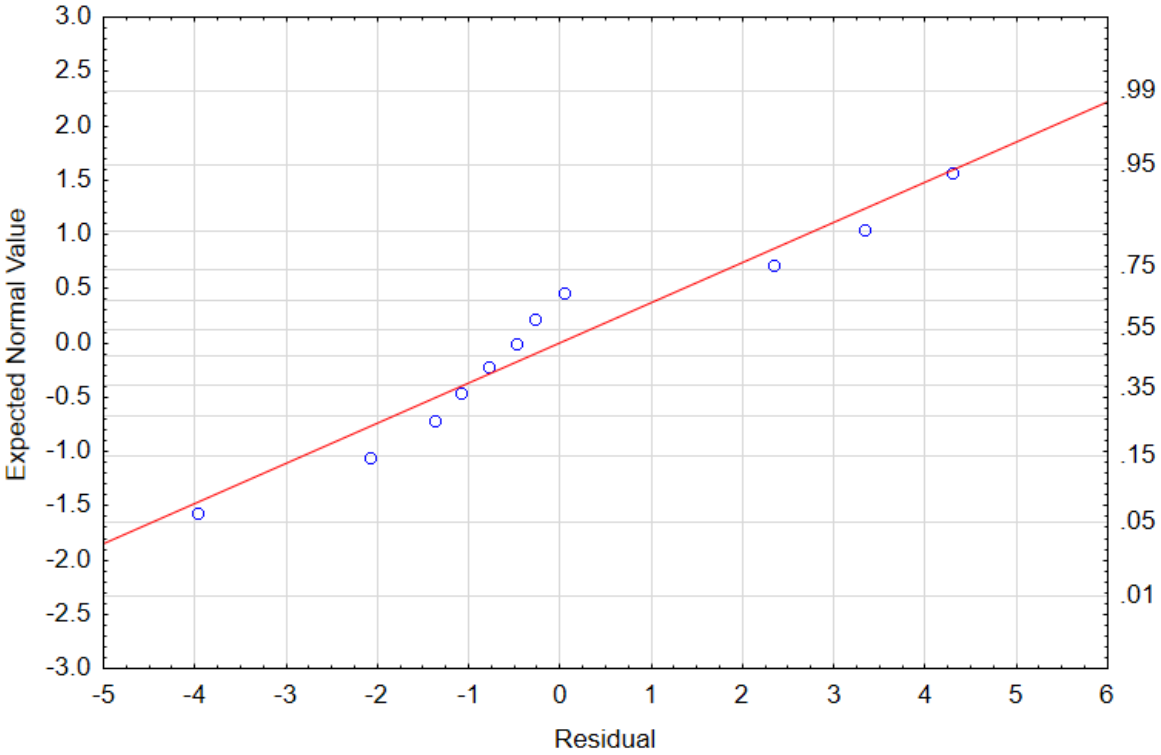

Figure 4-7: *Normal plot of the CST model*

4.2.2. Supernatant Turbidity

Supernatant turbidity was a particularly important parameter, as the results obtained with HPMA were significantly higher than those from the reference PAM. High supernatant turbidity is an undesired outcome as it indicates poor fines capture, which, by extension, negatively impacts on the quality of the recovered water. Turbidity measurements were run using a 2100 AN Hach turbidimeter after 24 hours of flocs sedimentation in 100 ml measuring cylinders. Turbidity values used for the CCD were obtained from the supernatant of samples corresponding to the optimal CST values.

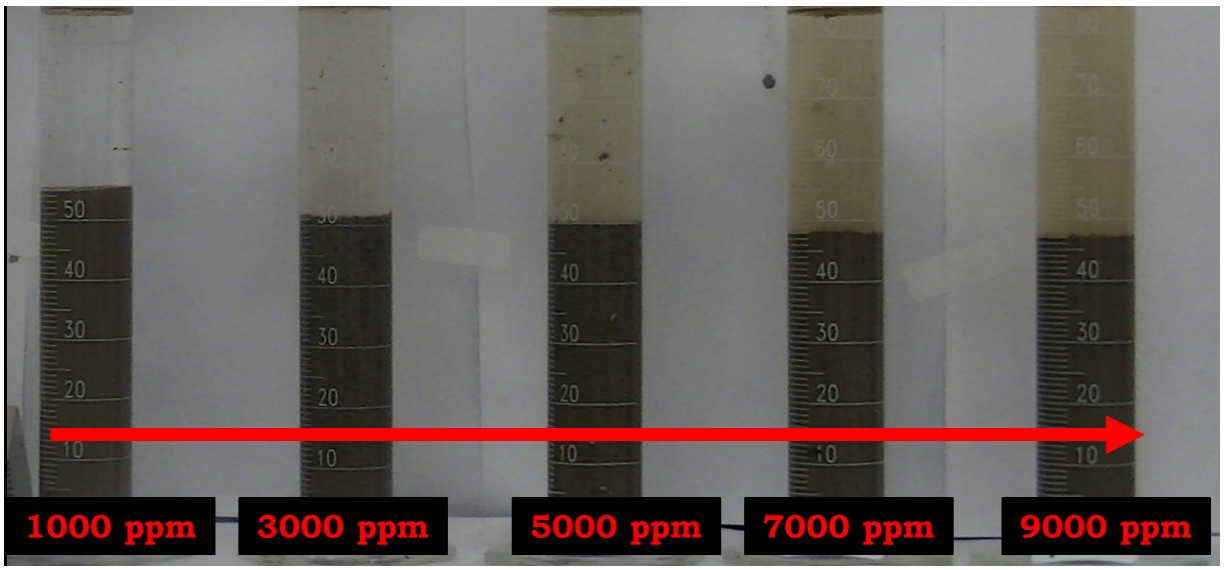

Figure 4-8: *An illustration of the typical increase in supernatant turbidity that was observed with increase in HPMA dosage.*

Supernatant turbidity worsened with increase in HPMA's dosage - an observation that was consistent in all cases regardless of the DOH (**Figure 4-8**). However, when the polymer dosage was held constant, we observed that HPMA flocculants with high DOH yielded more turbid supernatants than the lowly hydrolyzed variations. Based on these experimental observations, we came to the conclusion that turbidity was tied to an inherent property of the flocculant, namely the DOH. And on closer look at the DOH, we realized that the hydrolyzing agent, NaOH, was almost certainly the main cause of this undesired turbidity. Studies in various fields have confirmed the dispersive effect of sodium ions on clays (**Figure 4-9**).[47], [147]–[149] According to these studies, presence of a high amount of exchangeable sodium ions is considered to be the main reason for dispersivity in clay soils. Sodium ions have a relatively high hydration radius but, unlike calcium, they have a low valence charge and consequently their *charge sparsity* (CS) *index* (ratio of hydrated ionic radius to valency) is comparatively much higher. According to Thadeu et al. the

higher the CS index of a cation the poorer its ability to neutralize clay surface charge and the higher its dispersive effect on clays (**Table 4-5**).[3], [149], [150]

Table 4-4: *Key properties that influence clay dispersity.* [149], [150]

Cations	Hydrated ionic radius (HIR), 10^{-10} m	Valence	Charge Sparsity (CS), 10^{-10} m
Ca^{2+}	4.12	2	2.06
Mg^{2+}	4.28	2	2.14
K^{+}	3.31	1	3.31
Na^{+}	3.58	1	3.58

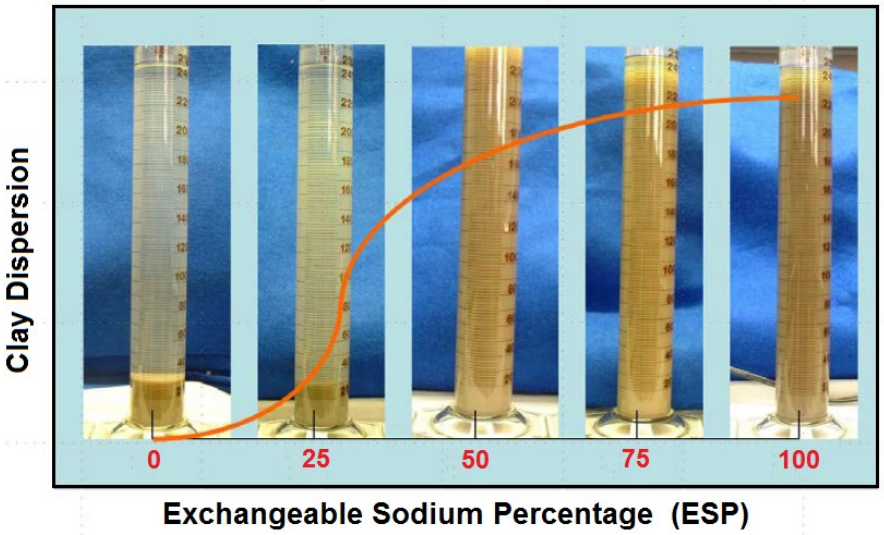

Figure 4-9: *Clay colloidal dispersion (turbidity) due to increase in exchangeable sodium content.[5]*

It is also known that pH plays a significant role in clay dispersion (**Figure 4-10**).[148] However, in our case, MFT maintained a pH that was relatively constant even after high dilution with DI water. Stable pH in MFT is thought to be a result of strong buffering from bicarbonate ions that form when hydroxyl ions, from caustic additives in MFT, react with absorbed atmospheric CO_2 in tailing ponds. So, with pH being constant, the other key variable that could affect fines capture in our case was the sodium content mostly from the hydrolyzing agent and partially from the surfactant. As can be seen from **Figure 4-11A**, at the *typical MFT pH* (~8), sodium-treated clays have a high surface charge that further enhances their electrostatic stability and encourages their dispersion. At this same pH (~8), calcium ions have a coagulative effect on fines (**Figure 4-11A**). And increasing Calcium dosage counters the dispersive effect of sodium ions, which might explain why we required a comparatively high calcium dosage in our flocculation tests (**Figure 4-11B**) .[42], [47]

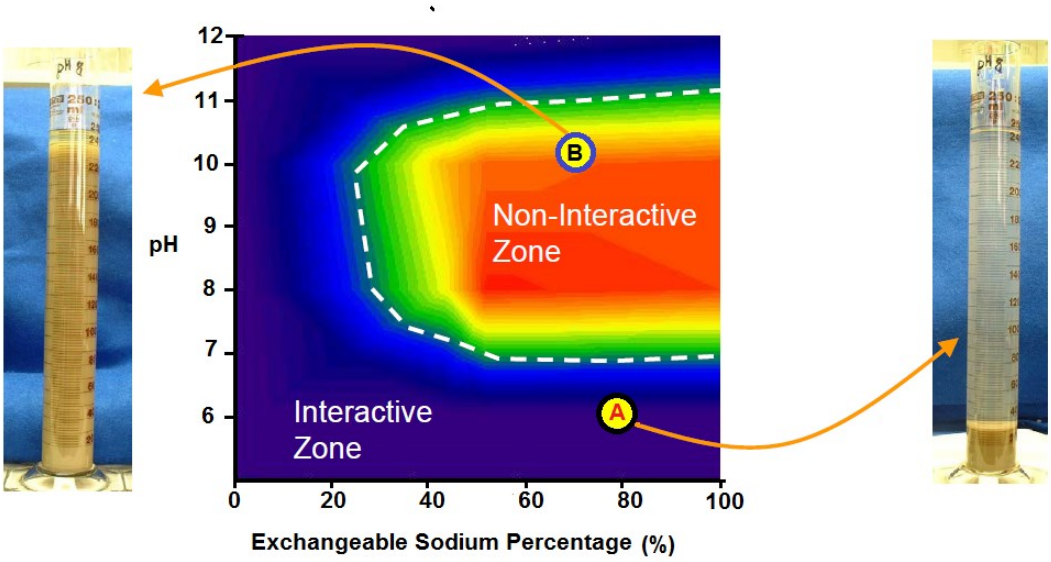

Figure 4-10: *Illustration of the dual effect that pH and sodium content have on clay colloidal dispersion. [42], [148]*

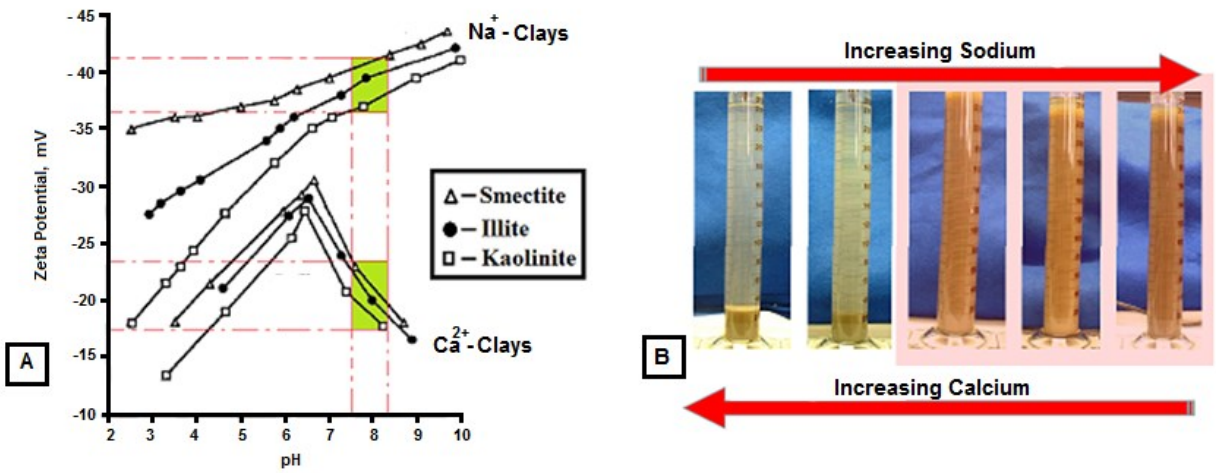

Figure 4-11: *(A) An illustration of the diametrically opposed effects that calcium and sodium ions have on the surface charge of clay minerals at the typical MFT pH (~8).[47] (B) Clay coagulation and dispersion resulting from an increase in calcium and sodium ions.[5], [148]*

$$\textbf{Turbidity} = 38.9 - 4.6\,\text{Log}[\text{I}] - 18.7\,\text{DOH} + 8.0\,\text{DOH}^2 \qquad \textbf{(4-3)}$$

In our statistical model, the DOH and the initiator concentration (MW) were both significant predictors in relation to this response. Equation **(4-3)** shows the resulting regression model based on coded factors. However, it is worth noting that the predictor variables where not equally significant - the DOH had predominantly higher influence on turbidity (**Figure 4-12**).

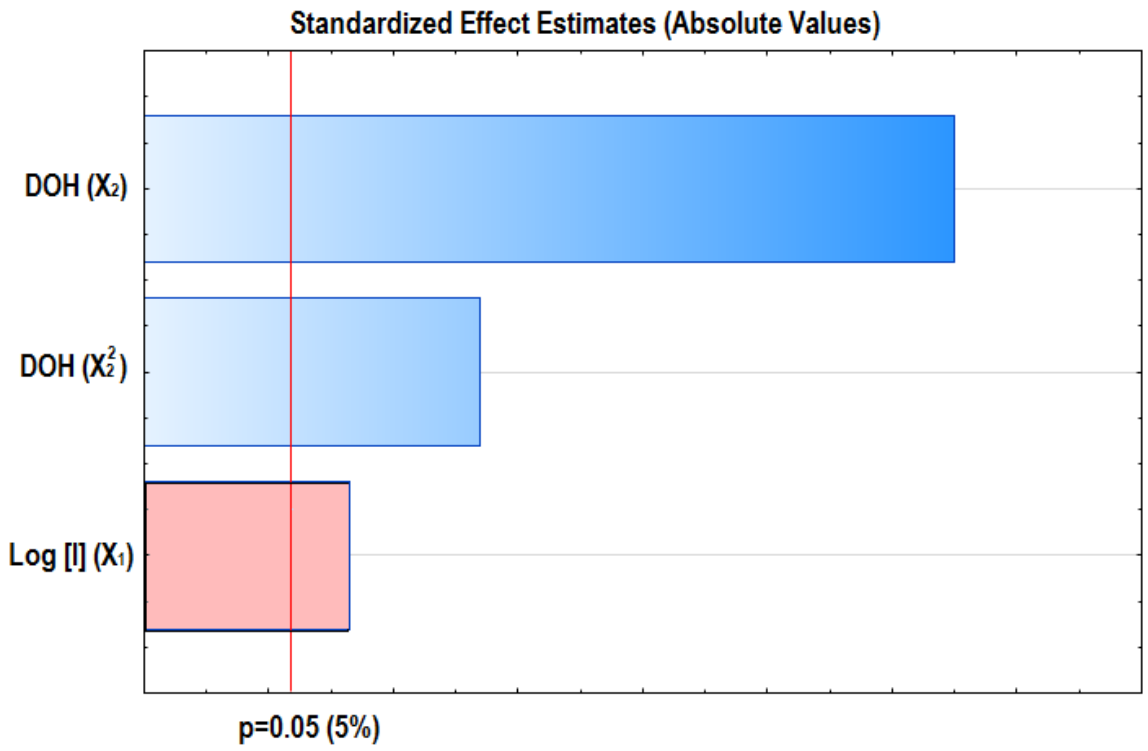

Figure 4-12: *A Pareto chart of standardized significant predictor variables.*

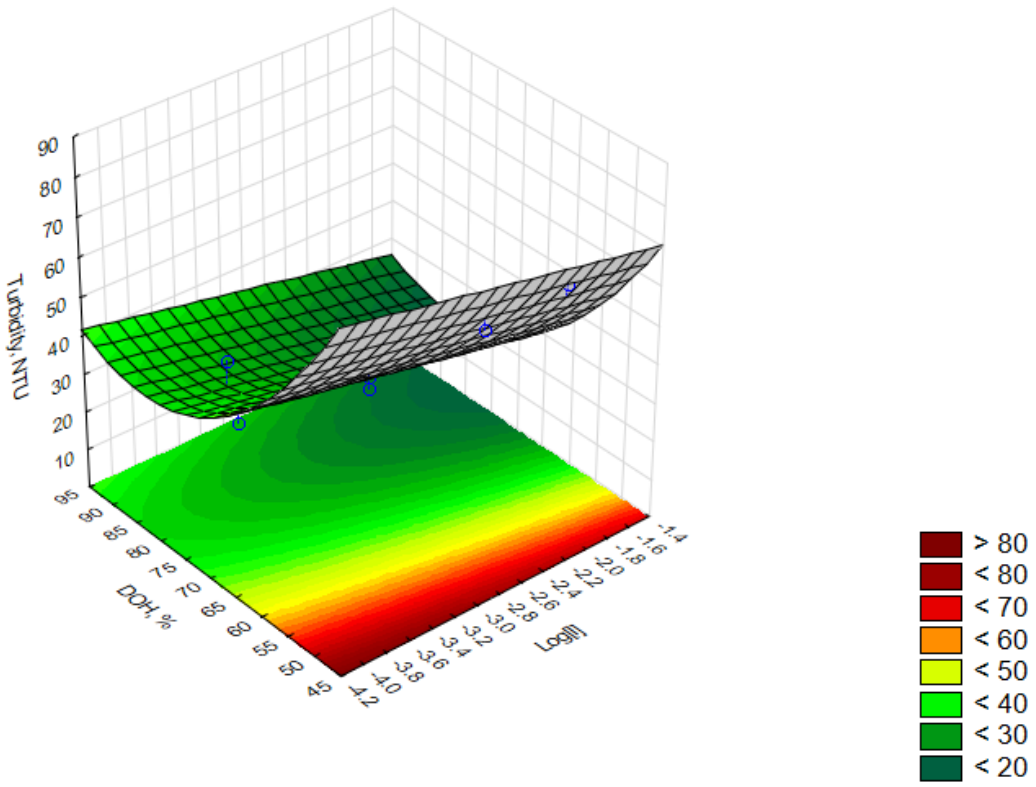

Figure 4-13: *Surface response of supernatant turbidity as a function of DOH and initiator concentration.*

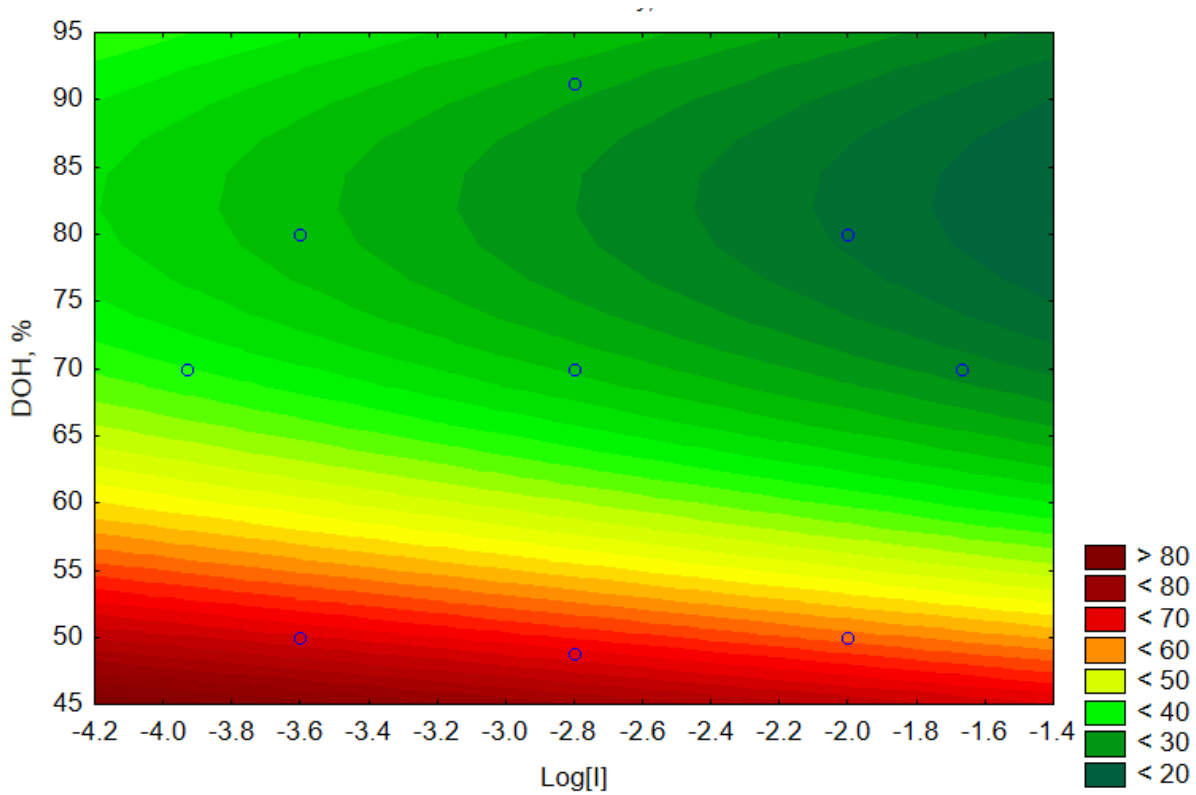

Figure 4-14: *A contour plot of the surface response of supernatant turbidity as a function of DOH and initiator concentration.*

As shown on the surface response (**Figure 4-13**) and contour profile (**Figure 4-14**) of the turbidity model, turbidity increased with decrease in DOH and decrease in initiator concentration. The higher turbidity at low DOH, we suppose, was due to the fact that higher polymer dosages were required to attain acceptable dewaterability, thus, resulting in a higher overall sodium content. Turning to other significant predictor, initiator concentration, we attributed the high turbidity values to poor fines capture associated with chains entanglement at high MW and/or the extra sodium hydroxide used to hydrolyze high MW chains. Fortunately, in all cases, supernatant turbidity was still relatively low at the polymer dosages that yielded optimal CST values.

The model's R^2 and R^2_{adj} values, which are statistical measures of how accurate the model is at capturing variations of the response variable, were desirably high (**Figure 4-15**). The model also met the regression assumptions of normality, as shown by the probability plot (**Figure 4-19**), and stochastic error, as shown by the turbidity residual plot (**APPENDIX E**).

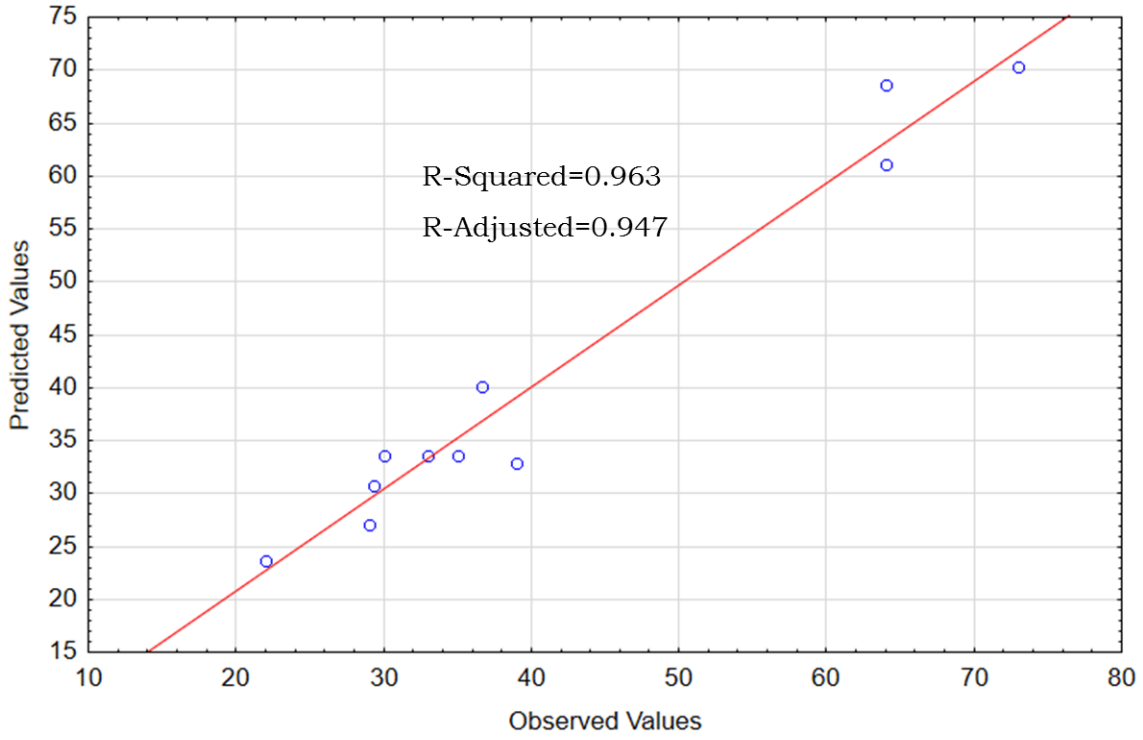

Figure 4-15: *Observed versus predicted values for the turbidity model.*

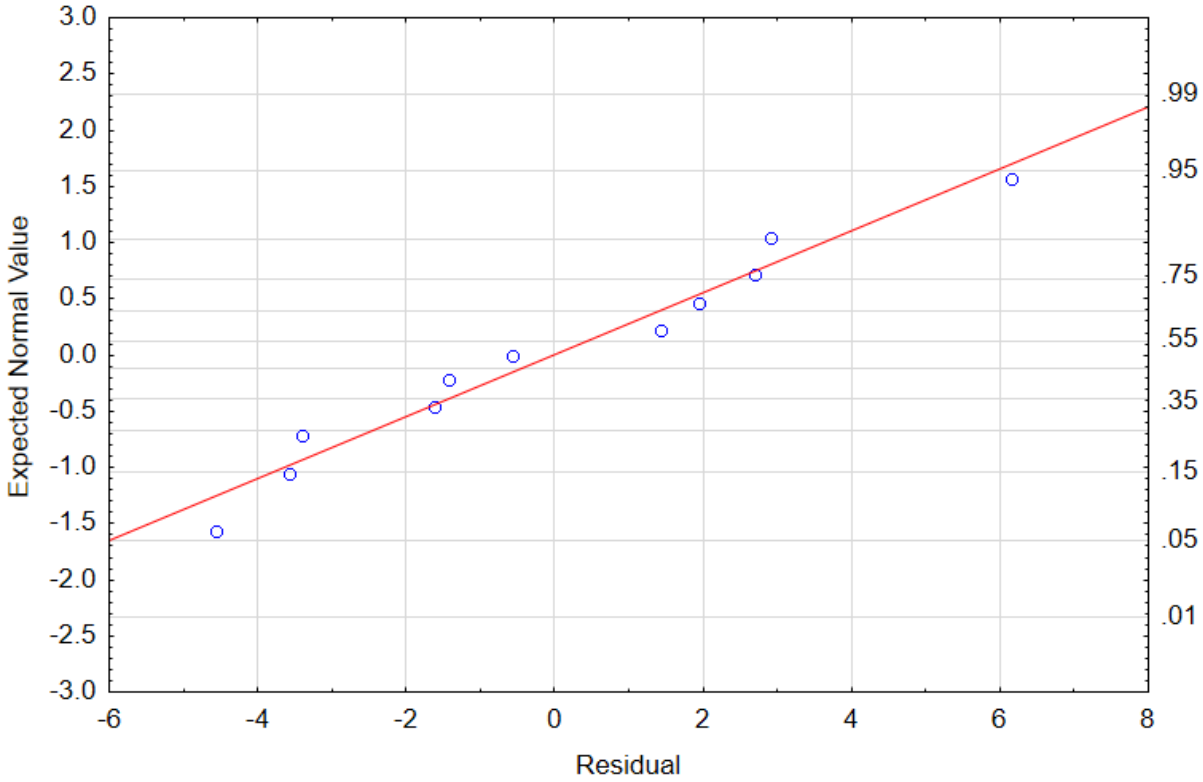

Figure 4-16: *Normal plot of the supernatant turbidity model.*

4.2.3. Initial Settling Rate (ISR)

This flocculation parameter, as the name suggests, determines the initial rate of floc sedimentation by following the change in the mudline (water-flocs interface) as the flocs settle immediately after flocculation. We calculated ISR values using the plots of the initial change in the mudline as a function of time. To be more precise, using the gradient of the linear part of the slopes from these plots. Generally, in alignment with the already discussed concept of polymer-induced flocculation, high MW flocculants with multiple binding sites form larger and denser flocs. And, congruent to Stokes' Law approximation, such flocs settle faster via gravitational sedimentation and, consequently, have higher ISR values.

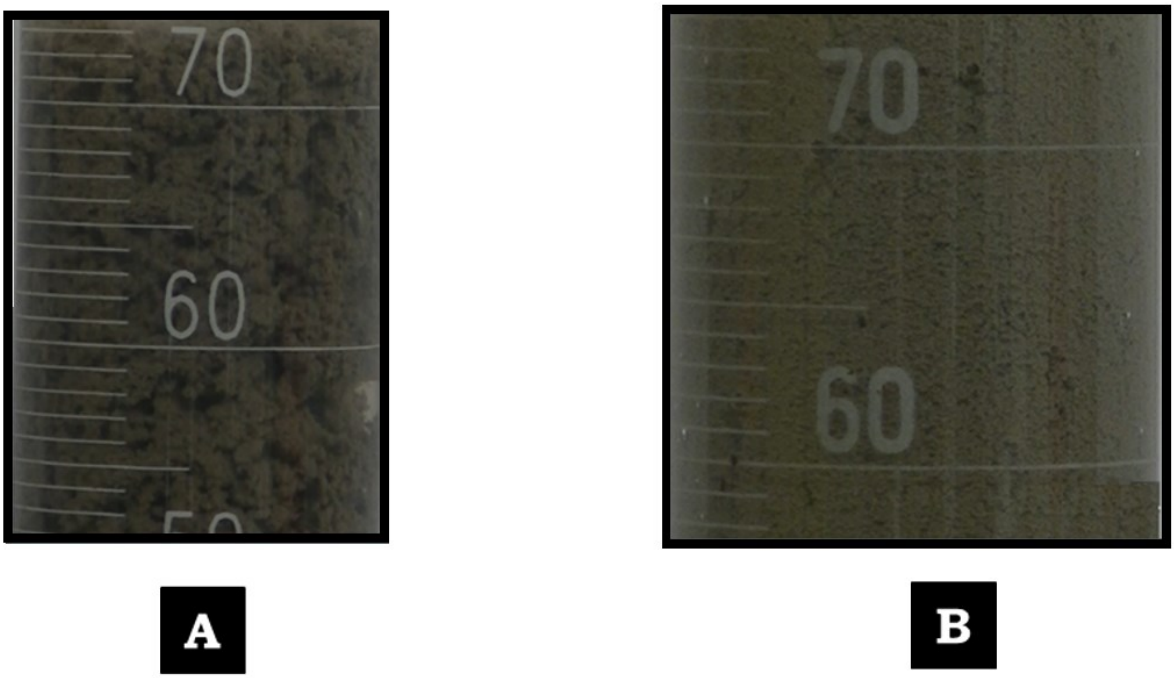

Figure 4-17: *The difference in floc size between two HPMA flocculants of equal dosage and hydrolyzed from the same PMA batch (1.58x10^{-3}M, KPS) but to different DOH: (A) ~70 % HPMA and (B) ~50 % HPMA.*

The ISR response variable had both the DOH and the initiator concentration as significant predictors. The resulting regression model, based on coded variables and factoring in both predictors, is described by Equation **(4-4)**. The DOH was once again the predominant predictor variable as shown by the Pareto chart in **Figure 4-18**. Generally, HPMA flocculants with a higher DOH formed visibly larger flocs (**Figure 4-20**). Again, we posit that this leverage observed in HPMA grades with a higher DOH is due to their higher number of active flocculation-sites, greater chain-extension and better water solubility, all of which facilitate flocculation.

$$\mathbf{ISR = 127.5 - 13.5\,Log[I] - 12.0\,(Log[I])^2 + 55.2\,DOH - 34.1\,DOH^2} \qquad \textbf{(4-4)}$$

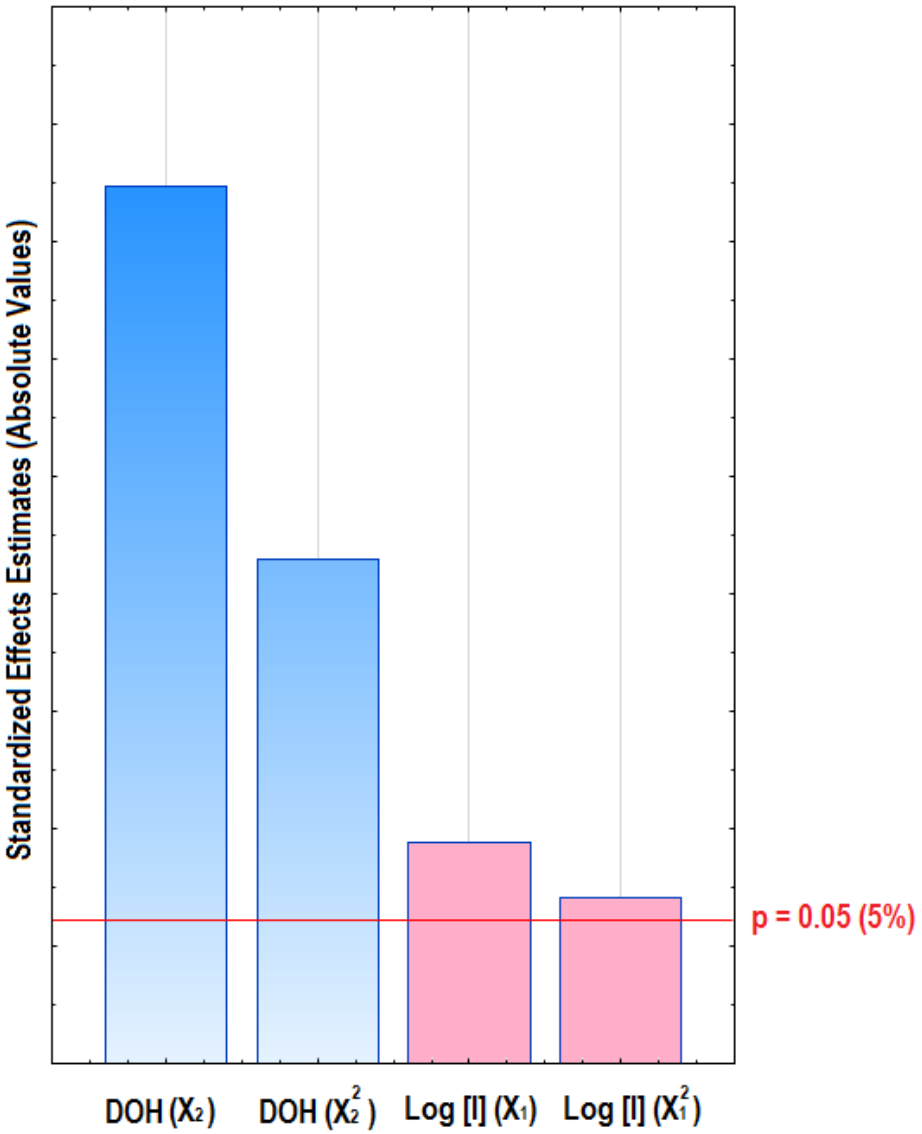

Figure 4-18: *A Pareto chart of standardized significant predictor variables for ISR.*

As expected, the ISR model showed that high molecular weight HPMAs with a moderately high DOH (water-soluble grades) had the highest settling rates (**Figure 4-19** and **Figure 4-20**). Therefore, based on this model and experimental observations, we can conclude that a DOH that enables water-solubility is sufficient to offer optimal flocculation results. Extensive hydrolysis (past solubility) seems to degrade the polymer (lower the molecular weight) and negatively affect flocculation. This model was also able to capture a high percentage of variation in ISR (**Figure 4-21**). The ISR model residuals adequately met the regression assumptions of normality and randomness as shown by the probability plot (**Figure 4-22**) and the residual plot (**APPENDIX E**), respectively.

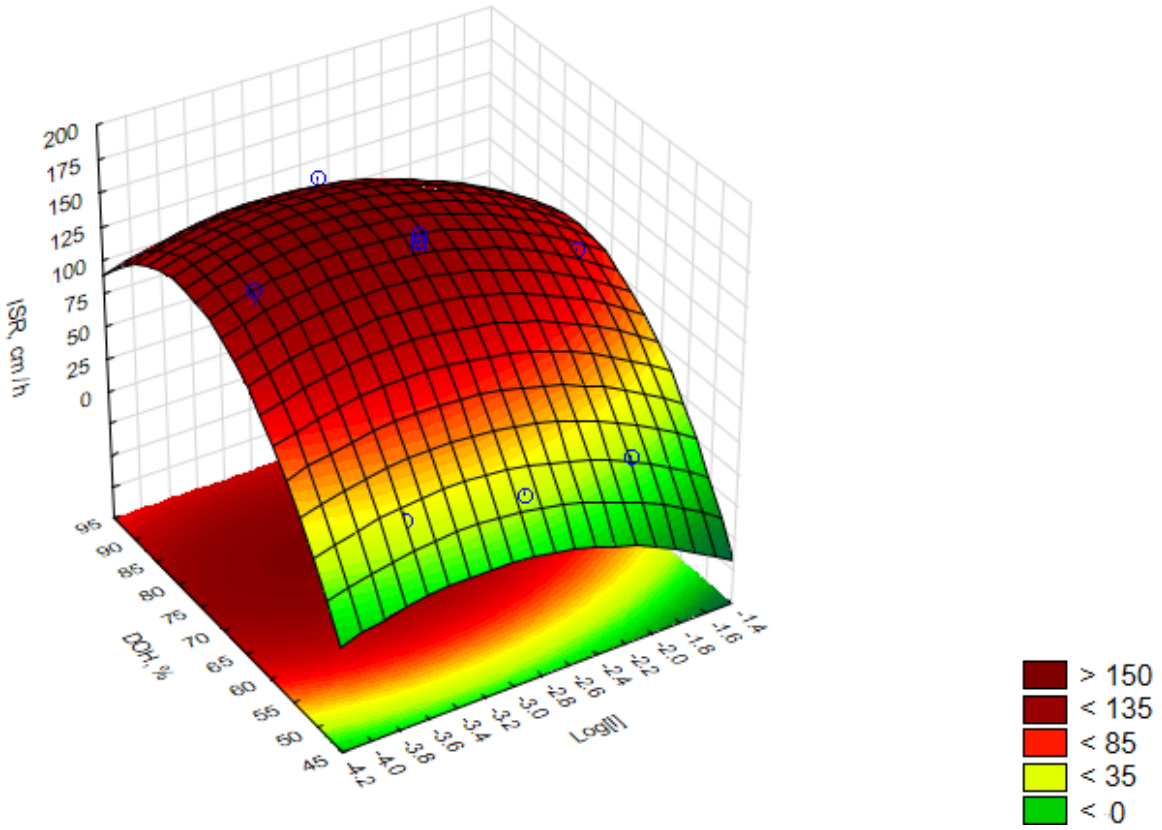

Figure 4-19: *Surface response of ISR as a function of DOH and initiator concentration.*

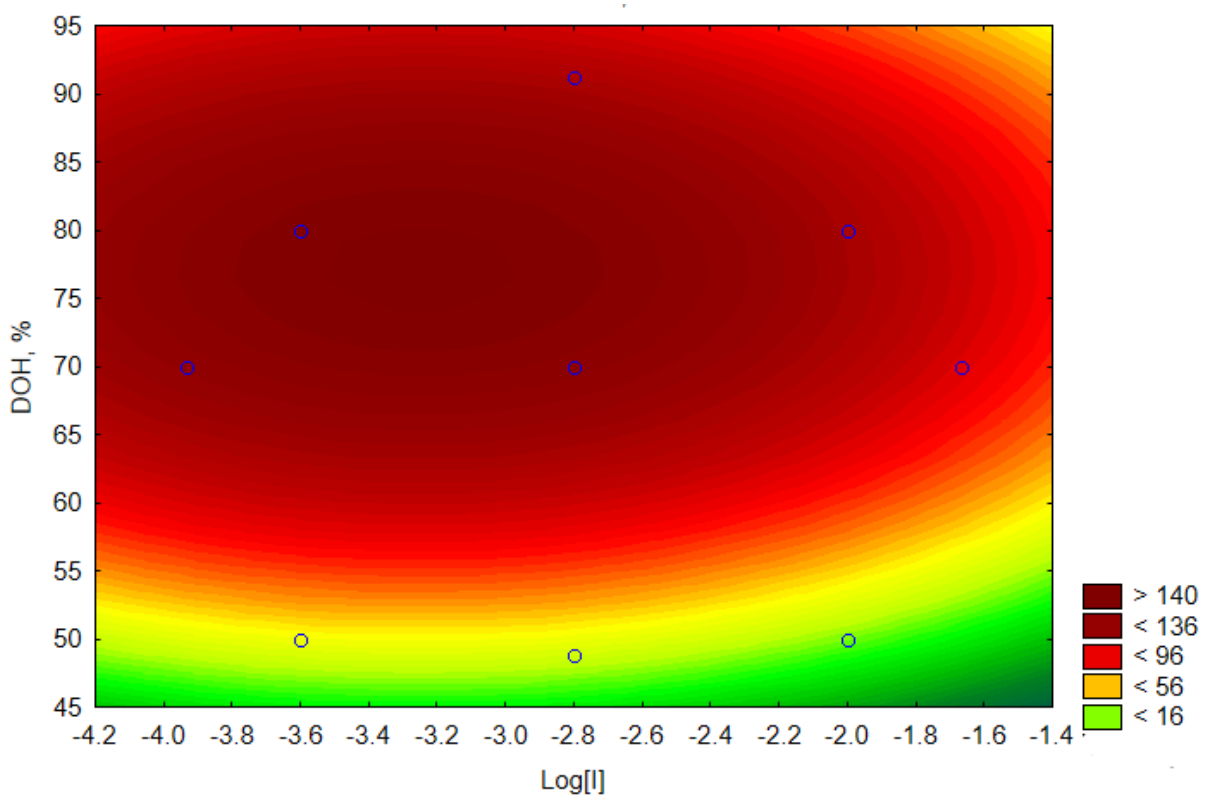

Figure 4-20: *A contour plot of the surface response of ISR as a function of DOH and initiator concentration.*

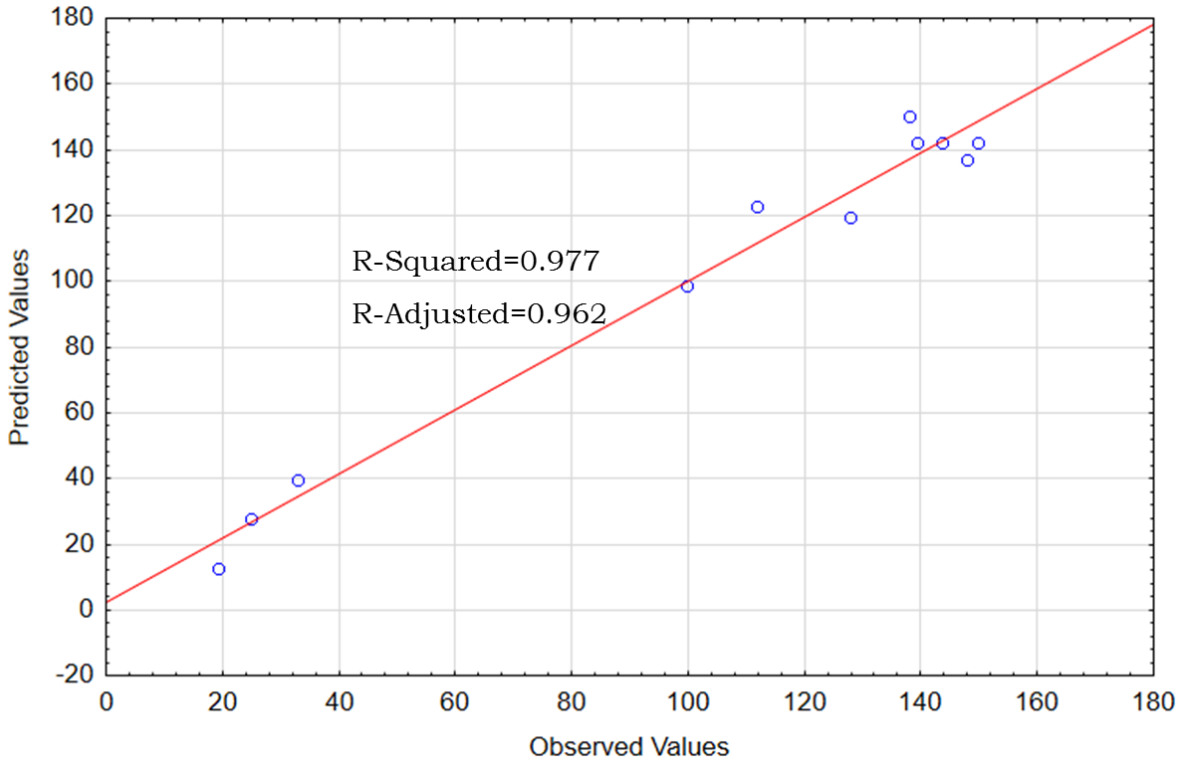

Figure 4-21: *Observed versus predicted values for the ISR model.*

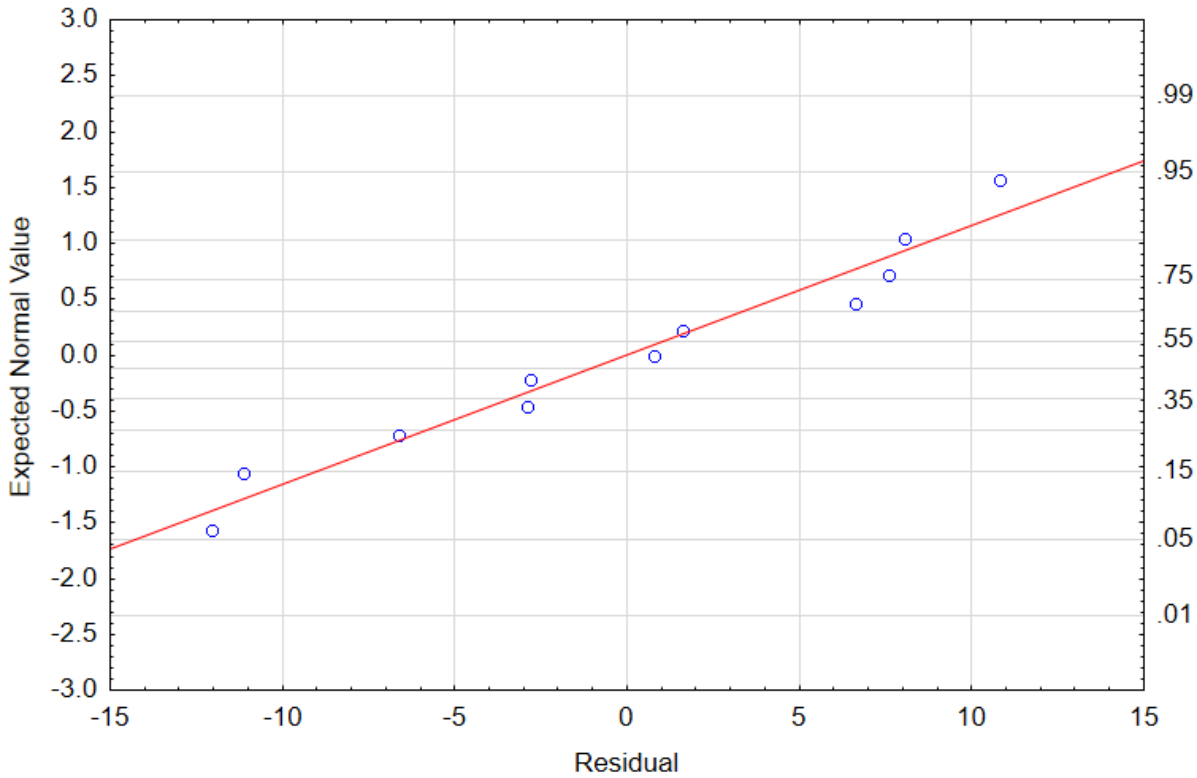

Figure 4-22: *Normal plot of the ISR model.*

4.3) High Density MFT Flocculation Tests

In the field, unlike in a lab setting, it would be impractical and counterproductive to highly dilute MFT prior to polymer-induced dewatering, especially considering the current tailings inventory. In this section, we ran a few flocculation tests on undiluted MFT using one of our high MW flocculants - HPMA (70 % DOH, 1.17×10^{-4} M, KPS). These tests were simple and aimed at assessing the possibility of using HPMA flocculant to treat high density MFT, and, hopefully, set the pace for more comprehensive future pilot tests on a commercial scale.

4.3.1. CST

As already mentioned, our operating hypothesis requires us to compare the dewatering ability of HPMA to an industrial PAM-based flocculant. Therefore, CST of the treated MFT was our first flocculation parameter to test. To gauge our success while using this flocculation parameter, we used the criteria proposed by the *Oil Sands Tailings Consortium (OSTC)* as our reference metric. According to the OSTC procedure, a successful polymer flocculant for use in treatment of high density oil sands tailings should have a CST that is less than 100 seconds.[33] The MFT sample that was used for this test was the same one characterized in **Table 4-1** and **Table 4-2** only that, in this case, it was undiluted (~33 wt. %). To homogenize the slurry, 100 g of undiluted MFT was mixed at 500 rpm in a 250 ml beaker for 5 minutes using an overhead electric mixer with an axial impeller. We maintained the same impeller diameter to beaker diameter ratio of ~0.7. For coagulation, 2000 ppm calcium was added and mixed for 2 minutes at the same rate. The procedure above was repeated in two separate beakers, one for our test HPMA flocculant and the other for the reference PAM, before adding the polymer flocculants. After coagulant addition, the mixing rate was reduced to 250 rpm and the polymer flocculants were added. Mixing was continued until the flocculant solution was evenly dispersed and visible flocs emerged.

Table 4-3: *CST results on undiluted MFT.*

	CST, seconds
OSCT (Syncrude) Proposed Standard	<100
Untreated and undiluted MFT (Control-1)	1988.6
MFT + Ca^{2+} Coagulant (Control-2)	915.7
Ref. PAM	242
HPMA (1.17×10^{-4}M, KPS; DOH-70%)	12.6

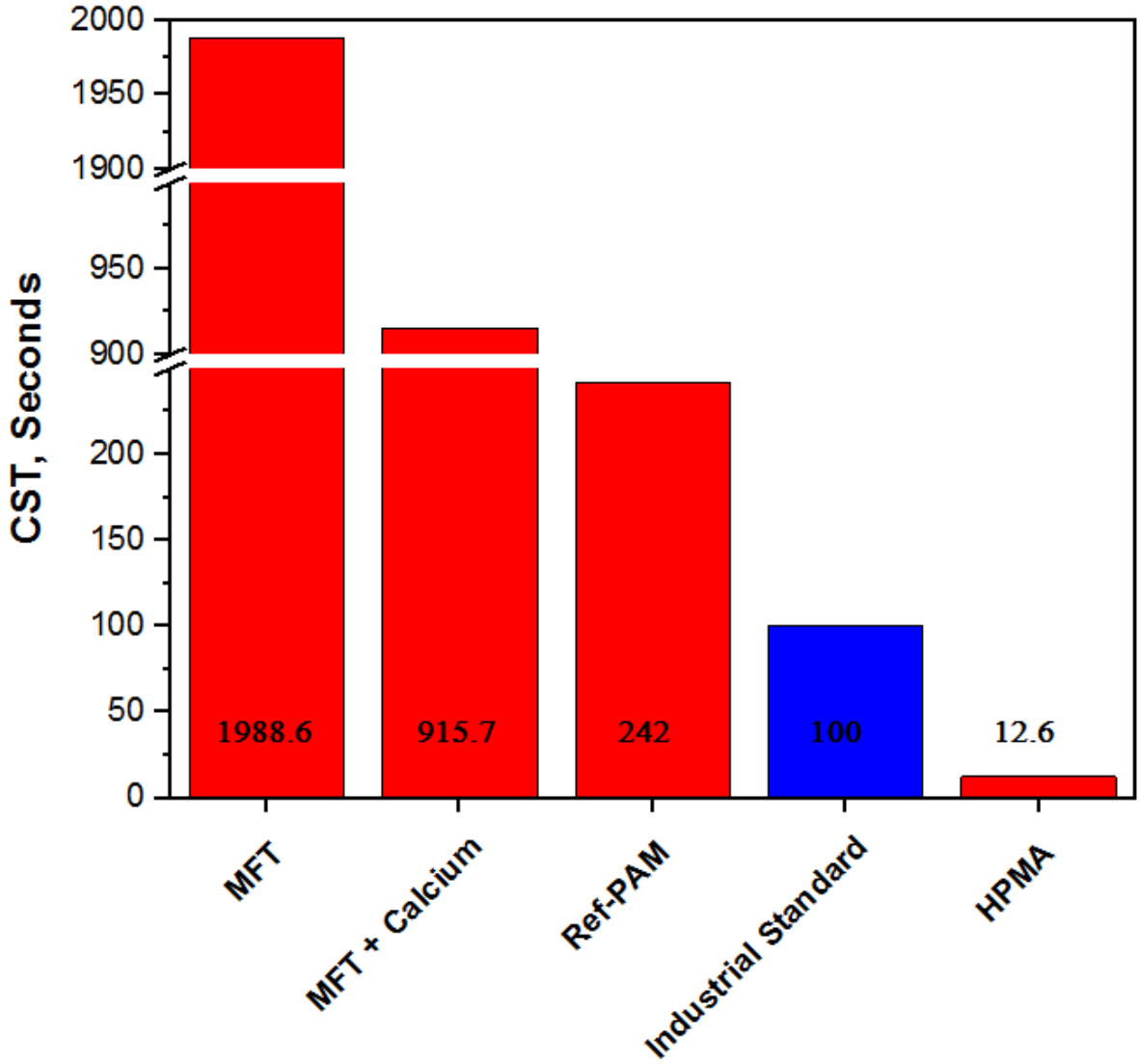

Figure 4-23: *CST values from the treatment of undiluted MFT.*

4.3.2. Pressure Filtration

A simple pressure filtration test was also run to assess the filterability and dewaterability of the flocculated MFT. We used the polymer-treated MFT samples that had optimal CST values as discussed above. The equipment used for this test was a filter press running at 10 psi pressure and each test was run for 5 minutes. For the same amount of treated MFT, HPMA (70 %, 1.17×10^{-4}M, KPS) recovered 37 ml of water in 5 minutes (30 ml within the first 30 seconds) whereas our reference PAM filtered out 24 ml in 5 minutes (9 ml within the first 30 seconds).

4.3.3. Supernatant Clarity: Centrate Solids Content

Flocculation of high density MFT lacks the clear mudline that is typical of highly diluted MFT, which makes it difficult to directly determine the clarity of the supernatant. The approach used to assess the quality of the recovered water was again borrowed from the *OSTC procedure.* This procedure proposes the use of centrifugation of polymer-treated MFT and subsequent analysis of the resulting centrate. A centrifuge centrate that has a total solids content that is below 0.5 wt. % is considered acceptable. [33] In our case, about 35 ml of the treated MFT that recorded optimal CST values was transferred to a 50 ml conical tube and centrifuged at 4200 rpm for 5 minutes. The solids content of the centrate was determined by drying triplicate samples in a moisture analyzer and was found to average 0.41 wt. % solids.

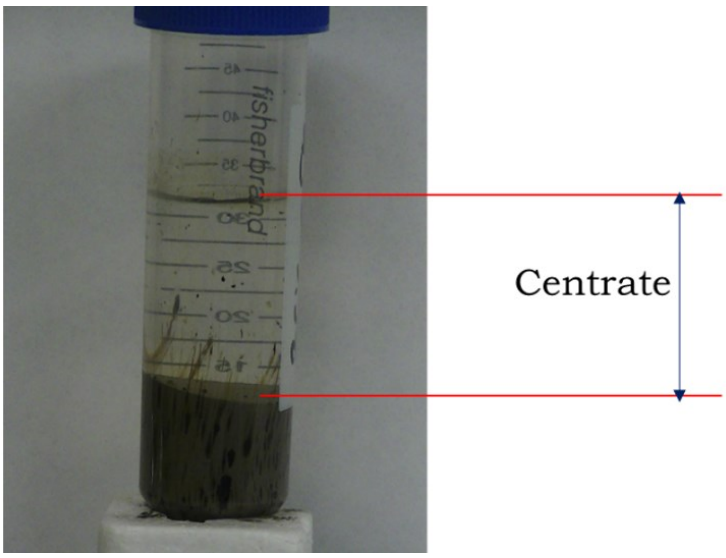

Figure 4-24: *Centrate clarity at optimal dewaterability of HPMA.*

4.3.4 Solids Content.

The solids content of the cake left behind after pressure filtration was also determined to assess the amount of solids consolidated in the cake. Solids content was determined by drying triplicate samples of the cake in an oven. HPMAs cake had a much higher solids content, which was expected considering that a significant portion of the treated MFT was recovered as filtrate water. A replication of these results on a larger scale, would lead to much better consolidation and reduction of MFT storage volume.

Table 4-5: *Solids content results on undiluted MFT.*

Polymer Flocculant	% Solids in Filtration Cake
HPMA (70%, 1.17×10^{-4}M, KPS)	49.76
Ref-PAM	40.97

5) Conclusions and Future Work

5.1) Main Contributions

I was able to successfully use emulsion polymerization to produce high batch-yields of PMA in stable latex solutions and ranging from high to relatively low molecular weights. Subsequently, I managed to use base-hydrolysis to obtain various HPMA grades from the PMA latex solutions.

Using a CCD and statistical modeling of flocculation results, I showed that the DOH was the most significant variable when using HPMA to flocculate and dewater MFT. I attributed this result to the crucial role that base hydrolysis plays in enhancing PMA's water-solubility, providing flocculation sites and extending the polymer chains.

Based on supernatant turbidity results, I concluded that using a caustic hydrolyzing agent caused dispersion of colloidal clays resulting in high turbidity of the supernatant. I also attributed the flocs shear-sensitivity to the low T_g of PMA.

Drawing from flocculation tests on undiluted MFT, I concluded that a water-soluble and high molecular weight HPMA flocculant would not only outperform an industrial PAM but it would also exceeded the industrial dewatering requirements for polymer flocculants used in treatment of high density MFT.

Lastly, from the results and insights I gained working with HPMA, I proposed a novel-group of acrylic-based flocculants for use in MFT treatment (**Figure 5-1**).

5.2) Future Work

In the future, I suggest the use of non-sodium based hydrolyzing agents like KOH and $Ca(OH)_2$, to help counter the unwanted turbidity that I attributed to sodium ions. And from a process set-up perspective, I recommend the use of a semi-batch emulsion polymerization process, which is much easier to control and reproduce than batch polymerization, especially on a commercial scale.

I also propose more detailed flocculation tests in the future, particularly with high density MFT. Polymer flocculants with varying properties (in this case DOH and MW) perform optimally at different *flocculation conditions* (clay and solids contents, mixing conditions, and polymer dosages). Comprehensive flocculation tests will help determine these optimal conditions and, in this way, lead to more effective practical applications. Also, flocculation studies on long term dewaterability and compaction will help further evaluate how these novel acrylate-based flocculants compare with their industrial counterparts.

Finally, this research work sets pace for a more comprehensive study that could lead to a novel group of hydrophobically modified acrylic polymer flocculants. This potential future endeavor will further examine the effect of increased hydrophobicity on water expulsion, verify the role of hydrogen bonding in water retention, and test the effect of *polymer* T_g (polymer elasticity) on the strength of resulting sediment flocs and subsequent compaction behavior. Based on the results from this thesis, I project that the extent to which acrylate-based polymers will form viable flocculants for use in tailings dewatering will mainly depend on their water solubility upon hydrolysis. Thus, determination of the possibility to attain water solubility via base hydrolysis will be a key step, particularly for higher acrylates. The use of water soluble acrylate-copolymers, like the one shown in **Figure 5-1**.**a**, will be especially useful in examining how flocculants with low hydrogen-bonding and high T_g perform compared to acrylate homopolymers with low Tg.

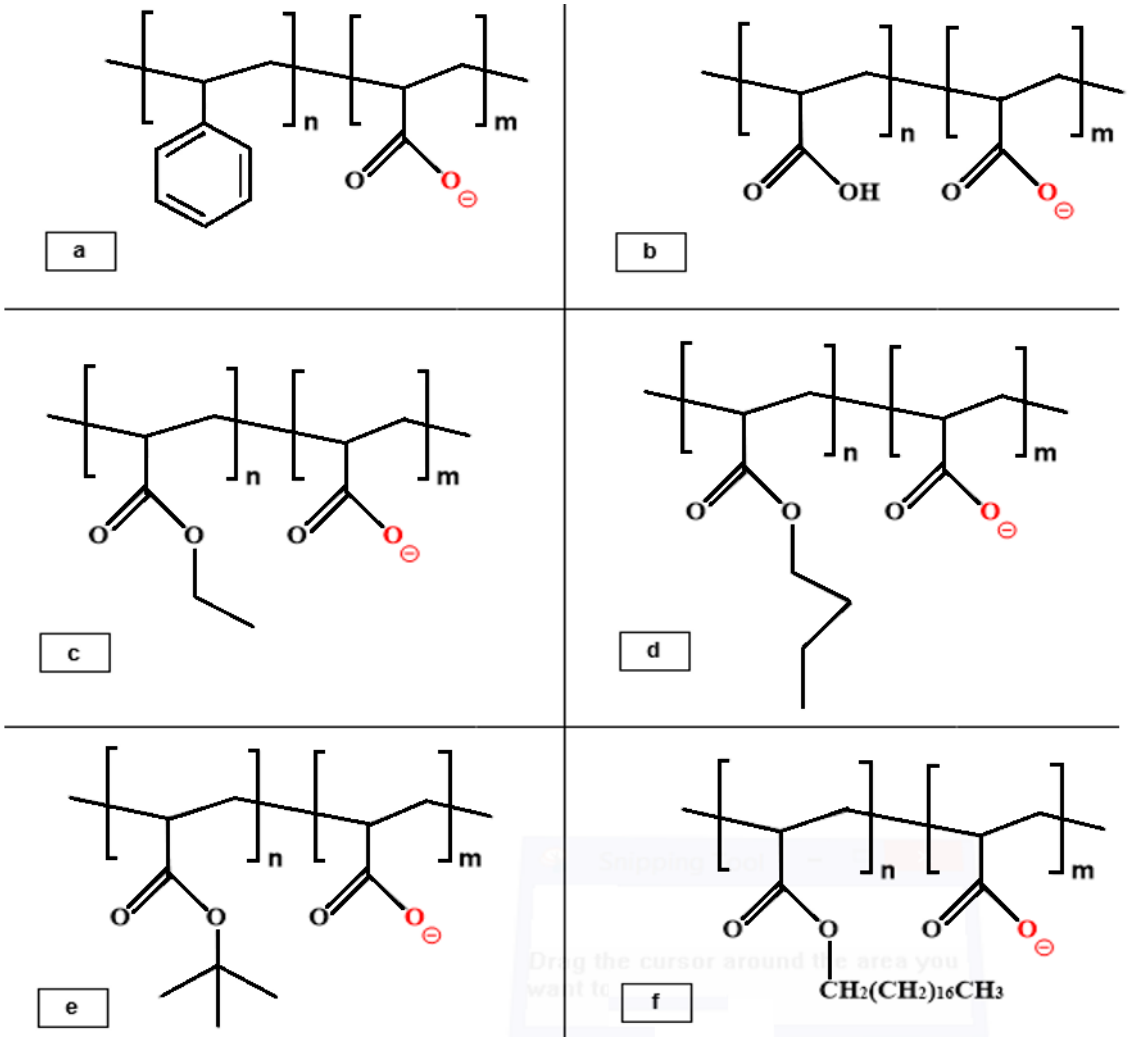

Figure 5-1: *(a) Hydrolyzed poly (styrene-acrylate) copolymer (flocculant with high T_g and low hydrogen bonding). (b) Partially hydrolyzed PAA homopolymer (high T_g and high hydrogen bonding). (c) Partially hydrolyzed PEA homopolymer (rubbery with low hydrogen bonding). (d) Partially hydrolyzed P-n-BA homopolymer. (e) Partially hydrolyzed P-t-BA homopolymer. (f) Partially hydrolyzed POA homopolymer.*

BIBLIOGRAPHY

[1] I. M. Head, D. M. Jones, and S. R. Larter, "Biological activity in the deep subsurface and the origin of heavy oil," Nature, vol. 426, no. 6964. pp. 344–352, 20-Nov-2003.

[2] M. Kleindienst, "The Athabasca oil sands in north-west Canada, a short geological overview."

[3] J. H. Masliyah, Z. Xu, and J. A. Czarnecki, Handbook on Theory and Practice of Bitumen Recovery from Athabasca Oil Sands. Kingsley Knowledge Publisher, 2011.

[4] "The Formation of Oil Sands," Alberta's Energy Heritage, Culture and Tourism | Government of Alberta. [Online]. Available: http://history.alberta.ca/energyheritage/sands/origins/the-geology-of-the-oil-sands/the-formation-of-oil-sands.aspx. [Accessed: 23-Sep-2019].

[5] P. H. J. Mercier, O. Omotoso, and D. Hockley, "Oil-Sands Clays," in Introduction to Oil Sands Clays CMS Workshop Lectures,22., 2018, pp. 9–32.

[6] "BP Statistical Review of World Energy 2019 | 68th edition," BP London UK, 2019. [Online]. Available: https://www.bp.com/content/dam/bp/business-sites/en/global/corporate/pdfs/energy-economics/statistical-review/bp-stats-review-2019-full-report.pdf. [Accessed: 23-Sep-2019].

[7] "Oil Sands Facts and Statistics," Government of Alberta. [Online]. Available: https://www.alberta.ca/oil-sands-facts-and-statistics.aspx. [Accessed: 23-Sep-2019].

[8] J. Masliyah, Z. J. Zhou, Z. Xu, J. Czarnecki, and H. Hamza, "Understanding Water-Based Bitumen Extraction from Athabasca Oil Sands," Can. J. Chem. Eng., vol. 82, no. 4, pp. 628–654, 2008.

[9] R. J. Chalaturnyk, J. D. Scott, and B. Özüm, "Management of oil sands tailings," Pet. Sci. Technol., vol. 20, no. 9–10, pp. 1025–1046, 2002.

[10] M. R. Gray, "Fundamentals of Partial Upgrading of Bitumen," Energy & Fuels, vol. 33, pp. 6843–6856, 2019.

[11] M. R. Gray, Upgrading Oilsands Bitumen and Heavy Oil. Edmonton, AB: University of Alberta Press, 2015.

[12] K. A. Clark and D. S. Pasternack, "Hot Water Seperation of Bitumen from Alberta Bituminous Sand," Ind. Eng. Chem., vol. 24, no. 12, pp. 1410–1416, 1932.

[13] K. A. Clark, "Hot-water separation of Alberta bituminous sand," Trans. Can. Inst. Min. Met., vol. 47, pp. 257–274, 1944.

[14] K. Takamura, "Microscopic structure of athabasca oil sand," Can. J. Chem. Eng., vol. 60, no. 4, pp. 538–545, 1982.

[15] J. Czarnecki, B. Radoev, L. L. Schramm, and R. Slavchev, "On the nature of Athabasca Oil Sands," Adv. Colloid Interface Sci., vol. 114–115, pp. 53–60, 2005.

[16] "ST98: Alberta Energy Outlook 2019 Executive Summary," Alberta Energy Regulator. [Online]. Available: http://www1.aer.ca/st98/2019/data/executive-summary/ST98-2019-Executive-Summary-May-2019.pdf. [Accessed: 14-Nov-2019].

[17] "Canada's Oil Sands Fact Book," Canadian Association of Petroleum Producers (CAPP), 2018. [Online]. Available: https://www.capp.ca/publications-and-statistics/publications/316441. [Accessed: 24-Sep-2019].

[18] "In-Situ Bitumen Extraction," Oil Sands Magazine. [Online]. Available: https://www.oilsandsmagazine.com/technical/in-situ. [Accessed: 24-Sep-2019].

[19] T. Hirsch, "Treasure in the Sand: An Overview of Alberta's Oil Sands Resources | Canada West Foundation," 2005. [Online]. Available: https://cwf.ca/research/publications/treasure-in-the-sand-an-overview-of-albertas-oil-sands-resources/. [Accessed: 09-Feb-2020].

[20] "Executive Summary," Alberta Energy Regulator, 2018. [Online]. Available: https://www.aer.ca/providing-information/data-and-reports/statistical-reports/executive-summary.htm#note2. [Accessed: 24-Sep-2019].

[21] "Economic Impacts of Canadian Oil and Gas Supply in Canada and the US (2017-2027)," Canadian Energy Research Institute, 2017. [Online]. Available: https://ceri.ca/assets/files/Study_166_Full-Report.pdf. [Accessed: 24-Sep-2019].

[22] "Oil and Gas," Invest Alberta| Government of Alberta. [Online]. Available: https://investalberta.ca/industry-profiles/oil-and-gas/. [Accessed: 24-Sep-2019].

[23] W. F. Eckert, J. H. Masliyah, M. R. Gray, and P. M. Fedorak, "Prediction of sedimentation and consolidation of fine tails," AIChE J., vol. 42, no. 4, 1996.

[24] P. M. Fedorak, D. L. Coy, M. J. Salloum, and M. J. Dudas, "Methanogenic potential of tailings samples from oil sands extraction plants," Can. J. Microbiol., vol. 48, no. 1, pp. 21–33, 2002.

[25] F. M. Holowenko, M. D. MacKinnon, and P. M. Fedorak, "Methanogens and sulfate-reducing bacteria in oil sands fine tailings waste," Can. J. Microbiol., vol. 46, no. 10, pp. 927–937, 2000.

[26] T. J. Penner and J. M. Foght, "Mature fine tailings from oil sands processing harbour diverse methanogenic communities," Can. J. Microbiol., vol. 56, no. 6, pp. 459–470, 2010.

[27] Z. Burkus, J. Wheler, and S. Pletcher, "GHG Emissions from Oil Sands Tailings Ponds: Overview and modelling based on fermentable substrates," 2014.

[28] C. Wang, D. Harbottle, Q. Liu, and Z. Xu, "Current state of fine mineral tailings treatment: A critical review on theory and practice," Minerals Engineering, vol. 58. pp. 113–131, Apr-2014.

[29] M. P. Davies and T. E. Martin, "Upstream constructed tailings dams: A review of the basics," in International conference; 7th, Tailings and Mine Waste, 2000, pp. 3–16.

[30] L. L. Schramm, E. N. Stasiuk, and M. MacKinnon, Surfactants in Athabasca Oil Sands Slurry Conditioning, Flotation Recovery, and Tailings Processes. 2010.

[31] S. Ren, H. Zhao, J. Long, Z. Xu, and J. Masliyah, "Understanding weathering of oil sands ores by atomic force microscopy," AIChE J., vol. 55, no. 12, pp. 3277–3285, Dec. 2009.

[32] "Bitumen Extraction Explained | Oil Sands Magazine." [Online]. Available: https://www.oilsandsmagazine.com/technical/mining/extraction. [Accessed: 28-Jun-2020].

[33] T. Xiaoli, "Research Techniques in Oil Sands - C HE 694 X02," in Chemical and Materials Engineering Dept., University of Alberta, 2019.

[34] "Alberta Environment and Parks Oil Sands Information Portal." [Online]. Available: http://osip.alberta.ca/map/. [Accessed: 12-Dec-2019].

[35] N. Dhadli et al., "Technical Guide for Fluid Fine Tailings Management," 2012.

[36] "Tailings Ponds 101 | Oil Sands Magazine." [Online]. Available: https://www.oilsandsmagazine.com/technical/mining/tailings-ponds?rq=tailings. [Accessed: 12-Dec-2019].

[37] S. Azam and J. D. Scott, "Revisiting the Ternary Diagram for Tailings Characterization and Management," 2006.

[38] H. Kaminsky et al., "Measuring Undrained Shear Strength of Oil Sands Tailings Deposits," 2015.

[39] J. Sobkowicz, A. Hyndman, R. Dawson, and B. Watts, "Guidelines for Performance Management of Oil Sands Fluid Fine Tailings Deposits to Meet Closure Commitments Canada's Oil Sands Innovation Alliance," 2014.

[40] N. Beier, W. Wilson, A. Dunmola, and D. Sego, "Impact of flocculation-based dewatering on the shear strength of oil sands fine tailings," Can. Geotech. J., vol. 50, no. 9, pp. 1001–1007, 2013.

[41] L. Botha and J. B. P. Soares, "The Influence of Tailings Composition on Flocculation," Can. J. Chem. Eng., vol. 93, no. 9, pp. 1514–1523, 2015.

[42] H. Kaminsky and A. Sedgwick, "Oil Sands Tailings 101," 2020.

[43] R. J. Mikula, K. L. Kasperski, R. D. Burns, and M. D. MacKinnorr, "Nature and fate of oil sands fine tailings," Adv. Chem. Ser., vol. 251, pp. 718–723, 1996.

[44] K. L. Konan et al., "Surface properties of kaolin and illite suspensions in concentrated calcium hydroxide medium," J. Colloid Interface Sci., vol. 307, no. 1, pp. 101–108, Mar. 2007.

[45] P. Zarzycki and B. Gilbert, "Long-Range Interactions Restrict Water Transport in Pyrophyllite Interlayers OPEN," Nat. Publ. Gr., 2016.

[46] S. Nimesh, R. Chan, and N. Gupta, Advances in nanomedicine for the delivery of therapeutic nucleic acids. .

[47] M. Chorom and P. Rengasamy, "Dispersion and zeta potential of pure clays as related to net particle charge under varying pH, electrolyte concentration and cation type," Eur. J. Soil Sci., vol. 46, no. 4, pp. 657–665, 1995.

[48] L. Yan, J. H. Masliyah, and Z. Xu, "Understanding suspension rheology of anisotropically-charged platy minerals from direct interaction force measurement using AFM," Current Opinion in Colloid and Interface Science, vol. 18, no. 2. pp. 149–156, Apr-2013.

[49] J. H. Adair, E. Suvaci, and J. Sindel, "Surface and Colloid Chemistry," in Encyclopedia of Materials: Science and Technology, Elsevier, 2001, pp. 1–10.

[50] Y. Guo and J. Q. Shang, "A study on electrokinetic dewatering of oil sands tailings," Environ. Geotech., vol. 1, no. 2, pp. 121–134, 2014.

[51] N. Ural, "The Importance of Clay in Geotechnical Engineering," in Current Topics in the Utilization of Clay in Industrial and Medical Applications, InTech, 2018.

[52] C. H. Benson and J. M. Trast, “Hydraulic conductivity of thirteen compacted clays,” Clays Clay Miner., vol. 43, no. 6, pp. 669–681, 1995.

[53] F. Tavenas, P. Jean, P. Leblond, and S. Leroueil, “The permeability of natural soft clays. Part II: permeability characteristics.,” Can. Geotech. J., vol. 20, no. 4, pp. 645–660, Nov. 1983.

[54] X. Ren, Y. Zhao, Q. Deng, J. Kang, D. Li, and D. Wang, “A relation of hydraulic conductivity — void ratio for soils based on Kozeny-Carman equation,” Eng. Geol., vol. 213, pp. 89–97, Nov. 2016.

[55] B. M. Das, “Principles of Foundation Engineering.,” 6th ed., Thomson, 2007, p. 480.

[56] C. M. Fellows and W. O. S. Doherty, “Insights into bridging flocculation,” Macromol. Symp., vol. 231, pp. 1–10, 2006.

[57] “Laboratory of Colloid and Surface Chemistry (LCSC).” [Online]. Available: http://www.colloid.ch/index.php?name=dlvo. [Accessed: 31-Dec-2019].

[58] R. Hogg, “Bridging flocculation by polymers,” KONA Powder Part. J., vol. 30, no. 30, pp. 3–14, 2012.

[59] D. R. L. Vedoy and J. B. P. Soares, “Water-soluble polymers for oil sands tailing treatment: A Review,” Can. J. Chem. Eng., vol. 93, no. 5, pp. 888–904, 2015.

[60] J. Long, H. Li, Z. Xu, and J. H. Masliyah, “Role of colloidal interactions in oil sand tailings treatment,” AIChE J., vol. 52, no. 1, pp. 371–383, Jan. 2006.

[61] P. H. J. Mercier et al., “Colloidal Clay Gelation: Relevance to Current Oil Sands Operations,” Pet. Sci. Technol., vol. 30, no. 9, pp. 915–923, Mar. 2012.

[62] M. S. Shoichet, “Polymer Scaffolds for Biomaterials Applications,” Macromolecules, vol. 43, no. 2, pp. 581–591, Jan. 2010.

[63] W. B. Liechty, D. R. Kryscio, B. V. Slaughter, and N. A. Peppas, “Polymers for Drug Delivery Systems,” Annu. Rev. Chem. Biomol. Eng., vol. 1, no. 1, pp. 149–173, Jun. 2010.

[64] R. E. Sojka, D. L. Bjorneberg, J. A. Entry, R. D. Lentz, and W. J. Orts, “Polyacrylamide in Agriculture and Environmental Land Management,” Advances in Agronomy, vol. 92. Academic Press, pp. 75–162, 01-Jan-2007.

[65] F. . Barvenik, Polyacrylamide Characteristics Related to Soil Applications, vol. 4, no. 158. Elsevier Inc., 1994.

[66] C. Aften and W. P. . Watson, “Improved friction reducer for hydraulic fracturing - Society of Petroleum Engineers,” 2009.

[67] A. Z. Abidin, T. Puspasari, and W. A. Nugroho, “Polymers for Enhanced Oil Recovery Technology,” Procedia Chem., vol. 4, pp. 11–16, Jan. 2012.

[68] S. S. Wong, T. T. Teng, A. L. Ahmad, A. Zuhairi, and G. Najafpour, “Treatment of pulp and paper mill wastewater by polyacrylamide (PAM) in polymer induced flocculation,” J. Hazard. Mater., vol. 135, no. 1–3, pp. 378–388, Jul. 2006.

[69] M. I. Aguilar et al., “Improvement of coagulation-flocculation process using anionic polyacrylamide as coagulant aid,” Chemosphere, vol. 58, no. 1, pp. 47–56, Jan. 2005.

[70] L. Botha, S. Davey, B. Nguyen, A. K. Swarnakar, E. Rivard, and J. B. P. Soares, “Flocculation of oil sands tailings by hyperbranched functionalized polyethylenes (HBfPE),” Miner. Eng., vol. 108, pp. 71–82, 2017.

[71] R. Hripko, V. Vajihinejad, F. LopesMotta, and J. B. P. Soares, “Enhanced Flocculation of Oil Sands Mature Fine Tailings Using Hydrophobically Modified Polyacrylamide Copolymers,” Glob. Challenges, vol. 2, no. 3, p. 1700135, Mar. 2018.

[72] L. G. Reis et al., “Using acrylamide/propylene oxide copolymers to dewater and densify mature fine tailings,” Miner. Eng., vol. 95, pp. 29–39, Sep. 2016.

[73] S. P. Gumfekar and J. B. P. Soares, “A novel hydrophobically-modified polyelectrolyte for enhanced dewatering of clay suspension,” Chemosphere, vol. 194, pp. 422–431, Mar. 2018.

[74] F. O. Garces, K. Sivadasan, P. Somasundaran, and N. J. Turro, “Interpolymer complexation of poly(acrylic acid) and polyacrylamide: structural and dynamic studies by solution- and solid-state NMR,” Macromolecules, vol. 27, no. 1, pp. 272–278, Jan. 1994.

[75] H. Li, J. Zhou, R. Chow, A. Adegoroye, and A. S. Najafi, “Enhancing treatment and geotechnical stability of oil sands fine tailings using thermo-sensitive poly(n -isopropyl acrylamide),” Can. J. Chem. Eng., vol. 93, no. 10, pp. 1780–1786, Oct. 2015.

[76] B. J. Lee and M. A. Schlautman, “Effects of polymer molecular weight on adsorption and flocculation in aqueous kaolinite suspensions dosed with nonionic polyacrylamides,” Water (Switzerland), vol. 7, no. 11, pp. 5896–5909, 2015.

[77] T. R. Rooney, S. P. Gumfekar, J. B. P. Soares, and R. A. Hutchinson, “Cationic Hydrolytically Degradable Flocculants with Enhanced Water Recovery for Oil Sands Tailings Remediation,” Macromol. Mater. Eng., vol. 301, no. 10, pp. 1248–1254, Oct. 2016.

[78] S. P. Gumfekar, T. R. Rooney, R. A. Hutchinson, and J. B. P. Soares, “Dewatering Oil Sands Tailings with Degradable Polymer Flocculants,” ACS Appl. Mater. Interfaces, vol. 9, no. 41, pp. 36290–36300, Oct. 2017.

[79] C. Klein, D. Harbottle, L. Alagha, and Z. Xu, “Impact of fugitive bitumen on polymer-based flocculation of mature fine tailings,” Can. J. Chem. Eng., vol. 91, no. 8, pp. 1427–1432, Aug. 2013.

[80] L. S. Kotlyar, B. D. Sparks, J. R. Woods, S. Raymond, Y. Le Page, and W. Shelfantook, “Distribution and types of solids associated with bitumen,” Pet. Sci. Technol., vol. 16, no. 1–2, pp. 1–19, 1998.

[81] G. Odian, Principles of Polymerization. John Wiley & Sons, Inc., 2004.

[82] D. Braun, “Origins and development of initiation of free radical polymerization processes,” International Journal of Polymer Science, vol. 2009. Hindawi Publishing Corporation, 2009.

[83] L. Peter and S. E.-A. Mohamed, Emulsion Polymerization and Emulsion Polymers. Wiley, 1997.

[84] C. Chern, Principles and applications of emulsion polymerization. 2008.

[85] D. H. Sebastian and J. A. Biesenberger, “Thermal ignition phenomena in chain-addition copolymerizations,” J. Appl. Polym. Sci., vol. 23, no. 3, pp. 661–686, Feb. 1979.

[86] J. A. Barton and P. F. Nolan, “Incidents in the chemical industry due to thermal-runaway chemical reactions.”

[87] P. Flory, Principles of polymer chemistry. 1953.

[88] D. R. Bassett and A. E. Hamielec, Eds., Emulsion Polymers and Emulsion Polymerization, vol. 165. Washington, D. C.: American Chemical Society, 1981.

[89] V. I. Eliseeva, S. S. Ivanchev, S. I. Kuchanov, and A. V. Lebedev, Emulsion Polymerization and Its Applications in Industry. New York: Consultants Bureau, 1981.

[90] A. M. van Herk, Chemistry and Technology of Emulsion Polymerisation: Second Edition. John Wiley and Sons, 2013.

[91] C. Anderson and E. Daniels, Emulsion polymerisation and latex applications. 2003.

[92] D. Feldman, "Polymer History," Des. Monomers Polym., vol. 11, pp. 1–15, 2008.

[93] J. Asua, Polymeric dispersions: principles and applications. 2012.

[94] H. Warson and C. Finch, Applications of Synthetic Resin Latices, Latices in Diverse Applications. 2001.

[95] J. W. Vanderhoff, E. B. Bradford, H. L. Tarkowski, J. B. Shaffer, and R. M. Wiley, "Inverse Emulsion Polymerization," 1962, pp. 32–51.

[96] J. W. Vanderhoff, F. V. DiStefano, M. S. El-Aasser, R. O'Leary, O. M. Shaffer, and D. L. Visioli, "Inverse emulsion polymerization of acrylamide: Polymerization kinetics and process development," J. Dispers. Sci. Technol., vol. 5, no. 3–4, pp. 323–363, Jan. 1984.

[97] J. M. Asua, "Miniemulsion polymerization," Progress in Polymer Science (Oxford), vol. 27, no. 7. Elsevier Ltd, pp. 1283–1346, 01-Sep-2002.

[98] F. J. Schork, Y. Luo, W. Smulders, J. P. Russum, A. Butté, and K. Fontenot, "Miniemulsion polymerization," Adv. Polym. Sci., vol. 175, pp. 129–255, 2005.

[99] F. M. Pavel, "Microemulsion Polymerization," J. Dispers. Sci. Technol., vol. 25, no. 1, pp. 1–16, Dec. 2004.

[100] J. S. Guo, M. S. El-Aasser, and J. W. Vanderhoff, "Microemulsion polymerization of styrene," J. Polym. Sci. Part A Polym. Chem., vol. 27, no. 2, pp. 691–710, Jan. 1989.

[101] B. Gupta and H. Singh, "Polymerization in microemulsion systems," Polym. Plast. Technol. Eng., vol. 31, no. 7–8, pp. 635–658, Aug. 1992.

[102] J. M. Asua, "Emulsion polymerization: From fundamental mechanisms to process developments," J. Polym. Sci. Part A Polym. Chem., vol. 42, no. 5, pp. 1025–1041, Mar. 2004.

[103] A. N. M. B. El-hoshoudy, "Emulsion Polymerization Mechanism," in Recent Research in Polymerization, InTech, 2018.

[104] M. B. Kirkham, Principles of Soil and Plant Water Relations | Chapter 3. Structure and Properties of Water. Elsevier Inc., 2005.

[105] H. Berber, "Emulsion Polymerization: Effects of Polymerization Variables on the Properties of Vinyl Acetate Based Emulsion Polymers," in Polymer Science, InTech, 2013.

[106] J. B. P. Soares, "Polymer Reaction Engineering - CME 694," in Chemical and Materials Engineering Dept., University of Alberta, 2019.

[107] S. C. Thickett and R. G. Gilbert, “Emulsion polymerization: State of the art in kinetics and mechanisms,” Polymer, vol. 48, no. 24. Elsevier BV, pp. 6965–6991, 16-Nov-2007.

[108] F. K. Hansen and J. Ugelstad, “Particle Nucleation in Emulsion Polymerization. I. A Theory for Homogeneous Nucleation,” J Polym Sci Polym Chem Ed, vol. 16, no. 8, pp. 1953–1979, Aug. 1978.

[109] J. Gao and A. Penlidis, “Mathematical modeling and computer simulator/database for emulsion polymerizations,” Prog. Polym. Sci., vol. 27, no. 3, pp. 403–535, 2002.

[110] W. D. Harkins, “A General Theory of the Reaction Loci in Emulsion Polymerization,” II J. Chem. Phys., vol. 13, no. 9, p. 17, 1945.

[111] W. D. Harkins, “A general theory of the reaction loci in emulsion polymerization. II [2],” The Journal of Chemical Physics, vol. 14, no. 1. American Institute of Physics, pp. 47–48, 22-Jan-1946.

[112] M. Nomura, H. Tobita, and K. Suzuki, “Emulsion polymerization: Kinetic and mechanistic aspects,” Adv. Polym. Sci., vol. 175, pp. 1–128, 2005.

[113] P. J. Feeney, D. H. Napper, and R. G. Gilbert, “Coagulative Nucleation and Particle Size Distributions in Emulsion Polymerization,” Macromolecules, vol. 17, no. 12, pp. 2520–2529, 1984.

[114] W. D. Harkins, “General theory of mechanism of emulsion polymerization. II,” J. Polym. Sci., vol. 5, no. 2, pp. 217–251, Apr. 1950.

[115] C. S. Chern, “Emulsion polymerization mechanisms and kinetics,” Progress in Polymer Science (Oxford), vol. 31, no. 5. Pergamon, pp. 443–486, 01-May-2006.

[116] R. Gilbert, Emulsion polymerization: a mechanistic approach. 1995.

[117] W. V. Smith and R. H. Ewart, “Kinetics of emulsion polymerization,” J. Chem. Phys., vol. 16, no. 6, pp. 592–599, Jun. 1948.

[118] C. S. Chern, “Desorption of free radicals in semibatch emulsion polymerization of methyl acrylate,” J. Appl. Polym. Sci., vol. 56, no. 2, pp. 231–238, Apr. 1995.

[119] M. Banerjee and R. S. Konar, “Mechanism of the emulsion polymerization of methyl acrylate: 2. Kinetics and growth of the polymers,” Polymer (Guildf)., vol. 27, no. 1, pp. 147–157, Jan. 1986.

[120] D. Mangaraj and S. K. Patra, “Autoacceleration in polymerisation of acrylic esters. Part 1. Ethyl and n-propyl acrylate,” Die Makromol. Chemie, vol. 104, no. 1, pp. 125–134, May 1967.

[121] K. J. Saunders, Organic Polymer Chemistry. Springer Netherlands, 1973.

[122] M. S. Matheson, E. E. Auer, E. B. Bevilacqua, and E. J. Hart, “Rate Constants in Free Radical Polymerizations. IV. Methyl Acrylate,” J. Am. Chem. Soc., vol. 73, no. 11, pp. 5395–5400, Nov. 1951.

[123] J. L. Kice, “Inhibition of polymerization. II. Methyl acrylate,” J. Polym. Sci., vol. 19, no. 91, pp. 123–140, Jan. 1956.

[124] K. G. McCurdy and K. J. Laidler, “Rates of polymerization of acrylates and methacrylates in emulsion systems,” Can. J. Chem., vol. 42, no. 4, pp. 825–829, Apr. 1964.

[125] N. M. Ahmad, F. Heatley, and P. A. Lovell, “Chain transfer to polymer in free-radical solution polymerization of n-butyl acrylate studied by NMR spectroscopy,” Macromolecules, vol. 31, no. 9, pp. 2822–2827, May 1998.

[126] S. D. Gadkary and S. L. Kapur, “Chain transfer in solution polymerization III. methyl acrylate.,” Die Makromol. Chemie, vol. 17, no. 1, pp. 29–38, Jan. 1955.

[127] J. Gao, A. Penlidis, and A. Penlidis’, “A Comprehensive Simulator/Database Package for Reviewing Free-Radical Homopolymerizations.,” 1996.

[128] “Glass Transition Temperatures.” [Online]. Available: http://polymerdatabase.com/polymer physics/Polymer Tg C.html. [Accessed: 10-Feb-2020].

[129] V. Vajihinejad, R. Guillermo, and B. Soares, “Dewatering Oil Sands Mature Fine Tailings (MFTs) with Poly(acrylamide-co-diallyldimethylammonium chloride): Effect of Average Molecular Weight and Copolymer Composition,” 2017.

[130] V. Czitrom, “One-factor-at-a-time versus designed experiments,” Am. Stat., vol. 53, no. 2, pp. 126–131, 1999.

[131] K. P. C. Vollhardt and N. E. Schore, “Chemistry of Esters,” in Organic chemistry : structure and function, 6th ed., W. H. Freeman and Company, 2011, pp. 936–938.

[132] S. Fujisawa and Y. Kadoma, “Relationships Between Base-Catalyzed Hydrolysis Rates or Glutathione Reactivity for Acrylates and Methacrylates and Their NMR Spectra or Heat of Formation,” Int. J. Mol. Sci., vol. 13, no. 5, pp. 5789–5800, May 2012.

[133] I. Sakurada, “Some Fundamental Aspects of Polymer Reactions,” in La Chimie Macromoléculaire—4 / Macromolecular Chemistry—4, Springer US, 1968, pp. 263–283.

[134] H. Kawabe and M. Yanagita, “Group Interactions in Polyelectrolytes. IV. Kinetics of the Alkaline Hydrolysis of Polymethyl Acrylate (Part II),” Bull. Chem. Soc. Jpn., vol. 44, no. 2, pp. 310–312, Feb. 1971.

[135] H. Kawabe and M. Yanagita, “Group Interactions in Polyelectrolytes. II. Kinetics of Alkaline Hydrolysis of Polymethyl Acrylate,” Bull. Chem. Soc. Jpn., vol. 42, no. 11, pp. 3109–3115, Nov. 1969.

[136] Y. V. Kudryavtsev, A. D. Litmanovich, and N. A. Platé, “On the kinetics of polyacrylamide alkaline hydrolysis,” Macromolecules, vol. 31, no. 14, pp. 4642–4644, Jul. 1998.

[137] J. Moens and G. Smets, “Alkaline and acid hydrolysis of polyvinylamides,” J. Polym. Sci., vol. 23, no. 104, pp. 931–948, Feb. 1957.

[138] K. Nagase and K. Sakaguchi, “Alkaline hydrolysis of polyacrylamide,” J. Polym. Sci. Part A Gen. Pap., vol. 3, no. 7, pp. 2475–2482, Jul. 1965.

[139] J. J. Max and C. Chapados, “Infrared Spectroscopy of Aqueous Carboxylic Acids: Comparison between Different Acids and Their Salts,” J. Phys. Chem. A, vol. 108, no. 16, pp. 3324–3337, Apr. 2004.

[140] D. L. Pavia, G. M. Lampman, G. S. Kriz, and J. R. Vyvyan, Introduction to spectroscopy, 5th ed. Vitalsource Technologies, Inc., 2015.

[141] "Particle Characterization - Guide to Particle Characterization Methods | Malvern Panalytical." [Online]. Available: https://www.malvernpanalytical.com/en/learn/knowledge-center/whitepapers/WP120620BasicGuidePartChar. [Accessed: 23-Mar-2020].

[142] "Zetasizer Nano ZSP | Expert Colloid & Protein Characterization | Malvern Panalytical." [Online]. Available: https://www.malvernpanalytical.com/en/products/product-range/zetasizer-range/zetasizer-nano-range/zetasizer-nano-zsp. [Accessed: 18-Mar-2020].

[143] Hong Wen Gao, "Mobility Control in Oil Recovery by Chemical Flooding State-of-the-Art Review," 1987.

[144] K. Spildo and E. I. Ø. Sæ, "Effect of Charge Distribution on the Viscosity and Viscoelastic Properties of Partially Hydrolyzed Polyacrylamide," Energy and Fuels, vol. 29, no. 9, pp. 5609–5617, Sep. 2015.

[145] S. Lee, D. H. Kim, C. Huh, and G. A. Pope, "Development of a comprehensive rheological property database for EOR polymers," in Proceedings - SPE Annual Technical Conference and Exhibition, 2009, vol. 5, pp. 3161–3174.

[146] A. M. S. Maia, M. A. Villetti, R. R. L. Vidal, R. Borsali, and R. C. Balaban, "Solution properties of a hydrophobically associating polyacrylamide and its polyelectrolyte derivatives determined by light scattering, small angle X-ray scattering and viscometry," J. Braz. Chem. Soc., vol. 22, no. 3, pp. 489–500, 2011.

[147] T. G. Parameswaran and P. V. Sivapullaiah, "Influence of Sodium and Lithium Monovalent Cations on Dispersivity of Clay Soil," J. Mater. Civ. Eng., vol. 29, no. 7, p. 04017042, Jul. 2017.

[148] Andrew Vietti, "Clay Mineralogy and Water Chemistry on Tailings Settling and Rheology," in Second Concrad Clay Workshop, 2011.

[149] T. Rodrigues De Melo, W. Machado, and J. Tavares Filho, "Charge sparsity: An index to quantify cation effects on clay dispersion in soils," Sci. Agric. v, vol. 77, no. 1, p. 2020, 2017.

[150] A. G. Volkov, S. Paula, and D. W. Deamer, "Two mechanisms of permeation of small neutral molecules and hydrated ions across phospholipid bilayers," in Bioelectrochemistry and Bioenergetics, 1997, vol. 42, no. 2, pp. 153–160.

APPENDIX A:

DLS Analysis

Batch	Temperature, °C	Z-Ave (d, nm)	PDI
2.14 x10^{-2}M, KPS	25	100.4	0.034
		100.1	0.033
		100.4	0.031
1.00 x10^{-2}M, KPS	25	101.5	0.035
		101.4	0.020
		100.2	0.041
1.58 x10^{-3}M, KPS	25	107.3	0. 034
		106.6	0.016
		106.5	0.035
2.51 x10^{-4}M, KPS	25	115.2	0.048
		113.0	0.036
		113.2	0.029
1.17 x10^{-4}M, KPS	25	122.8	0.044
		121.6	0.037
		120.2	0.048

APPENDIX B:

CMC Determination

Surface Tension [mN/m]	[Surfactant],mM (mol/L.10^{-3})
72.572	0
55.630	1.82
43.804	3.64
35.84	5.46
35.252	6.37
34.575	7.28
34.045	8.2
35.603	9.1
36.451	10.01
38.044	11.8
38.322	12.74
38.483	13.65
38.449	14.56
38.357	15.47
38.473	16.38
38.424	18.2
38.512	20.02

APPENDIX C:

Batch Solids Content

	1	2	3	4	5
[Initiator], M	*1.17 x10^{-4}*	*2.51x10^{-4}*	*1.58 x10^{-3}*	*1.00 x10^{-2}*	*2.14 x10^{-2}*
Solids Content, %	*27*	*29*	*30*	*28*	*27*

$$\boldsymbol{Solids\ Content} = \frac{(\boldsymbol{Initial\ Mass\ of\ Latex\ Solution}) - (\boldsymbol{Final\ Mass\ after\ Heating})}{\boldsymbol{Initial\ Mass\ of\ Latex\ Solution}}\ \boldsymbol{x\ 100}$$

Or,

$$\boldsymbol{Solids\ Content} = [\mathbf{1} - \boldsymbol{Moisture\ Content}^{*}]\ \boldsymbol{x\ 100}$$

**Heating was done using a programmable OHAUS moisture analyzer. The mass of the aluminum pan containing the latex solution was tared to zero before adding the polymer samples.*

APPENDIX D:

CCD Experimental Design Matrix.

Log [I]	DOH, %	CST, Seconds	Turbidity, NTU	ISR, cm/h	Dosage, ppm
-3.6	80	10	39	138	3000
-3.93	70	9.5	36.7	148	7000
-2.8	90	12.7	29.3	127.8	1000
-2.0	80	11	22	111.9	3000
-2.8	48	45	64	25	9000
-3.6	50	34	73	33	12000
-2.8	70	9.5	35	143.7	5000
-2.0	50	38	64	19.2	9000
-2.8	70	8.4	30	149.7	5000
-1.67	70	9	29	99.7	1000
-2.8	70	8.7	33	139.3	5000

APPENDIX E:

CST Residual Plot

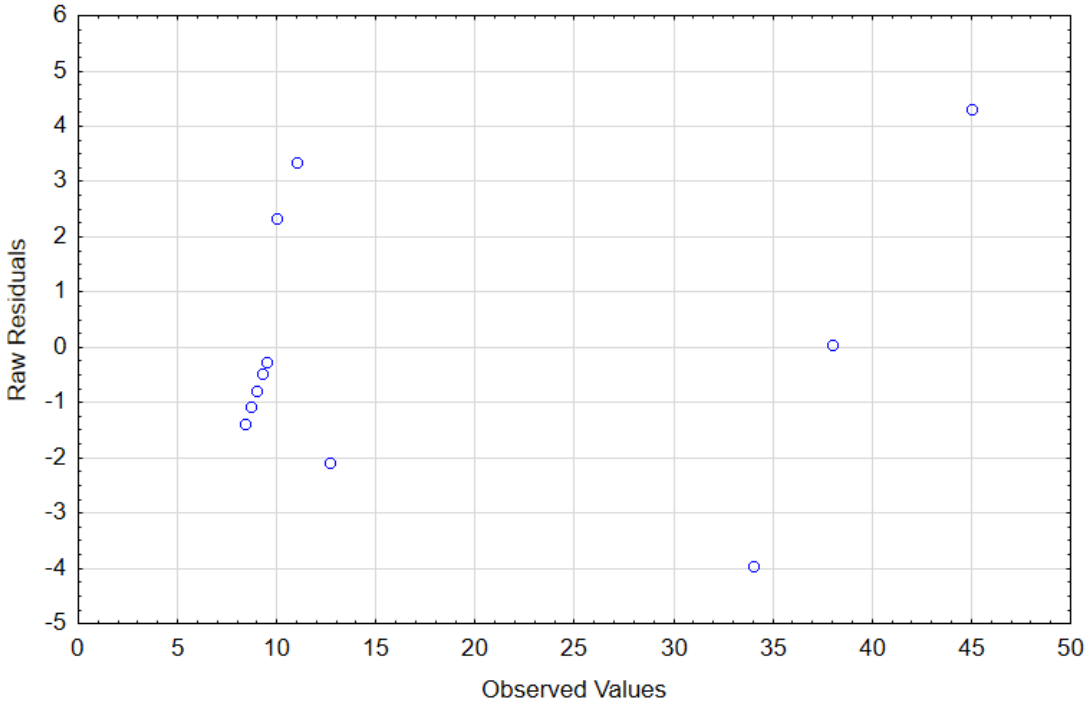

Turbidity Residual Plot

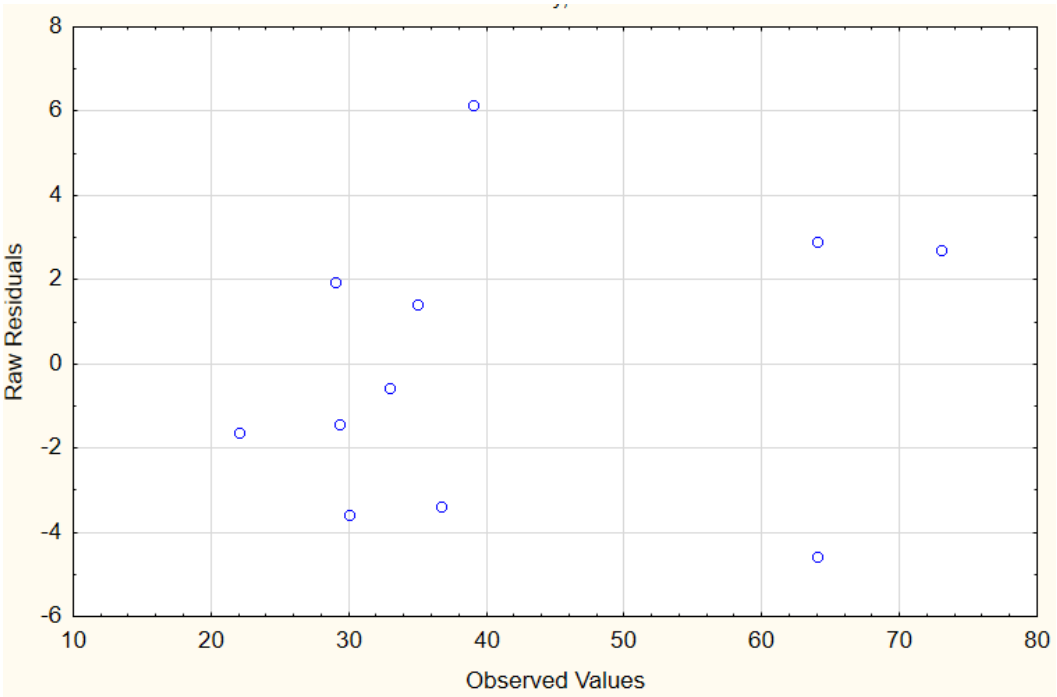
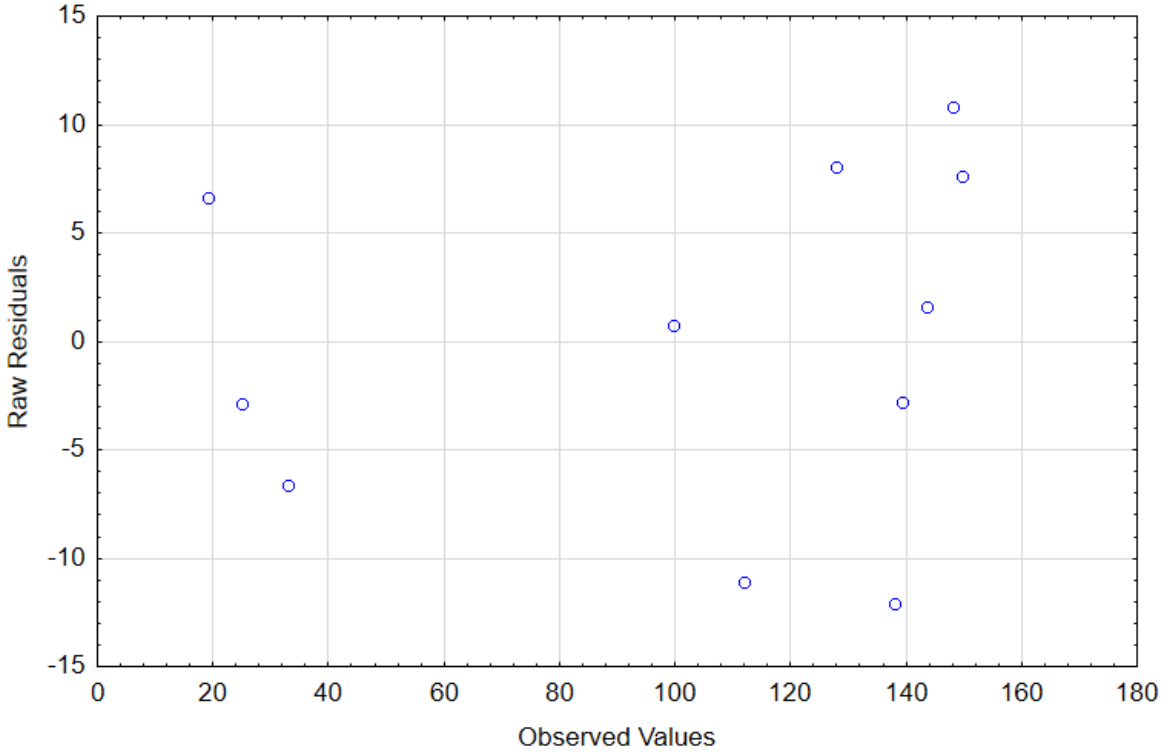
ISR Residual Plot